Title
Metabolic Regulation of Preimplantation Mouse Embryo Development

Author
Chi, Fangtao

Publication Date
2020

Peer reviewed|Thesis/dissertation

UNIVERSITY OF CALIFORNIA

Los Angeles

Metabolic Regulation of Preimplantation Mouse Embryo Development

A dissertation submitted in partial satisfaction of the

requirements for the degree Doctor of Philosophy

in Molecular Biology

by

Fangtao Chi

2020

ABSTRACT OF THE DISSERTATION

Metabolic Regulation of Preimplantation Mouse Embryo Development

by

Fangtao Chi

Doctor of Philosophy in Molecular Biology

University of California, Los Angeles, 2020

Professor Utpal Banerjee, Chair

Preimplantation mammalian embryo is a critical stage in embryonic development, during which the totipotent zygote goes through zygotic genome activation (ZGA) at 2-cell stage, and then generates the first two cell lineages, trophectodem (TE), the inner cell mass (ICM) at the blastocyst stage. The nutritional requirements of the preimplantation embryo are minimal and are largely derived from the oviductal fluid in which it floats. An *in vitro* culture medium with only pyruvate, lactate, and glucose as nutrients, but lacking any amino acids, fats or proteins supports normal development through the 4.5 days of preimplantation stages.

Extensive studies in the past have shown that lack of these metabolites during culture result in specific developmental phenotypes. Zygote cultured in the medium lacking pyruvate is viable but fails to develop beyond the 2-cell stage. Lack of glucose in

the culture medium blocks preimplantation development at the morula stage. The mechanism by which specific nutrients control different developmental processes is still unclear.

In this thesis, I interrogated the roles of pyruvate and glucose during mammalian embryogenesis. We found pyruvate mediated *O*-glycosylation and mitochondrial enzymes nuclear localization are critical steps in mammalian ZGA at 2-cell stage (Chapter 2), while glucose metabolism distinguishes TE from ICM fate at 8- to 16-cell stages (Chapter 3).

In Chapter 2, we made the novel and surprising finding that a number of enzymatically active mitochondrial enzymes associated with the TCA cycle are transiently localized to the nucleus where they directly make the metabolites that are essential for ZGA and the associated global genome organization. We also found that pyruvate, *O*-glycosylation, and chaperones are essential for this nuclear localization. In Chapter 3, we found that at morula stage critical pathways of glucose catabolism are the pentose pathway (PPP) and the hexosamine biosynthetic pathway (HBP) and blocking these pathways recapitulate distinct aspects of the glucose phenotype. Analysis of the roles of the PPP and the HBP further showed that these pathways have non-over lapping roles in the regulation of specific transcription factors that are essential for the establishment of the TE fate.

The dissertation of Fangtao Chi is approved.

Christofk, Heather R

Coller, Hilary Ann

Fan, Guoping

Lowry, William Edward

Banerjee, Utpal, Committee Chair

University of California, Los Angeles

2020

Acknowledgement

First and foremost, I would like to sincerely thank my mentor Dr. Utpal Banerjee, who has always been extremely supportive to my research and career. I joined Banerjee laboratory as an undergraduate research intern in the summer of 2013, and then as a full-time graduate student in 2014. It is really a great honor for me to join this nice academic family. Utpal has become my lifelong idol, with extremely strong working ethics, broad vision and optimistic characteristics. The training I received in Banerjee lab is critical to my success not only for my PhD, but also for my future scientific career.

Infinite thanks to my supervisor Raghavendra Nagaraj and colleague Mark Sharpley for generous share of their knowledge in science, and collaboration on the project. I would also thank Cory Evans, Bama Charan Mondal, Jiwon Shim and Ting Liu for supervising me for the summer project. I thank all other current and past members in Banerjee lab, Win Lam, Cheng-Wei Wang, Carolyn Spratford, Lauren Goins, Juliet Girard, Yonggang Zhou, Shubhendu Sen Roy, Wei Liao, for their generous sharing of research reagents and valuable comments on my project, my research would not be so successful without them.

I also want to thank my thesis committee members, Drs. Heather Christofk, Hilary Coller, Guoping Fan, Bill Lowry for their support and feedbacks on my dissertation project, as well as the helpful suggestions for my career development.

Last but not least, I would like to express my deepest thanks to my family. My parents gave me deepest love and support. My wife, Huachun, has always been supporting me, and taking care of me daily life.

The work for this dissertation was performed under the direction of Dr. Utpal Banerjee. The thesis is based upon work from the manuscripts:

Nagaraj, R., Sharpley, M. S., Chi, F., Braas, D., Zhou, Y., Kim, R., Clark, A. T., & Banerjee, U. (2017). Nuclear localization of mitochondrial TCA cycle enzymes as a critical step in mammalian zygotic genome activation. *Cell*, 168(1-2), 210-223.

Chi, F., Sharpley, M. S., Nagaraj, R., Roy, S. S., & Banerjee, U. (2020). Glycolysis-independent glucose metabolism distinguishes TE from ICM fate during mammalian embryogenesis. *Developmental Cell*, 53(1), 9-26.

Table of Contents

List of Figures

Chapter 2

Chapter 3

Vita

Education

- PhD candidate, Molecular Biology, UCLA, USA 2014 – present
- Bachelor of Science**,** College of Life, Zhejiang University, China 2010 – 2014

Publications

- **Chi F**, Sharpley MS, Nagaraj R, Roy SS, Banerjee U. (2020). Glycolysis-Independent Glucose Metabolism Distinguishes TE from ICM Fate during Mammalian Embryogenesis. ***Developmental Cell***, 2020, 53: 9–26.
- Nagaraj R, Sharpley MS, **Chi F**, Braas D, Zhou Y, Kim R, Clark AT, Banerjee U. (2017). Nuclear Localization of Mitochondrial TCA Cycle Enzymes as a Critical Step in Mammalian Zygotic Genome Activation[J]. ***Cell***, 2017, 168(1): 210-223. e11.
- Dai X, She P, **Chi F**, Feng Y, Liu H, Jin D, Zhao Y, Guo X, Jiang D, Guan KL, Zhong TP, Zhao B. (2013). Phosphorylation of angiomotin by Lats1/2 kinases inhibits F-actin binding, cell migration, and angiogenesis. ***Journal of Biological Chemistry*** 288(47): 34041-34051.
- Liu H, Jiang D, **Chi F**, Zhao B. (2012). The Hippo pathway regulates stem cell proliferation, self-renewal, and differentiation. ***Protein & Cell*** 3: 291-304.
- Liu J-J, Zhang X-Q, **Chi F-T**, Pan J, Sun C, Wu M. (2014). Gemmobacter megaterium sp. nov., isolated from coastal planktonic seaweeds. ***Int J Syst Evol Microbiol*** 64(Pt 1): 66-71
- **Chi F**, Beniwal AS, Liu H. (2017). The apical domain defines the trophectoderm

differentiation in early mammalian embryo by regulating YAP nuclear translocation. ***AME Medical Journal***, 2017, 2(10)

Presentations

- *Poster*: Glucose metabolism during preimplantation mouse embryo development. (Keystone Symposia Conference-Tumor Metabolism, Keystone, Colorado, February, 2019).
- *Poster*: Glucose Function during preimplantation mouse embryo development. (UCLA-BSCRC 13th & 14th & 15th Annual Stem Cell Symposium, February, 2017 & 2018 & 2019)
- *Oral Presentation*: Metabolic regulation of preimplantation mouse embryo development (Cold Spring Harbor Asia - Cancer & Metabolism, Suzhou, China, March 2018).
- *Guest Lecturer*: Metabolic regulation of preimplantation mouse embryo development (UCLA-CDB Club, Hosted by Dr. Jeff Long & Dr. Edward M. De Robertis, February 9, 2018)

Awards and Honors

- The Philip Whitcome Predoctoral Fellowship 2019 – 2020
- California Institute for Regenerative Medicine Predoctoral Fellowship 2016 – 2019
- Helmsley Scholarship, Cold Spring Harbor Laboratory 06/2015
- China Scholarship Council (CSC) Scholarship 2014 – 2016

Chapter 1: Introduction

Mammalian preimplantation development initiates with the release of oocytes from the ovary, followed by fertilization resulting in a single-cell zygote. In mouse, the zygote undergoes three rounds of cell division, generating eight gently connected blastomeres which show no obvious differences in developmental potencies. The first lineage specification of mouse embryos happens during the compacted 8- to 16-cell transition; these cells eventually differentiate into the extra-embryonic trophectoderm (TE) and the pluripotent inner cell mass (ICM) at blastocyst stage. TE cells will form extra-embryonic tissues, while ICM will give rise to the definitive structure of the fetus. Preimplantation development takes approximately 4 days in mice and 6 days in humans, and the blastocyst then implants into the uterine wall (Cockburn and Rossant, 2010, Li et al., 2010).

Several critical cellular events occur during the 1-cell and 2-cell stages of mouse preimplantation development. By the end of the 2-cell stage, maternal endowments of most RNAs and some proteins are depleted, and development beyond this point requires the productive activation of the embryonic genome (Li et al., 2010). Major zygotic/embryonic genome activation (ZGA/EGA) takes place at the 2-cell stage in mouse (Aoki et al., 1997) and EGA in humans, occurs during the 4- to 8-cell stage (Niakan and Eggan, 2013). As expected, these processes are dependent on many structural and epigenetic changes to the maternal and the paternal genomes that are reprogrammed for the purpose of the embryo (Weaver et al., 2009). Epigenetic modification dynamics that involve in ZGA have been studied extensively in the past

several years (Du et al., 2017; Ke et al., 2017; Xu et al., 2019; Zheng and Xie, 2019; Du et al., 2020). The high DNA methylation is known to associated with the silencing of gene expression. Embryonic genome inherited from the parents is heavily methylated, and whole-genome bisulfite sequencing analysis reveals there are both passive and active DNA demethylation during ZGA (Shen et al., 2014; Smith et al., 2014; Messerschmidt et al., 2014; Guo et al., 2014). In addition to DNA demethylation, histone modifications remodeling is also essential for preimplantation development (Zheng et al., 2016; Xia et al,. 2019). Such major reprogramming of the genome requires metabolites such as α-ketoglutarate (α-KG), essential for protein and DNA demethylation, Acetyl-CoA required for protein acetylation, ATP for phosphorylation of substrates, and UDP-GlcNAc for glycosylation (Hardivillé and Hart, 2014, Martinez-Pastor et al., 2013), production of each is dependent on the mitochondrial enzymes driving the tri-carboxylic acid (TCA) cycle and the utilization of pyruvate by pyruvate dehydrogenase. How metabolism regulates ZGA during early embryogenesis is largely unknown.

The preimplantation embryo derives and exchanges nutrients with the oviductal fluid, while the post-implantation embryo is vascularized and is exposed to the considerably larger repertoire of nutrients and growth factors from the maternal blood supply. Extensive studies in the late 1960s and early 1970s have revealed three critical nutrients, pyruvate, glucose and lactate that can support the whole process of preimplantation embryos development. This developmental program is recapitulated *ex vivo* when the zygote is grown in a defined medium (potassium-supplemented simplex optimized medium [KSOM]), containing pyruvate, glucose, lactate, salts and buffer

systems (Lawitts and Biggers, 1991). Such cultured embryos can be transplanted to produce normal progeny in diverse mammalian species (McLaren and Biggers, 1958).

Analysis of the early cleavage stages shows that the embryo has low metabolic activity (Leese, 2012) compared with the metabolic activity in the blastocyst or in adult tissues (Brinster, 1967a). The mitochondria appear small and rounded, lacking cristae at the 1- to 2-cell stages but are well formed in later stages (Calarco and Brown, 1969). Measurements of glucose metabolism (Brinster, 1967b, Lane and Gardner, 2000, Leese and Barton, 1984) have shown that glucose consumption in cleavage-stage preimplantation embryos is often more than 10-fold lower than in blastocysts. Metabolic processes such as the TCA cycle are coupled to the overall energetics of the cell and are therefore also attenuated (Barbehenn et al., 1978, Houghton et al., 1996). Similarly, the fate of metabolites consumed by the embryos is unusual. For example, only a fraction of pyruvate is completely oxidized in the mitochondria or reduced to lactate by lactate dehydrogenase (Lane and Gardner, 2000)

Both lactate, pyruvate and glucose are present in the oviductal fluid and are included in similar proportions in the *ex vivo* growth medium. Zygotes fail to survive in medium lacking both lactate and pyruvate. However, if only pyruvate is left out of the growth medium, the embryo is viable but fails to develop beyond the 2-cell stage (Brown and Whittingham, 1991). Under these conditions, lactate is not efficiently utilized because of the low NAD^+/NADH ratio in the 2-cell embryo. Glucose is not substantially oxidized until the morula stage, and added glucose cannot be converted to pyruvate (Barbehenn et al., 1978, Brinster, 1969). Rather, Whittingham and co-workers established a specific requirement for glucose during the compacted morula to

blastocyst transition (Brown and Whittingham, 1991). This requirement for glucose is absolute, and glucose cannot be substituted by pyruvate and lactate that fully support the earlier developmental stages (Martin and Leese, 1995). While this might suggest a bioenergetic role of glucose at this stage, early studies reported minimal oxidation of glucose in the mitochondria (Fridhandler, 1961; Fridhandler et al., 1967). Historically, metabolites were originally considered as having two functions: to provide the energy sources required by the embryos to maintain homeostasis and as biosynthetic precursors for other macromolecules. Recent studies, however, suggest an additional important role for these metabolites in cellular signaling (Sturmey et al., 2009; Dunning et al., 2010; Jungheim et al., 2011; McKeegan et al., 2011).

In my thesis, I studied the roles of pyruvate and glucose during mammalian embryogenesis. We found pyruvate mediated *O*-glycosylation and mitochondrial enzymes nuclear localization are critical steps in mammalian zygotic genome activation at 2-cell stage (Chapter 2), while glucose metabolism distinguishes TE from ICM fate at 8- to 16-cell stages (Chapter 3).

References

Aoki, F., Worrad, D.M., and Schultz, R.M. (1997). Regulation of transcriptional activity during the first and second cell cycles in the preimplantation mouse embryo. Dev Biol 181, 296-307.

Barbehenn, E.K., Wales, R.G., and Lowry, O.H. (1978). Measurement of metabolites in single preimplantation embryos; a new means to study metabolic control in early embryos. J Embryol Exp Morphol 43, 29-46.

Brinster, M.a. (1967a). Oxygen consumption of preimplantation embryos. Experimental cell research 47, 337-344.

Brinster, R.L. (1967b). Carbon dioxide production from glucose by the preimplantation mouse embryo. Experimental cell research 47, 271-277.

Brinster, R.L. (1969). Incorporation of carbon from glucose and pyruvate into the preimplantation mouse embryo. Experimental cell research 58, 153-158.

Brown, J.J., and Whittingham, D.G. (1991). The roles of pyruvate, lactate and glucose during preimplantation development of embryos from F1 hybrid mice in vitro. Development 112, 99-105.

Calarco, P.G., and Brown, E.H. (1969). An ultrastructural and cytological study of preimplantation development of the mouse. The Journal of experimental zoology 171, 253-283.

Cockburn, K., and Rossant, J. (2010). Making the blastocyst: lessons from the mouse. J Clin Invest 120, 995-1003.

Du, Z., Zheng, H., Huang, B., Ma, R., Wu, J., Zhang, X., ... & Ma, J. (2017). Allelic reprogramming of 3D chromatin architecture during early mammalian

development. Nature, 547(7662), 232-235.

Du, Z., Zheng, H., Kawamura, Y. K., Zhang, K., Gassler, J., Powell, S., ... & Ozonov, E. A. (2020). Polycomb group proteins regulate chromatin architecture in mouse oocytes and early embryos. Molecular Cell, 77(4), 825-839.

Dunning, K. R., Cashman, K., Russell, D. L., Thompson, J. G., Norman, R. J., & Robker, R. L. (2010). Beta-oxidation is essential for mouse oocyte developmental competence and early embryo development. Biology of reproduction, 83(6), 909-918.

Fridhandler, L. (1961). Pathways of glucose metabolism in fertilized rabbit ova at various pre-implantation stages. Experimental cell research 22, 303-316.

Fridhandler, L., Wastila, W.B., and Palmer, W.M. (1967). The Role of Glucose in Metabolism of the Developing Mammalian Preimplantation Conceptus. Fertility and Sterility 18, 819-830.

Guo, F., Li, X., Liang, D., Li, T., Zhu, P., Guo, H., ... & Walsh, C. P. (2014). Active and passive demethylation of male and female pronuclear DNA in the mammalian zygote. Cell stem cell, 15(4), 447-459.

Hardiville, S., and Hart, G.W. (2014). Nutrient regulation of signaling, transcription, and cell physiology by O-GlcNAcylation. Cell Metab 20, 208-213.

Jungheim, E. S., Louden, E. D., Chi, M. M. Y., Frolova, A. I., Riley, J. K., & Moley, K. H. (2011). Preimplantation exposure of mouse embryos to palmitic acid results in fetal growth restriction followed by catch-up growth in the offspring. Biology of reproduction, 85(4), 678-683.

Ke, Y., Xu, Y., Chen, X., Feng, S., Liu, Z., Sun, Y., ... & Chen, H. (2017). 3D chromatin

structures of mature gametes and structural reprogramming during mammalian embryogenesis. Cell, 170(2), 367-381.

Lane, M., and Gardner, D.K. (2000). Lactate regulates pyruvate uptake and metabolism in the preimplantation mouse embryo. Biology of reproduction 62, 16-22.

Lawitts, J.A., and Biggers, J.D. (1991). Optimization of mouse embryo culture media using simplex methods. Journal of reproduction and fertility 91, 543-556.

Leese, H.J., and Barton, A.M. (1984). Pyruvate and glucose uptake by mouse ova and preimplantation embryos. Journal of reproduction and fertility 72, 9-13.

Leese, H.J. (2012). Metabolism of the preimplantation embryo: 40 years on. Reproduction 143, 417-427.

Li, L., Zheng, P., and Dean, J. (2010). Maternal control of early mouse development. Development 137, 859-870.

Martinez-Pastor, B., Cosentino, C., and Mostoslavsky, R. (2013). A tale of metabolites: the cross-talk between chromatin and energy metabolism. Cancer Discov 3, 497-501.

Martin, K.L., and Leese, H.J. (1995). Role of glucose in mouse preimplantation embryo development. Mol Reprod Dev 40, 436-443.

McKeegan, P. J., & Sturmey, R. G. (2011). The role of fatty acids in oocyte and early embryo development. Reproduction, Fertility and Development, 24(1), 59-67.

McLaren, and Biggers, J.D. (1958). Successful development and birth of mice cultivated in vitro as early as early embryos. Nature 182, 877-878.

Messerschmidt, D. M., Knowles, B. B., & Solter, D. (2014). DNA methylation dynamics during epigenetic reprogramming in the germline and preimplantation embryos.

Genes & development, 28(8), 812-828.

Niakan, K.K., and Eggan, K. (2013). Analysis of human embryos from zygote to blastocyst reveals distinct gene expression patterns relative to the mouse. Dev Biol 375, 54-64.

Shen, L., Inoue, A., He, J., Liu, Y., Lu, F., & Zhang, Y. (2014). Tet3 and DNA replication mediate demethylation of both the maternal and paternal genomes in mouse zygotes. Cell stem cell, 15(4), 459-471.

Smith, Z. D., Chan, M. M., Humm, K. C., Karnik, R., Mekhoubad, S., Regev, A., ... & Meissner, A. (2014). DNA methylation dynamics of the human preimplantation embryo. Nature, 511(7511), 611-615.

Sturmey, R. G., Hawkhead, J. A., Barker, E. A., & Leese, H. J. (2009). DNA damage and metabolic activity in the preimplantation embryo. Human Reproduction, 24(1), 81-91.

Weaver, J.R., Susiarjo, M., and Bartolomei, M.S. (2009). Imprinting and epigenetic changes in the early embryo. Mamm Genome 20, 532-543.

Xia, W., Xu, J., Yu, G., Yao, G., Xu, K., Ma, X., ... & Chen, X. (2019). Resetting histone modifications during human parental-to-zygotic transition. Science, 365(6451), 353-360.

Xu, Q., Xiang, Y., Wang, Q., Wang, L., Brind'Amour, J., Bogutz, A. B., ... & Du, Z. (2019). SETD2 regulates the maternal epigenome, genomic imprinting and embryonic development. Nature genetics, 51(5), 844-856.

Zheng, H., & Xie, W. (2019). The role of 3D genome organization in development and cell differentiation. Nature Reviews Molecular Cell Biology, 1.

Zheng, H., Huang, B., Zhang, B., Xiang, Y., Du, Z., Xu, Q., ... & Xu, F. (2016). Resetting epigenetic memory by reprogramming of histone modifications in mammals. Molecular cell, 63(6), 1066-1079.

Chapter 2: Pyruvate mediated *O*-glycosylation and mitochondrial enzymes nuclear localization are critical steps in mammalian zygotic genome activation

2.1 Abstract

Transcriptional control requires epigenetic changes directed by mitochondrial tricarboxylic acid (TCA) cycle metabolites. In the mouse embryo, global epigenetic changes occur during zygotic genome activation (ZGA) at the 2-cell stage. Pyruvate is essential for development beyond this stage, which is at odds with the low activity of mitochondria in this period. We now show that a number of enzymatically active mitochondrial enzymes associated with the TCA cycle are essential for epigenetic remodeling and are transiently and partially localized to the nucleus. Pyruvate is essential for this nuclear localization, and a failure of TCA cycle enzymes to enter the nucleus correlates with loss of specific histone modifications and a block in ZGA. At later stages, however, these enzymes are exclusively mitochondrial. In humans, the enzyme pyruvate dehydrogenase is transiently nuclear at the 4/8-cell stage coincident with timing of human embryonic genome activation, suggesting a conserved metabolic control mechanism underlying early preimplantation development.

2.2 Introduction

Mammalian preimplantation development initiates with the release of oocytes from the ovary, followed by fertilization resulting in a single-cell zygote. In mouse, the zygote undergoes three to four rounds of cell division, compacts at the 8-cell stage and then gives rise to a morula. The first differentiation step results in a blastocyst containing an inner cell mass (ICM) of cells, progenitors to the embryo proper and a surrounding lining of trophectoderm (TE) cells that will form extra-embryonic tissues. Preimplantation development takes approximately 4 days in mice and 6 days in humans, and the blastocyst then implants into the uterine wall (Cockburn and Rossant, 2010, Li et al., 2010). The preimplantation embryo derives and exchanges nutrients with the oviductal fluid, while the post-implantation embryo is vascularized and is exposed to the considerably larger repertoire of nutrients and growth factors from the maternal blood supply. This developmental program is recapitulated *ex vivo* when the zygote is grown in a defined medium (potassium-supplemented simplex optimized medium [KSOM]), most of whose components are present in the oviductal fluid (Lawitts and Biggers, 1991). Such cultured embryos can be transplanted to produce normal progeny in diverse mammalian species (McLaren and Biggers, 1958).

Several critical cellular events occur during the 1-cell and 2-cell stages of mouse preimplantation development. By the end of the 2-cell stage, maternal endowments of most RNAs and some proteins are depleted, and development beyond this point requires the productive activation of the embryonic genome (Li et al., 2010). Major zygotic/embryonic genome activation (ZGA/EGA) takes place at the 2-cell stage in

mouse (Aoki et al., 1997) and EGA in humans, occurs during the 4- to 8-cell stage (Niakan and Eggan, 2013). As expected, these processes are dependent on many structural and epigenetic changes to the maternal and the paternal genomes that are reprogrammed for the purpose of the embryo (Weaver et al., 2009). Such major reprogramming of the genome requires metabolites such as α-ketoglutarate (α-KG), essential for protein and DNA demethylation, acetyl-CoA required for protein acetylation, ATP for phosphorylation of substrates, and UDP-GlcNAc for glycosylation (Hardivillé and Hart, 2014, Martinez-Pastor et al., 2013), production of each is dependent on the mitochondrial enzymes driving the tri-carboxylic acid (TCA) cycle and the utilization of pyruvate by pyruvate dehydrogenase. However, analysis of the early cleavage stages shows that the embryo has low metabolic activity (Leese, 2012) compared with the metabolic activity in the blastocyst or in adult tissues (Brinster, 1967a). The mitochondria appear small and rounded, lacking cristae at the 1- to 2-cell stages but are well formed in later stages (Calarco and Brown, 1969). Measurements of glucose metabolism (Brinster, 1967b, Lane and Gardner, 2000, Leese and Barton, 1984) have shown that glucose consumption in cleavage-stage preimplantation embryos is often more than 10-fold lower than in blastocysts. Metabolic processes such as the TCA cycle are coupled to the overall energetics of the cell and are therefore also attenuated (Barbehenn et al., 1978, Houghton et al., 1996). Similarly, the fate of metabolites consumed by the embryos is unusual. For example, only a fraction of pyruvate is completely oxidized in the mitochondria or reduced to lactate by lactate dehydrogenase (Lane and Gardner, 2000)

Both lactate and pyruvate are present in the oviductal fluid and are included in similar proportions in the *ex vivo* growth medium. Zygotes fail to survive in medium lacking both lactate and pyruvate. However, if only pyruvate is left out of the growth medium, the embryo is viable but fails to develop beyond the 2-cell stage (Brown and Whittingham, 1991). Under these conditions, lactate is not efficiently utilized because of the low NAD^+/NADH ratio in the 2-cell embryo. Glucose is not substantially oxidized until the morula stage, and added glucose cannot be converted to pyruvate (Barbehenn et al., 1978, Brinster, 1969). However, glucose is also included in the growth medium to support the entire preimplantation developmental program from 1-cell to blastocyst, in serum-free conditions (Biggers et al., 1967, Leese, 2012, Brown and Whittingham, 1991). Embryos develop normally without requiring the import of proteins and amino acids from the medium, and, astonishingly, the 1-cell and 2-cell embryos complete their entire homeostatic processes even though amino acid accumulation, mitochondrial oxygen consumption, and glucose oxidation are all at very low levels (Brinster, 1969, Houghton et al., 1996). Low metabolic activity at early stages is thought to keep ROS levels low, thus avoiding DNA damage at a totipotent stage (Baumann et al., 2007).

In this chapter, we demonstrate that a subset of mitochondrial enzymes of the TCA cycle briefly localize to and are active within the nucleus of the early stage embryo and are essential for the production of key metabolites that play a role in epigenetic remodeling during zygotic genome activation and developmental progression beyond the 2-cell stage.

2.3 Results

2.3.1 Pyruvate requirement in early stages of embryogenesis

The first step in this study was to optimize the conditions of growth in a medium that is devoid of all amino acids or proteins and yet capable of sustaining preimplantation development. Since the standard KSOM medium contains both, we developed a modified medium (mKSOM) (see Materials and Methods for details) that only contains the metabolites lactate, glucose and pyruvate, plus salts/buffer, and poly vinyl alcohol (PVA, to replace BSA added to standard KSOM) ((Biggers et al., 1997). Zygotes are obtained from PMSG/hCG induced super-ovulating young female mice (Watson et al., 1977). Naturally fertilized single cell zygotes are isolated 18 hours post hCG injection and cultured either in mKSOM medium that contains pyruvate (called +P medium in this chapter for simplicity) or in mKSOM lacking pyruvate (or –P medium). The results are found to be identical to those from previous studies that used different media, supplemented with BSA and glutamine (Biggers et al., 1967; Brown and Whittingham, 1991). Embryos grown in +P medium transition at the proper rate to the blastocyst stage (Figure 2-1A-D), while those grown in –P medium are arrested at the 2-cell stage (Figure 2-1E-H). A subset of embryos is blocked at the 1 cell stage in –P, as was also reported in earlier studies (Biggers et al., 1967).

To identify more precisely the period during which pyruvate is required for the progression of embryonic development, the medium was switched from +P to –P (and vice versa) at various time points (Figure S2-1). The critical period is a 30-hour window between 24hrs post-hCG and 54hrs post-hCG (Figure 2-1I-K'). At time periods outside this window, pyruvate can be replaced by lactate for normal development.

The precise cell cycle stage in which the 2-cell embryos are blocked in the absence of pyruvate was mapped using cell cycle and cytosketetal markers. Bromo-deoxy Uridine (BrdU) incorporation and PCNA expression, marking the S-phase of the 2-cell stage, remain unchanged between embryos grown in +P or –P media (Figure 2-1L-O). The marker phospho-Histone3 (PH3), can be first detected at very low levels at 45hrs post-hCG with a significant rise in its expression seen at 54hrs post-hCG. The initial PH3 incorporation (45hrs post-hCG) appears to be pyruvate independent (Figure 2-1P, Q). However, in late G2 (54hrs post-hCG), PH3 staining in embryos grown on +P medium shows a dramatic up-regulation, while the –P embryos remain weak (Figure 2-1R, S). As a result, the pyruvate deprived 2-cell embryo fails to enter M phase and does not progress to the spindle assembly stage (Figure 2-1T, U). Interestingly, this strict requirement for exogenous pyruvate for G2/M transition is only seen at these stages, and not in controlling cell cycle beyond the 2-cell stage.

2.3.2 Pyruvate requirement in zygotic genome activation

Transcriptional activation of the zygotic genome marks the transition from maternal to zygotic control of development (Li et al., 2013). An early, and largely unproductive minor activation takes place during the 1-cell to 2-cell transition (Aoki et al., 1997). But the major zygotic genome activation (ZGA) in mouse embryos initiates during the G2 phase of the 2-cell embryo (Aoki et al., 1997). As this is precisely the stage when the embryos arrest in the absence of pyruvate, we used several different strategies to explore whether these two events might be linked. First, we used BrUTP to assay for incorporation into newly synthesized transcripts (Aoki et al., 1997; Zheng et

al., 2010). This assay revealed that +P medium grown embryos display a robust incorporation of BrUTP in the late 2-cell stage. In contrast, those grown in –P medium fail to show detectable BrUTP staining (Figure 2-2A-C). Second, we took advantage of the fact that the phosphorylation status of Ser5 and Ser2 on the C-terminal domain of RNA Polymerase II are excellent measures of transcription-initiation as RNA Pol II requires these serine phosphorylation events to become part of the initiation and the elongation complex, respectively (Egloff and Murphy, 2008). Embryos grown in +P and –P media were stained with RNA Pol II Ser-5P and RNA Pol II Ser-2P specific antibodies. A significant reduction of these staining patterns in a –P medium demonstrated that RNA Pol II is not engaged in the steps that are essential for genome activation (Figure 2-2D-I). This is not a result of a change in the abundance of total RNA Pol II protein in pyruvate-deprived embryos (Figure S2-2A-D). Finally, we compared the protein expression of SIRT1, the product of an early zygotic transcript, in +P and –P media. SIRT1 is robustly detected at the 2-cell stage when pyruvate is included in the medium, but is eliminated when grown in the absence of pyruvate (Figure 2-2J-L). Taken together, we find that exogenously supplied pyruvate is essential for activation of the zygotic genome.

2.3.3 Subcellular localization of enzymes involved in pyruvate metabolism

Results from many different laboratories, using independent functional assays such as oxygen consumption, ATP generation, mitochondrial morphology and measurement of membrane potential (Acton et al., 2004; Brinster, 1973; Houghton et al., 1996; Komatsu et al., 2014; Thouas et al., 2004; Trimarchi et al., 2000), have

established that early stage mitochondria show low energetic activity compared to later stages such as the blastocyst. Other studies have shown that the mitochondria at this stage can be distinguished into two populations based on their membrane potential (Acton et al., 2004; Komatsu et al., 2014). As culture conditions and genetic backgrounds can affect mitochondrial function (Kawahara et al., 2015; Williams et al., 2016), it was important for us to make sure that these previously well-established conclusions are also seen under our culture conditions. Indeed, in agreement with previous studies (Komatsu et al., 2014), we found that the early cleavage stage embryo has a large number of mitochondria (Figure 2-3A) that fall into two distinct groups when stained with the JC1 dye (Figure 2-3B). Mitochondria along the edge stain red (indicating high membrane potential) while the vast majority stain green (suggesting low membrane potential). Similar results were obtained upon staining with Rhodamine-2AM, a dye sensitive to Ca2+ concentration, as an indirect but independent marker of mitochondrial membrane potential (Figure 2-3D). Once again, a relatively small number of the mitochondria along the periphery show high Ca2+ compared with the majority that is dispersed within the tissue. It is important to point out that JC1 and Rhodamine-2AM can penetrate the tissue since extensive mitochondrial staining is readily detected throughout the depth of the embryo at many developmental stages (e.g., Figure S2-3B, C). As further controls, we verified that addition of FCCP, a mitochondrial membrane un-coupler causes loss of Rhodamine-2AM staining and conversion of all mitochondrial JC1 staining to green, indicating loss of membrane potential (Figure 2-3C, E).

The enzyme PDH that converts pyruvate to Acetyl-CoA in the mitochondrion is a multi-subunit complex with an active site within the PDH-E1α subunit. The activity of the

PDH complex is regulated by the phosphorylation status of PDH-E1α (Kolobova et al., 2001). Un-phosphorylated PDH is active, and converts pyruvate to Acetyl-CoA. A kinase called PDH-kinase (PDK) phosphorylates PDH-E1α rendering it inactive (Behal et al., 1993; Holness and Sugden, 2003). A corresponding phosphatase, called PDH-phosphatase (PDP), allows the inactive PDH to revert to its active non-phosphorylated form (Holness and Sugden, 2003).

In the unfertilized oocyte, PDK protein is at marginally detectable levels (Figure S2-3D). Following fertilization at pronuclear stages PN2-3 of the one-cell embryo, PDK protein expression is seen at a low level. By PN4-5 stages, as the pro-nuclei are about to fuse, this expression is further enhanced (Figure S2-3E). PDK protein is robustly seen in the mitochondria of the 2-cell embryo (Figure 2-3F; S2-3F). Given that the PDH complex activity is the primary entry point into the TCA cycle, its inactivation by rising PDK is expected to decrease TCA cycle activity.

The activity pattern of PDH can also be directly judged by staining with a series of antibodies. The first, generated against the phosphorylated epitope of PDH-E1α, specifically recognizes the inactivating phosphorylation site (called α-PDH^{inactive} in this chapter). This antibody has been extensively used to detect inactive PDH in both *in vivo* and *in vitro* assays (Donohoe and Bultman, 2012). Staining with α-PDH^{inactive} decorates a majority of the mitochondria in the cell (Figure 2-3G; S2-3G-I). This supports the notion that the mitochondrial PDH is largely inactive. Consistent with this notion, embryos treated with dichloroacetate (DCA) that blocks PDK function results in loss of α-PDH^{inactive} staining and increases the mitochondrial Ca2+ level (Figure S2-3I-K).

A second antibody, generated against the N-terminal 131 amino acids (31-161) of PDH-E1α protein recognizes both the active and the inactive forms of the protein (called α-PDH^{total} here; Edmunds et al 2014, Sutendra et al 2014). Immuno-staining with α-PDH^{total} reveals that total PDH is not only localized to the mitochondrion, but also prominently in the nuclear compartment (Figure 2-3H, I). Nuclear PDH is not recognized by α-PDH^{inactive}, and is therefore un-phosphorylated and likely active. Screening amongst the large collection of commercially available PDH antibodies, we found one (Davoudi et al., 2014; Tomilov et al., 2014) that specifically recognizes this nuclear component (Figure 2-3J-L). We refer to this antibody as α-PDH^{nuc}. This same antibody exclusively stains mitochondria at the blastocyst stage (Figure S2-3L) as is also true of the α-PDH^{total} staining (Figure 2-3M) suggesting that α-PDH^{nuc} likely recognizes the active enzyme. The E2 and E3 subunits of PDH also show dual localization to the mitochondrion and the nucleus (Figure S2-3M, N). The nuclear localization of PDH initiates during the S phase of the mitotic cycle based on timing as well as co-localization with PCNA (Figure S2-3O-V). Thus, in the 1-cell stage, PDH is first detected at PN3 with increased accumulation through PN4. Likewise, during the transition to the 2-cell embryos, nuclear PDH level is extremely low during the short G1 phase but is again robustly seen in the nucleus during the S phase (independently marked by PCNA staining, Figure S2-3R-V) and in the prolonged G2 phase that follows (Figure S2-3T). These results are consistent with an earlier study that reported nuclear PDH starts rising in the S phase in lung fibroblasts and carcinomas (Sutendra et al., 2014; see Chapter 4). Strikingly, *in vivo* isolated 4-cell embryos occasionally show two of the cells with mitochondrial localization and the other two with largely a nuclear pattern, while other

embryos from the same collection, show identical, nuclear localization pattern in all four cells (Figure S2-3W, X). As each pair of cells of a 4-cell embryo can be slightly asynchronous in their cell cycle with the other, these results suggest that nuclear localization follows the final cyclic pattern at the 4-cell stage. Also, these images indicate an exchange of the enzyme between the mitochondrial and nuclear compartments.

Pyruvate has multiple roles within the cell, one unexpected role, relevant to the current context, is revealed upon staining with PDH antibodies in a pyruvate-deprived embryo. In contrast to embryos grown in the normal +P medium, those that are grown without pyruvate (–P medium), show a complete lack of nuclear PDH (Figure 2-3N-P). Further support for the involvement of pyruvate in nuclear localization is suggested by rescue experiments. Embryos cultured until the late 2-cell stage without pyruvate, when returned to a +P medium, and allowed to develop for an additional 12 hours, show partial rescue of nuclear PDH (Figure 2-3Q). However, the 2-cell mitotic block is not rescued by this delayed pyruvate addition (not shown).

Conversion of phosphorylated PDH-E1α to an active un-phosphorylated form requires pyruvate dehydrogenase phosphatase (PDP). Antibody staining reveals that PDP is localized to the nucleus at the 2-cell stage (Figure 2-3R). The exclusive localization of PDK to the mitochondrion (Figure 2-3F) and PDP to the nucleus (Figure 2-3R) indicates a concerted regulatory mechanism that keeps the mitochondrial PDH relatively inactive and the nuclear PDH complex active at this specific stage of development. Later in the chapter, we describe a functional assay directly demonstrating that the nuclear component of PDH is indeed enzymatically active.

2.3.4 Localization of pyruvate carboxylase (PCB) and enzymes of the TCA cycle

The metabolite, citrate, is very abundant in the early mouse preimplantation embryo compared to that usually seen in somatic cells (Barbehenn et al., 1978). Citrate is generated by the condensation of the metabolites acetyl-CoA and oxaloacetate (OAA). In principle, pyruvate can be converted to acetyl-CoA by PDH (reviewed in Holness and Sugden, 2003), additionally, pyruvate can be directly converted to OAA in the presence of pyruvate carboxylase (PCB) (Graves and Biggers, 1970; Jitrapakdee and Wallace, 1999). Indeed early embryonic PCB activity has been reported in the literature (Quinn and Wales, 1974).

Upon immuno-staining for PCB, we found a fraction of it to be present in the nucleus (Figure 2-4C). Unlike for PDH, antibodies that discriminate between active and inactive versions of PCB, or the other enzymes described in this section, are not available. Although the nuclear staining is clearly discernable, the stronger mitochondrial component makes it harder to tell apart from that in the nucleus. We followed 4 steps to establish nuclear localization. First, we isolated and immediately fixed single nuclei from the embryos (see materials and methods), stained them with the antibody and with DAPI and imaged them directly. This would prevent any artifacts due to spillover staining or saturation issues with microscopy due to the dominant mitochondrial staining. Second, to ensure that the nuclear staining is not an artifact of the ex vivo culture system, we isolated older, 2-cell embryos instead of zygotes, directly from the mother by adjusting the collection time, and fixed and stained them with no time spent in culture. Third, we cultured embryos in +P and –P media followed by

immunohistochemistry to determine if the enzyme, as for PDH, requires pyruvate for nuclear localization. Finally, we repeated our staining protocol on multiple embryos to quantitate the strength of staining with and without the presence of pyruvate.

Following this protocol, we determined that isolated nuclei show the presence of PCB (Figure 2-4A, A'), 2-cell embryos from in vivo collection show nuclear localization (Figure 2-4B) similar to that seen following culture in +P medium (Figure 2-4C) and that the nuclear localization of PCB is entirely pyruvate dependent (Figure 2-4C'). Quantitation of multiple isolates clearly established that the pyruvate dependence is statistically significant (Figure 2-4C"). In principle, nuclear PCB and PDH could metabolize pyruvate to generate OAA and acetyl-CoA respectively, in the nucleus. To make citrate however, involves the enzyme citrate synthase (CS) that is a component of the TCA-cycle. We therefore looked for the localization patterns of the mitochondrial TCA cycle proteins at the 2-cell stage of embryogenesis.

Following the four steps elaborated above for PCB, we found that a fraction of the CS enzyme also localizes to the nucleus of the 2-cell embryo (Figure 2-4D-F) and that this nuclear localization is dependent on the presence of pyruvate (Figure 2-4F-F"). While nuclear localization of PDH has been reported in other systems (Chueh et al., 2011; Sutendra et al., 2014), nuclear localization of a TCA cycle enzyme such as citrate synthase is an unexpected finding and led us to investigate the 2-cell embryo localization status of all TCA cycle enzyme isoforms that normally function in the mitochondrion. Beyond CS, the next TCA cycle step uses the mitochondrial enzyme aconitase 2 (ACO2) to metabolize citrate to iso-citrate (Tong and Rouault, 2007). Like the enzymes for the earlier steps, ACO2 expression is distinctly nuclear in a pyruvate

dependent fashion at the 2-cell stage (Figure 2-4G-I"). Next is the enzyme mitochondrial isocitrate dehydrogenase (IDH3), which uses isocitrate as a substrate to generate α-ketoglutarate (α-KG), an important metabolite required for DNA and histone demethylation enzyme function (Xiao et al., 2012). IDH3 is also nuclear at this stage of development only in the presence of pyruvate (Figure 2-4J-L"). None of the above enzymes is nuclear at later stages such as in the blastocyst where they are exclusively localized to the mitochondrion (Figure 2-4M-P). The next set of TCA cycle enzymes is either detected at very low levels in the nucleus (KGDH, Figure 2-4Q, Q'), or not detected (SCS, SDHA, MDH2) in the nucleus at all (Figure 2-4R-T') even in the presence of pyruvate. Finally, embryos isolated after in vivo development to the 2-cell stage and then immediately fixed and stained with SDHA antibody gave no detectable signal in the nucleus, as was seen for the cultured embryos (Figure 2-4U).

As important controls, most mitochondrial enzymes are excluded from the nucleus in cultured cell lines that we tested, including cultured HeLa cells (Figure S2-4A-H). Several bona fide mitochondrial membrane proteins such as ATP synthase and OPA-1 remain mitochondrial throughout development, including at the 2-cell stage, and are not detected in the nucleus (Figure S2-4I,J) and finally, typical nuclear proteins such as SP1 and Myc (Figure S2-4K,L) or RNA Polymerase II (Figure S2-2C,D) remain nuclear in the absence of pyruvate.

The process of nuclear transport is suppressed when mitochondrial entry of pyruvate is blocked (Figure S2-4M, N). This suggests that mitochondrial pyruvate facilitates the transport process. This function is presumably in addition to its role in maintaining energy homeostasis. This notion is further supported by rescue

experiments described later in this chapter. Additionally, we show that a functional protein translation machinery is equally essential for maintaining both the mitochondrial and the nuclear levels of PDH (Figure S2-4O, P). The simplest explanation is that export of the TCA related proteins from the mitochondrion is a pyruvate dependent and a stage-specific process that requires pyruvate to be exogenously provided.

In summary, in the 1-2 cell stages of mouse preimplantation embryo, half of the TCA cycle proteins, CS, ACO2, IDH3, and perhaps low amounts of KGDH as well as two other proteins involved in pyruvate metabolism, PDH and PCB, are readily detected in the nucleus, whereas, the enzymes that function later in the TCA cycle remain strictly mitochondrial. Given the low activity of the TCA cycle, in the mitochondrion, in principle, this nuclear localization affords the ability to generate metabolites important for transcription, acetyl-CoA, citrate, isocitrate and α-KG directly within the nucleus. This hypothesis was next tested by multiple assays for enzyme function and metabolite levels.

2.3.5 Activity assays in isolated nuclei for key mitochondrial enzymes

We have shown that nuclear PDH complexes are largely un-phosphorylated and therefore predicted to be catalytically active. The first step in this enzymatic activity involves the decarboxylation of pyruvate and this process generates CO2 derived from the carbon at position 1 of pyruvate. To directly assay this activity, we adapted a technique previously described for larger sample sizes (Sies et al., 1983; Williamson et al., 1979) to work with isolated nuclei from two-cell embryos. In this setup, nuclei adhering to a glass coverslip are suspended over a reservoir of bicarbonate solution in

a small air-tight container. Using approximately 200 isolated nuclei for each preparation, and incubating them for 5 hours in 1-^{14}C-pyruvate added to the coverslip, we clearly established that the isolated nuclei formed 14CO2 from the 1-^{14}C-pyruvate in the medium (Figure 2-5A). This direct assay for enzymatic activity, combined with the observation that nuclear PDH remains un-phosphorylated allows us to conclude that the PDH we detect in the nucleus is catalytically active. Consistent with this direct measurement, lipoic acid modification, essential for PDH complex function is detected in the nucleus in the presence of pyruvate (Figure S2-5A, B).

We proceeded to test whether IDH3, the last enzyme along the TCA cycle detected within the nucleus, is also catalytically active (Figure 2-5B-G). Active IDH3 converts isocitrate to α-KG and in the process generates NADH from NAD^+. The production of NADH is monitored using a nitro-tetrazolium dye (cyano-tetrazolium), which fluoresces red and precipitates upon reduction (Dikov et al., 2004). Once again, adapting this technique to work for individual nuclei, it becomes readily apparent that embryos cultured in the +P medium have active IDH3 in their nuclei (Figure 2-5B, C) in contrast to nuclei of embryos from –P medium (Figure 2-5D, E). Importantly, the IDH3 signal is completely dependent on the presence of isocitrate in the assay solution demonstrating the specificity of the assay for this specific dehydrogenase enzyme reaction (Figure 2-5F, G). The signal in this assay requires the presence of NAD^+. $NADP^+$ does not support this enzyme reaction further establishing that the assay is specific in reporting IDH3 activity since the IDH1 and IDH2 enzymes convert $NADP^+$ to NADPH. Together, these experiments demonstrate that key mitochondrial enzymes that feed pyruvate into the half cycle of enzymes and the final component of that pathway

are not only localized to, but are also catalytically active in, the nuclei of two-cell embryos. Combined with the measurements of metabolic dynamics described below, these data provide strong support to a model in which the nuclear localization of a subset of TCA cycle and associated proteins is functionally relevant.

2.3.6 Metabolite measurements

The spatial separation of the TCA cycle components suggests that the metabolites formed by the TCA cycle enzymes that are found in the nucleus have different dynamic properties than the ones that are not seen in the nucleus. In classical studies, using cycling assays, Lowry and coworkers used a short period of starvation of pyruvate, lactate and glucose followed by re-feeding with only one of the metabolites to determine the relative activities of enzymes in the glycolytic pathway (Barbehenn et al., 1974, 1978). We adapted this assay for measuring TCA cycle metabolites. Instead of the cycling assays, we used highly sensitive capillary ion chromatography for separation, followed by high-resolution mass spectrometry to measure metabolite levels. We were successful in measuring small quantities of most TCA cycle metabolites except oxaloacetate and isocitrate, both of very low abundance.

Approximately 300 embryos were subject to the starvation pulse of 30 minutes and then re-fed with pyruvate for 20 minutes in each sample. Metabolite levels were measured and compared from embryos for three sets of growth conditions: 1. Metabolites measured following incubation in +P medium, no starvation. 2. Metabolites measured after incubation in starvation medium and 3. Metabolites measured following recovery from starvation. Of the TCA cycle metabolites, citrate, aconitate and α-KG

levels are significantly reduced upon starvation and significantly restored during the short, 20 minute, re-feeding session (Figure 2-5H, I). Remarkably, succinate, fumarate and malate, which are generated by enzymes that are not localized to the nucleus, are not diminished following starvation nor do their levels rise following re-feeding with pyruvate (Figure 2-5H, I). The observation that malate levels in fact fall upon re-feeding is in agreement with some of Lowry's observations (Barbehenn et al., 1974, 1978).

In a second analysis, we isolated zygotes, cultured them until the 2-cell stage under +P and –P conditions, and then directly measured TCA cycle metabolites. Figure 2-5J shows that metabolites formed by enzymes present in the nucleus decrease significantly more in –P medium than metabolites formed by enzymes that are exclusively mitochondrial. Collectively, these data demonstrate that the TCA metabolites have different dynamic properties. Those generated by enzymes with a nuclear component are more dependent on the presence of exogenously provided pyruvate compared with metabolites generated by the later enzymes of the TCA cycle that are not detected in the nucleus.

2.3.7 Rescue experiments

We designed rescue experiments to test the above ideas and to further characterize which aspects of pyruvate dependent metabolism are critical for progression beyond the 2-cell stage. We focused on α-KG, the terminal product of the TCA cycle enzymes localized to the nucleus. Embryos cultured with a cell permeable α-KG analog supplementing the –P medium develop to blastocysts in a manner identical

to embryos cultured in +P media (Figure 2-5K,L), and α-KG also restores the translocation of the mitochondrial enzymes to the nucleus (Figure 2-5M-O).

Metabolite measurements show that the GSH/GSSG ratio, indicative of oxidative stress is unchanged in the absence of pyruvate (Figure S2-5G) whereas the ATP/ADP ratio (Figure S2-5F), the amount of ATP (Figure 2-5Q) and the NAD^+/NADH ratio (Figure 2-5P) are all affected if the growth medium lacks pyruvate. Under normal growth conditions, these ratios are critical for the embryonic development, and the redox ratio in particular, is too low in the absence of pyruvate to support progress beyond 2-cells. Interestingly, and somewhat unexpectedly, we found that the embryos rescued with α-KG added to the –P medium continue to exhibit reduced NAD^+/NADH ratio (Figure 2-5P) and reduced ATP levels (Figure 2-5Q) similar to embryos cultured in –P media rather than those grown in +P.

It is pertinent that the rescue by α-KG requires the presence of lactate. This observation, as well as previous data (Brinster, 1967), suggests that lactate is utilized, but the rate of lactate to pyruvate conversion is not sufficiently high to maintain the levels of Class I metabolite levels in the absence of pyruvate.

Currently, it is unclear at which point the perturbed NAD^+/NADH ratio limits lactate utilization. It is likely that the conversion of lactate to pyruvate by LDH is affected, but it is also possible that subsequent steps of the pathway are also limited at abnormally low NAD^+/NADH ratios. The decrease in the levels of Class I metabolites, such as α-KG, will compromise the important biosynthetic and signaling processes, which drive developmental progression, and are fueled by carbon from lactate and pyruvate. In the absence of pyruvate, the provision of exogenous α-KG is able to supply

a portion of the carbon requirement of these processes, rendering the redox state of the embryos less critical, allowing them to progress beyond the two-cell stage even under energetic (Figure 2-5Q) or redox (Figure 2-5P) stress.

Within the cell, catabolism of amino acids can generate α-KG. We therefore asked if non-essential amino acids rescue –P embryo phenotypes. Interestingly, the only two that are capable of such a rescue are proline and arginine, both known to generate α-KG ((Cox, 2013) Figure 2-5R; Figure S2-5 C, D). None of the other non-essential amino acids substantially rescue the phenotype, including the pyruvate-generating metabolites such as alanine and serine (Figure 2-5R).

Similar to α-KG, proline does not rescue the NAD^+/NADH ratio while rescuing the 2-cell block, once again demonstrating that early embryos can develop into blastocysts even if the NAD^+/NADH ratio is perturbed (Figure 2-5S). Even more remarkably, ATP levels are not rescued in the presence of proline or arginine even as the developmental and molecular phenotypes are fully normal (Figure S2-5E). Currently, it is unclear whether the abnormal NAD^+/NADH ratio that is generated in –P media also limits proline catabolism, but the extent of the rescue suggests that such a deficit is not sufficient to compromise development. It is surprising that proline is able to rescue development, but glutamine is not. Our preliminary (not shown) metabolite measurements suggest that exogenously provided 2-KG or proline raises glutamate level in the embryo, but providing glutamine is much less effective in causing this change. The reason for this observation remains unclear, but in this respect, the metabolism of the early embryo provides a contrast to normal, and more significantly, cancer cells, where glutamine is a more effective anaplerotic substrate.

Thus, in the absence of pyruvate, two-cell embryos can normally progress to the blastocyst even under energetic (Figure 2-5Q; Figure S2-5C-E) or redox stress (Figure 2-5P, S).

2.3.8 Role of *O*-linked glycosylation in nuclear localization

The mechanism by which mitochondrial complexes are moved from the mitochondrion to the nucleus is not yet fully clear (see Chapter 4). However, our data point to an important role for *O*-linked glycosylation in this process. In 2-cell embryos grown in +P media, *O*-glycosylated proteins are seen both inside the nucleus and are also associated with the nuclear membrane (Figure 2-6A). When incubated in the –P medium, the glycosylated protein level inside the nucleus is substantially reduced, while the nuclear membrane component remains relatively unchanged (Figure 2-6A-C). Import of nuclear proteins from the cytosol largely relies on the presence of canonical nuclear localization signals (NLS) (Lange et al., 2007). A second, well-characterized mode of protein transport involves *O*-linked glycosylation of the transported protein, followed by binding to a chaperone molecule such as HSP90 or HSP70, and the subsequent transport of this complex through the heavily glycosylated nuclear pore (Guinez et al., 2005). In a remarkable demonstration of this process, it was shown that introduction of a single *O*-glycosylation site on bovine serum albumin (BSA) causes this cytoplasmic protein to localize to the nucleus (Duverger et al., 1996). The enzyme necessary for transferring the *O*-glycosyl moiety derived from UDP-GlcNAc to the target protein is *O*-linked *N*-acetyglucosamine transferase (OGT). In +P medium OGT is seen in the nucleus, as well as in cytoplasmic punctae, but in –P embryos, OGT is no longer

nuclear (Figure S2-6A-F). Additionally, the inhibitor STO45849 that specifically blocks OGT function causes loss of PDH nuclear localization (Figure 2-6D-F), a reduction in glycosylation and a 2-cell block (Figure S2-6M-P). The chaperon proteins HSP70 and HSP90 are indeed prominently expressed at this stage (Figure S2-6G, H), and most strikingly, a specific inhibitor of HSP90, 17-AAG, gives rise to a 2-cell block in development (Figure S2-6Q-T) and prevents nuclear localization of PDH (Figure 2-6G-I). One potential model is that *O*-glycosylated mitochondrial enzymes could utilize a chaperon dependent transport process to locate within the nucleus (see Chapter 4).

2.3.9 Pyruvate dependent Histone modifications

A number of epigenetic changes result from addition or deletion of acetyl or methyl groups to histones and have been linked to genome activation (Gut and Verdin, 2013) as well as to the presence of appropriate metabolites (Martinez-Pastor et al., 2013). We therefore investigated if such marks are dependent on the presence of exogenously supplied pyruvate. We find that pyruvate deprived embryos show a significant reduction in H3K4 acetylation (Figure 2-6J-L). H3K27 acetylation is also somewhat reduced (Figure 2-6M-O), but acetylation at other sites such as H3K9, H3K14 and H4K5 is not affected by the lack of pyruvate (Figure S2-6U-V'). Similarly, H3K27 trimethylation is significantly reduced in the absence of pyruvate (Figure 2-6P-R) while trimethylation on other histones such as H3K4 and H3K9 remains unchanged (Figure S2-6W-X'). To understand why some of the epigenetic marks are affected more than others, we will first need to identify the status of individual sites by CHIP-seq analysis and also the activity of each chromatin modifier protein at this stage of

development. This is beyond the scope of this investigation but will be followed up in the very near future.

2.3.10 PDH localization in human embryos

The surprising finding that the first half of the mouse TCA cycle enzymes can be detected in the nucleus at the 2-cell stage, led us to investigate whether a similar mechanism might operate in human embryos. A conserved mechanism would be relevant to human fertility and in vitro fertilization protocols and we were therefore granted access to a small number of human embryos from fertilization clinics, through a fully consented and documented process. Due to the very limited tissue availability, we have restricted our study to the localization of PDH to serve as a guide. A mixture of two sets of antibodies was used: α-PDH^{inactive} (recognizes only the inactive phosphorylated version) and α-PDH^{total} (recognizes both active and inactive forms). In both 1-cell pronuclear fusion (Figure 2-7A-C) and at the 2-cell stage (Figure 2-7D-F), no nuclear PDH is detected in human embryos. This is unlike the situation in mouse where these stages have robust expression of un-phosphorylated PDH^{active} in the nucleus. Similar to that seen in mouse, however, the mitochondrial PDH detected in the human embryo is largely phosphorylated (inactive). At the 4-cell stage of the human embryo, a burst of nuclear PDH^{active}, becomes readily detectable (Figure 2-7G-L). This nuclear localization peaks at the 8-cell stage (Figure 2-7M-R). A single stage later, in the morula, there is no hint of nuclear PDH^{active} in the human embryo (Figure 2-7S-U). Thus, in mouse embryos, nuclear PDH initiates at 1-cell, peaks at 2-cell and starts declining beyond the 4-cell stage. In contrast, human embryos initiate nuclear PDH localization at the 4-cell

stage, peaking at the 8-cell stage and is excluded from the nucleus in the morula. Nuclear PDH is never detected in the morula or blastocyst of either mammal. Remarkably, the delayed nuclear entry in human compared to mouse embryo corresponds exactly to the natural ZGA timing, which takes place in the mouse, at the late 2-cell stage, while in humans, between the 4-cell and 8-cell stages (Niakan and Eggan, 2013; Xue et al., 2013). These stages of genomic remodeling fully coincide in both species with the time when PDH^{active} is localized to the nucleus.

2.4 Acknowledgments

We would like to thank Wei Liao for help in bioinformatics analysis of RNA expression, Shubhendu Senroy for setting up the embryo culture system during the early phases of this work, and all members of our laboratory for their suggestions and support. The human embryo studies were approved by the full UCLA Institutional Review Board (IRB#11-002027) and the UCLA Embryonic Stem Cell Research Oversight (ESCRO) Committee (2007-005). We thank Dr. David Jelinek and Dr. Hilary Coller at UCLA for help with the IDH enzyme assay. We thank the UCLA metabolism group including Drs. Lowry, Coller, Plath, Graeber, and Christofk for advice and discussions.

We are extremely grateful for the support provided by the NIH Director's Pioneer Award to U.B. (DP1DK098059-04) that enabled this laboratory to initiate research in metabolism and development of mammalian embryos. We would also like to gratefully acknowledge critical research support from the UCLA Broad Stem Cell Research Center and thank Director Owen Witte for his continued support. F.C. is supported by a China Scholarship Council Award and a California Institute for Regenerative Medicine pre-doctoral fellowship.

2.5 Materials and Methods

2.5.1 Mouse embryo culture

All animal care and procedures used in this study are approved by the Animal Regulatory Committee (ARC) of the University of California at Los Angeles (UCLA).

Mouse zygotes and preimplantation embryos were collected from super-ovulated 4-week old C57BL/6J X C3He (Jackson labs) F1 females. Mice were super-ovulated by peritoneal injection of 7.5 IU of PMSG (Pregnant Mare Serum Gonadotropin) to stimulate egg production, followed by 7.5 IU of hCG (human Chorionic Gonadotropin) 48hrs after PMSG. Embryos were obtained by mating the super-ovulated females with C57BL/6 X C3He F1 males. Mating was confirmed by the presence of vaginal plug. For isolation of fertilized 1-cell zygotes, super-ovulated females were euthanized 18hrs post-hCG and zygotes were dissected out of the ampulla in the oviduct. The embryo-cumulus complexes were treated with 300 μg/ml of hyaluronidase to disperse the cumulus cells, washed in mKSOM medium without pyruvate and transferred to the appropriate culture medium (+P or –P) and cultured at 37°C in 5% CO_2. For embryo isolation at later stages, the embryos were flushed from the oviduct at the appropriate times, washed in mKSOM medium and either cultured or fixed immediately for immuno-fluorescence analysis. All mouse embryos used in this study were cultured in a modified KSOM medium whose composition is identical to KSOM in salts, glucose, lactate and pyruvate (95mM NaCl, 2.5mM KCl, 0.35mM KH_2PO_4, 0.20mM $MgSO_4$, 25mM $NaHCO_3$, 1.71mM $Cacl_2$, 0.01 mM EDTA, 0.20mM glucose, 10mM lactate, 0.20mM pyruvate) but

was devoid of all amino acids and BSA. The osmolarity of the medium was maintained using 0.1% PVA (poly vinly alcohol) (Biggers et al., 1997).

2.5.2 Human embryo culture

The human embryo studies were approved by the full UCLA Institutional Review Board (IRB#11-002027) and the UCLA Embryonic Stem Cell Research Oversight (ESCRO) Committee (2007-005). Human preimplantation embryos for this project were received cryopreserved from an IVF clinic following consent. A total of 10 2PN embryos from 2 donors were used for this project. Human embryos were slow thawed using Thaw-Kit 1 (Vitrolife) according to the manufacturer's protocol. The embryos were cultured in drops of Continuous Single Culture media (Irvine Scientific) supplemented with 20% Quinn's Advantage SPS Serum Protein Substitute (Sage Media) for 0 to 4 sequential days at 37°C, 6% CO_2 and 5% O_2. At varying stages of development from 2PN to compacting morula, the zona pellucida was removed with Tyrode's Acidified Solution (Irvine Scientific) and fixed in 4% paraformaldehyde for 30 min and stained with antibodies as in the previous protocol.

2.5.3 BrUTP incorporation

BrUTP incorporation was performed using the protocol described by Aoki et al., 1997. BrUTP incorporation was also performed using the Click-iT RNA imaging kit from Invitrogen (cat no. C10330). Live embryos were incubated in 5-ethynyl uridine (EU) for 30mins for incorporation into nascent transcripts, following which they were fixed in 4% paraformaldehyde for 30mins at room temperature and permeabilized in PBST for

20mins. Click-iT cocktail was freshly prepared and the embryos were incubated in it for 30mins at room temperature protected from light. The embryos were subsequently washed in Click-iT reaction rinse buffer and incubated in To-Pro in PBS to mark the nuclei and mounted in Vectashield medium for microscopy.

2.5.4 Immuno-localization in isolated nuclei

Staining nuclei devoid of the surrounding cytoplasm followed the methods developed by Coonen et al., 1994. Embryos are removed from the mKSOM medium, washed several times with PBS, transferred with minimal amounts of PBS to a microdrop of 0.01N HCl / 0.1% Tween20 in distilled sterile water on a glass slide. Within a few minutes the Zona and the cytoplasm begin to disintegrate and the nucleus becomes clearly visible and following removal of all the cytoplasm, the nuclei remain attached to the glass slide. The slides are washed with several rounds of PBS to remove the remaining cytoplasm. The attached nuclei are fixed with 4% paraformaldehyde, washed in PBST, and stained with specific antibodies.

2.5.5 Antibody staining for immunofluorescence

Staged embryos are fixed in 4% paraformaldehyde for 30 min at room temperature, permeabilized for 30mins in PBS with 0.4% Triton (PBST), blocked in PBST with 3% albumin for 30mins and incubated with the desired primary antibody in PBST plus 3% albumin (PBSTA) overnight at 4°C. The following day the embryos were washed in PBST four times for 10min each, blocked with PBSTA, incubated with the appropriate secondary antibody (1/300 dilution) overnight at 4°C. Embryos were

washed again 3 times for 10min each in PBST. Nuclei were counterstained with To-Pro for 10mins, washed once again in PBST for 10mins, deposited on glass slides and mounted in Vecta-shield (Vector Laboratories) medium. Images were captured using a Zeiss LSM 700 confocal microscope. Data were quantified using the Prism software package, using a two-tailed unpaired t test. The numbers of embryos used for each experiment are reported in the Figure legend. Data are considered significant if $p < 0.05$, and the error bars are ± SEM.

2.5.6 JC1 and Rhod-2AM staining

Live 2-cell embryos were incubated in mKSOM containing 0.1 µg/ml of JC1 (Life Technologies) or 5 µM Rhod-2AM (Life Technologies) for 30 min in 5% CO_2 at 37°C. After incubation, embryos were washed several times in mKSOM, transferred to depression slides and mounted in the medium.

2.5.7 Measurement of metabolite levels

ATP was measured using the ENLIGHTEN ATP assay system according to the manufacturer's instructions (Promega, WI, USA). Briefly, ATP was extracted from embryos using 2.5% TCA and neutralized with 0.1 M Tris-acetate buffer pH 7.75. Following addition of an equal volume of rL/L Reagent (Promega), luminescence was measured as readout for ATP levels. ADP was measured using the ADP-glo detection kit (Promega, WI, USA). Reduced glutathione levels were determined using the GSH-Glo bioluminescent assay (Promega, WI, USA). Embryos (in 10 µL mKSOM) were snap frozen in liquid nitrogen. The thawed samples were added directly to 2X GSH-Glo

reagent containing a modified luciferin and glutathione transferase, and incubated in the dark for 30 min at room temperature. An equal volume of luciferin detection reagent was added and the luminescence detected after 15 min. NAD^+ and NADH levels were determined using the NAD^+/NADH Glo cycling assay, according to the manufacturer's instructions (Promega, WI, USA). Briefly, both NAD^+ and NADH were extracted from the embryos in a carbonate buffered base solution containing 1% DTAB, 10 mM nicotinamide, 0.05% Triton X-100, pH 10.7. The embryos were freeze-thawed in liquid nitrogen and centrifuged through a filter with a 10kDa mW cut-off. Samples for NAD^+ determination were neutralized with 0.4 N HCl. Both NAD^+ and NADH samples were heated for 20 min at 60°C. The assay reagent was added to the samples, which were then incubated for 3 hr for cycling, after which the luminescence was determined.

The assay to measure the response of the TCA cycle metabolites to starvation and re-feeding was adapted from the approach of Lowry. For each condition, approximately 250 embryos were cultured in +P media until 48 hr post-hCG. Each condition was assayed in triplicate, with each replicate containing approximately 250 embryos, the exact number of which was used to normalize the data. For the fully fed condition, embryos were washed twice in a large volume of fresh +P media, but which lacked lactate and glucose, and incubated for 30 min. Following which, the embryos were incubated for a further 20 min in fresh +P media (lacking lactate and glucose but containing pyruvate) and then the metabolites were extracted using cold 80% methanol. For the starved condition, embryos were washed twice in starvation media (lacking pyruvate, lactate and glucose), incubated for 30 min, following which the embryos were

washed with fresh starvation medium and the metabolites isolated. For the re-fed condition, following a 30 min starvation, embryos were incubated with +P media (containing pyruvate, but not lactate or glucose) for 20 min. The embryos were washed twice in fresh +P media (containing pyruvate, but not lactate or glucose) and the metabolites extracted using cold 80% methanol. For samples analyzed under steady state conditions (Figure 2-5J), embryos were transferred into 80% methanol in 5 µl of +P or –P media, which contained 10 mM lactate. The lactate level in the media is in excess and therefore insensitive to culture conditions. In Figure 2-5J, the lactate level was used as an internal control (this was not possible in Figure 2-5H, I since lactate was omitted from the media). Dried metabolites were re-suspended in 15 µl 50% ACN and 10 µl were injected for chromatographic separation using the Thermo Scientific Ion Chromatography System (ICS) 5000 coupled to a Thermo Scientific Q Exactive run in negative polarity mode. The gradient ran from 10 mM to 90 mM KOH over 25 min with a flow rate of 350 µl / min. The settings for the HESI-II source were: S-lens 50, Sheath Gas 18, Aux Gas 4, spray heater 320°C, and spray voltage −3.2 kV. Metabolites were identified based on accurate mass (±3 ppm) and retention times of pure standards. Relative amounts of metabolites were quantified using TraceFinder 3.3. Oxaloacetate and isocitrate could not be measured accurately using this approach with tractable numbers of embryos. The data were analyzed using the Prism software package. The difference between metabolites in each condition was compared using unpaired two-tailed Student’s t tests.

2.5.8 Enzymatic Analyses in Isolated Nuclei

Nuclei were isolated from two-cell embryos as described above. PDH activity was measured by adopting a method described by Lane and Gardner to measure pyruvate oxidation in live embryos (Lane and Gardner, 2000). In these experiments pyruvate dehydrogenase activity was measured by incubating 200 isolated nuclei with assay solution (50 mM MOPS pH 7.4, 0.2 mM $MgCl_2$, 0.01 mM $CaCl_2$, 0.3 mM thiamine pyrophosphate, 0.12 mM coenzyme A, 2 mM NAD^+, 2.64 mM L-cysteine HCl) containing containing [1-^{14}C]pyruvate 0.085 mCi/ml. Each condition was performed in triplicate (and each replicate contained 200 nuclei). The nuclei were attached to pre-cut coverslips that were fixed in the lid of a microcentrifuge vial and a 3 µL drop of assay medium was placed on the nuclei. The vial lid was placed on a vial containing 1.65 mL of 25 mM $NaHCO_3$ pre-gassed with 5% CO_2 in air, which trapped labeled CO_2 generated from pyruvate. Samples were incubated for 5 hr at 37°C. Controls included a 3 µL drop of assay medium on the lid without nuclei in order to control for spontaneous breakdown of the label. Total counts were determined by the addition of a 3 µL drop of medium straight into the 1.65 mL $NaHCO_3$. After 5 hr the vials were opened, and 1 mL of the NaHCO3 removed and placed into a scintillation vial containing 200 µL of 0.1 M NaOH. Vials were sealed and stored overnight. The following morning, 10 mL of scintillation fluid was added to each vial. The vials were vortexed and counted for 4 min each, and the results were normalized against the total number of counts in the assay medium. Quantification was performed using an unpaired two-tailed Student's t test.

2.5.9 IDH3A assay

Nuclei were isolated from embryos cultured either in +P or –P medium on a glass slide were washed in PBS twice and IDH3 activity was determined in situ using an enzymatic assay. The assay buffer (Tris pH 7.4 (50mM), Mg_2SO_4 (1mM), NAD^+ (1mM), isocitrate (10mM), Cynoditoly Tetrazolium (500 µg/ml) (Polysciences 19292-100) and PMS (25 µg/ml)). For negative controls, isocitrate was eliminated from the assay buffer. The nuclei were incubated for 4 hr, washed in PBS several times and mounted on Vectashield medium and the images were collected using confocal microscope.

2.5.10 Quantification and Statistical Analysis

Statistical parameters are reported in the figures and figure legends. Data is considered significant if $p < 0.05$ (see Method Details). Statistical analysis was performed using the Graphpad Prism 7 software.

2.5.11 Key Resources Table

REAGENT or RESOURCE	SOURCE	IDENTIFIER
Antibodies		
Mouse anti-PCNA	Abcam	Cat #ab29
Rabbit anti-phosphohistone 3	Abcam	Cat #ab47297
Rat anti-tubulin	Abcam	Cat #ab6160
Mouse anti-Pol II	Santa Cruz	Cat #8WG16
Rabbit anti-Sirt1	Abcam	Cat #ab7343
Mouse anti-O-linked glycolysation antibody (RL2)	Abcam	Cat #ab2739
Rabbit anti-H3K4 acetylation	Abcam	Cat #ab113672
Rabbit anti-H3K27 acetylation	Abcam	Cat #ab45173
Mouse anti-H3K9 acetylation	Abcam	Cat #ab12179
Mouse anti-H3K4 tri-methylation	Abcam	Cat #ab12209
Rabbit anti-phospho-PDH	Abcam	Cat #ab92696
Mouse anti-PDH	Abcam	Cat #ab110334
Mouse anti-PDH	Santa Cruz	Cat #sc377092
Rabbit anti-PDK1 antibody	Abcam	Cat #ab110025
Goat anti-PDP1 antibody	Santa Cruz	Cat #sc87354
Mouse anti-PCB antibody	Abcam	Cat #ab110314
Rabbit anti-CS antibody	Abcam	Cat #ab96600

Mouse anti-Aconitase 2 antibody	Abcam	Cat #ab110321
Rabbit anti-IDH3A antibody	Abcam	Cat #ab58641
Goat anti-KGDH antibody	Santa Cruz	Cat #sc48589
Rabbit anti-SCS antibody	Cell Signaling	Cat #8071
Mouse anti-SDH antibody	Abcam	Cat #ab14715
Mouse anti-MDH2 antibody	Abcam	Cat #ab92867
Mouse anti-HSP70 antibody	Santa Cruz	Cat #sc24
Mouse anti-HSP90 antibody	Abcam	Cat #ab13492
Mouse anti-H3K9me3 antibody	Abcam	Cat #ab8898
Rabbit anti-H3K14 acetylation	Epigenetik	Cat #A4032
Mouse anti-Sp1 antibody	Abcam	Cat #ab77441
Rabbit anti-myc antibody	Santa Cruz	Cat #sc40
Chemicals, Peptides, and Recombinant Proteins		
17-AAG	Tocris	Cat #1515
ST045849	TimTec	Cat #ST045849
JC1	Thermo Fisher	Cat #T3168
Rhod-2AM	Thermo Fisher	Cat #R1244
5-Cyano-2,3-di-(p-tolyl)tetrazolium chloride	Polysciences	Cat #19292
Pyruvic Acid, sodium salt 1-^{14}C	Perkin Elmer	Cat #NEC255050UC
Pregnant Mare Serum Gonadotropin (PMSG)	ProSpec	Cat #hor-272
Chorionic gonadotropin human (hCG)	Sigma-Aldrich	Cat #CG10
Critical Commercial Assays		
NAD^+/NADH measurement	Promega	Cat #G9071
GSH/GSSG measurement	Promega	Cat #V6611
ATP measurement	Promega	Cat #FF2000
ADP measurement	Promega	Cat #V6930
EU Click-iT RNA imaging kit	Thermo Fisher	Cat #C10330
Experimental Models: Cell Lines		
Human: embryo culture	This lab	N/A
Mouse: embryo culture	This lab	N/A
Experimental Models: Organisms/Strains		
Mouse: B6C3F1/J	Jackson Laboratory	Stock No: 100010
Software and Algorithms		
Graphpad Prism 7	GraphPad	http://www.graphpad.com/
TraceFinder 3.3	Thermo Scientific	N/A
ImageJ	NIH	https://imagej.nih.gov/ij/

2.6 References

Acton, B.M., Jurisicova, A., Jurisica, I., and Casper, R.F. (2004). Alterations in mitochondrial membrane potential during preimplantation stages of mouse and human embryo development. Molecular human reproduction 10, 23-32.

Aoki, F., Worrad, D.M., and Schultz, R.M. (1997). Regulation of transcriptional activity during the first and second cell cycles in the preimplantation mouse embryo. Dev Biol 181, 296-307.

Baltz, J.M. (2013). Connections between preimplantation embryo physiology and culture. J Assist Reprod Genet 30, 1001-1007.

Banerjee, P.S., Ma, J., and Hart, G.W. (2015). Diabetes-associated dysregulation of O-GlcNAcylation in rat cardiac mitochondria. Proceedings of the National Academy of Sciences of the United States of America 112, 6050-6055.

Barbehenn, E.K., Wales, R.G., and Lowry, O.H. (1974). The explanation for the blockade of glycolysis in early mouse embryos. Proceedings of the National Academy of Sciences of the United States of America 71, 1056-1060.

Barbehenn, E.K., Wales, R.G., and Lowry, O.H. (1978). Measurement of metabolites in single preimplantation embryos; a new means to study metabolic control in early embryos. J Embryol Exp Morphol 43, 29-46.

Baumann, C.G., Morris, D.G., Sreenan, J.M., and Leese, H.J. (2007). The quiet embryo hypothesis: molecular characteristics favoring viability. Mol Reprod Dev 74, 1345-1353.

Behal, R.H., Buxton, D.B., Robertson, J.G., and Olson, M.S. (1993). Regulation of the pyruvate dehydrogenase multienzyme complex. Annu Rev Nutr 13, 497-520.

Biggers, J.D. (1971). Metabolism of mouse embryos. J Reprod Fertil Suppl 14, 41-54.

Biggers, J.D., Summers, M.C., and McGinnis, L.K. (1997). Polyvinyl alcohol and amino acids as substitutes for bovine serum albumin in culture media for mouse preimplantation embryos. Hum Reprod Update 3, 125-135.

Biggers, J.D., Whittingham, D.G., and Donahue, R.P. (1967). The pattern of energy metabolism in the mouse oocyte and zygote. Proceedings of the National Academy of Sciences of the United States of America 58, 560-567.

Bond, M.R., and Hanover, J.A. (2015). A little sugar goes a long way: the cell biology of O-GlcNAc. The Journal of cell biology 208, 869-880.

Brinster, M.a. (1967a). Oxygen consumption of preimplantation embryos. Experimental cell research 47, 337-344.

Brinster, R.L. (1967b). Carbon dioxide production from glucose by the preimplantation mouse embryo. Experimental cell research 47, 271-277.

Brinster, R.L. (1968). Hexokinase activity in the preimplantation mouse embryo. Enzymologia 34, 304-308.

Brinster, R.L. (1969). Incorporation of carbon from glucose and pyruvate into the preimplantation mouse embryo. Experimental cell research 58, 153-158.

Brinster, R.L. (1973). Lactate dehydrogenase isozymes in the preimplantation rabbit embryo. Biochemical genetics 9, 229-234.

Brown, J.J., and Whittingham, D.G. (1991). The roles of pyruvate, lactate and glucose during preimplantation development of embryos from F1 hybrid mice in vitro. Development 112, 99-105.

Brown, J.J., and Whittingham, D.G. (1992). The dynamic provision of different energy

substrates improves development of one-cell random-bred mouse embryos in vitro. Journal of reproduction and fertility 95, 503-511.

Calarco, P.G., and Brown, E.H. (1969). An ultrastructural and cytological study of preimplantation development of the mouse. The Journal of experimental zoology 171, 253-283.

Chueh, F.Y., Leong, K.F., Cronk, R.J., Venkitachalam, S., Pabich, S., and Yu, C.L. (2011). Nuclear localization of pyruvate dehydrogenase complex-E2 (PDC-E2), a mitochondrial enzyme, and its role in signal transducer and activator of transcription 5 (STAT5)-dependent gene transcription. Cell Signal 23, 1170-1178.

Cloos, P.A., Christensen, J., Agger, K., and Helin, K. (2008). Erasing the methyl mark: histone demethylases at the center of cellular differentiation and disease. Genes Dev 22, 1115-1140.

Cockburn, K., and Rossant, J. (2010). Making the blastocyst: lessons from the mouse. J Clin Invest 120, 995-1003.

Cox, N.a. (2013). Lehninger Principles of Biochemistry.

Davoudi, M., Kallijarvi, J., Marjavaara, S., Kotarsky, H., Hansson, E., Leveen, P., and Fellman, V. (2014). A mouse model of mitochondrial complex III dysfunction induced by myxothiazol. Biochemical and biophysical research communications 446, 1079-1084.

Dikov, A., Dimitrova, M., Krieg, R., and Halbhuber, K.J. (2004). New fluorescent method for the histochemical detection of tripeptidyl peptidase I using glycyl-l-prolyl-l-met-2-anthraquinonyl hydrazide as substrate. Cellular and molecular biology 50 Online Pub, OL565-568.

Donohoe, D.R., and Bultman, S.J. (2012). Metaboloepigenetics: interrelationships between energy metabolism and epigenetic control of gene expression. Journal of cellular physiology 227, 3169-3177.

Duverger, E., Roche, A.C., and Monsigny, M. (1996). N-acetylglucosamine-dependent nuclear import of neoglycoproteins. Glycobiology 6, 381-386.

Egloff, S., and Murphy, S. (2008). Cracking the RNA polymerase II CTD code. Trends Genet 24, 280-288.

Graves, C.N., and Biggers, J.D. (1970). Carbon dioxide fixation by mouse embryos prior to implantation. Science 167, 1506-1508.

Guinez, C., Morelle, W., Michalski, J.C., and Lefebvre, T. (2005). O-GlcNAc glycosylation: a signal for the nuclear transport of cytosolic proteins? Int J Biochem Cell Biol 37, 765-774.

Gut, P., and Verdin, E. (2013). The nexus of chromatin regulation and intermediary metabolism. Nature 502, 489-498.

Hardiville, S., and Hart, G.W. (2014). Nutrient regulation of signaling, transcription, and cell physiology by O-GlcNAcylation. Cell Metab 20, 208-213.

Hart, G.W., Housley, M.P., and Slawson, C. (2007). Cycling of O-linked beta-N-acetylglucosamine on nucleocytoplasmic proteins. Nature 446, 1017-1022.

Holness, M.J., and Sugden, M.C. (2003). Regulation of pyruvate dehydrogenase complex activity by reversible phosphorylation. Biochemical Society transactions 31, 1143-1151.

Houghton, F.D., Thompson, J.G., Kennedy, C.J., and Leese, H.J. (1996). Oxygen consumption and energy metabolism of the early mouse embryo. Mol Reprod Dev

44, 476-485.

Jitrapakdee, S., and Wallace, J.C. (1999). Structure, function and regulation of pyruvate carboxylase. The Biochemical journal 340 (Pt 1), 1-16.

Kawahara, M., Koyama, S., Iimura, S., Yamazaki, W., Tanaka, A., Kohri, N., Sasaki, K., and Takahashi, M. (2015). Preimplantation death of xenomitochondrial mouse embryo harbouring bovine mitochondria. Scientific reports 5, 14512.

Keefer, C.L. (2015). Artificial cloning of domestic animals. Proceedings of the National Academy of Sciences of the United States of America 112, 8874-8878.

Koivunen, P., Hirsila, M., Remes, A.M., Hassinen, I.E., Kivirikko, K.I., and Myllyharju, J. (2007). Inhibition of hypoxia-inducible factor (HIF) hydroxylases by citric acid cycle intermediates: possible links between cell metabolism and stabilization of HIF. The Journal of biological chemistry 282, 4524-4532.

Kolobova, E., Tuganova, A., Boulatnikov, I., and Popov, K.M. (2001). Regulation of pyruvate dehydrogenase activity through phosphorylation at multiple sites. The Biochemical journal 358, 69-77.

Komatsu, K., Iwase, A., Mawatari, M., Wang, J., Yamashita, M., and Kikkawa, F. (2014). Mitochondrial membrane potential in 2-cell stage embryos correlates with the success of preimplantation development. Reproduction 147, 627-638.

Lane, M., and Gardner, D.K. (2000). Lactate regulates pyruvate uptake and metabolism in the preimplantation mouse embryo. Biology of reproduction 62, 16-22.

Lane, M., and Gardner, D.K. (2005). Mitochondrial malate-aspartate shuttle regulates mouse embryo nutrient consumption. The Journal of biological chemistry 280, 18361-18367.

Lange, A., Mills, R.E., Lange, C.J., Stewart, M., Devine, S.E., and Corbett, A.H. (2007). Classical nuclear localization signals: definition, function, and interaction with importin alpha. The Journal of biological chemistry 282, 5101-5105.

Lawitts, J.A., and Biggers, J.D. (1991). Optimization of mouse embryo culture media using simplex methods. Journal of reproduction and fertility 91, 543-556.

Leese, H.J. (1995). Metabolic control during preimplantation mammalian development. Hum Reprod Update 1, 63-72.

Leese, H.J. (2002). Quiet please, do not disturb: a hypothesis of embryo metabolism and viability. BioEssays : news and reviews in molecular, cellular and developmental biology 24, 845-849.

Leese, H.J. (2012). Metabolism of the preimplantation embryo: 40 years on. Reproduction 143, 417-427.

Leese, H.J. (2015). History of oocyte and embryo metabolism. Reproduction, fertility, and development.

Leese, H.J., and Barton, A.M. (1984). Pyruvate and glucose uptake by mouse ova and preimplantation embryos. Journal of reproduction and fertility 72, 9-13.

Li, L., Lu, X., and Dean, J. (2013). The maternal to zygotic transition in mammals. Mol Aspects Med 34, 919-938.

Li, L., Zheng, P., and Dean, J. (2010). Maternal control of early mouse development. Development 137, 859-870.

Martin, K.L., and Leese, H.J. (1995). Role of glucose in mouse preimplantation embryo development. Mol Reprod Dev 40, 436-443.

Martinez-Pastor, B., Cosentino, C., and Mostoslavsky, R. (2013). A tale of metabolites:

the cross-talk between chromatin and energy metabolism. Cancer Discov 3, 497-501.

McLaren, and Biggers, J.D. (1958). Successful development and birth of mice cultivated in vitro as early as early embryos. Nature 182, 877-878.

Mitra, K., Rangaraj, N., and Shivaji, S. (2005). Novelty of the pyruvate metabolic enzyme dihydrolipoamide dehydrogenase in spermatozoa: correlation of its localization, tyrosine phosphorylation, and activity during sperm capacitation. The Journal of biological chemistry 280, 25743-25753.

Niakan, K.K., and Eggan, K. (2013). Analysis of human embryos from zygote to blastocyst reveals distinct gene expression patterns relative to the mouse. Dev Biol 375, 54-64.

Quinn, P., and Wales, R.G. (1974). Fixation of carbon dioxide by preimplantation rabbit embryos in vitro. Journal of reproduction and fertility 36, 29-39.

Rossant, J., and Tam, P.P. (2009). Blastocyst lineage formation, early embryonic asymmetries and axis patterning in the mouse. Development 136, 701-713.

Shi, L., and Wu, J. (2009). Epigenetic regulation in mammalian preimplantation embryo development. Reprod Biol Endocrinol 7, 59.

Shyh-Chang, N., Daley, G.Q., and Cantley, L.C. (2013). Stem cell metabolism in tissue development and aging. Development 140, 2535-2547.

Sies, H., Graf, P., and Crane, D. (1983). Decreased flux through pyruvate dehydrogenase during calcium ion movements induced by vasopressin, alpha-adrenergic agonists and the ionophore A23187 in perfused rat liver. The Biochemical journal 212, 271-278.

Stern, S., Biggers, J.D., and Anderson, E. (1971). Mitochondria and early development of the mouse. The Journal of experimental zoology 176, 179-191.

Summers, M.C. (2013). A brief history of the development of the KSOM family of media. J Assist Reprod Genet 30, 995-999.

Sutendra, G., Kinnaird, A., Dromparis, P., Paulin, R., Stenson, T.H., Haromy, A., Hashimoto, K., Zhang, N., Flaim, E., and Michelakis, E.D. (2014). A nuclear pyruvate dehydrogenase complex is important for the generation of acetyl-CoA and histone acetylation. Cell 158, 84-97.

Thomson, J.L. (1967). Effect of inhibitors of carbohydrate metabolism on the development of preimplantation mouse embryos. Experimental cell research 46, 252-262.

Thouas, G.A., Trounson, A.O., Wolvetang, E.J., and Jones, G.M. (2004). Mitochondrial dysfunction in mouse oocytes results in preimplantation embryo arrest in vitro. Biology of reproduction 71, 1936-1942.

Tomilov, A., Bettaieb, A., Kim, K., Sahdeo, S., Tomilova, N., Lam, A., Hagopian, K., Connell, M., Fong, J., Rowland, D., et al. (2014). Shc depletion stimulates brown fat activity in vivo and in vitro. Aging cell 13, 1049-1058.

Tong, W.H., and Rouault, T.A. (2007). Metabolic regulation of citrate and iron by aconitases: role of iron-sulfur cluster biogenesis. Biometals : an international journal on the role of metal ions in biology, biochemistry, and medicine 20, 549-564.

Trimarchi, J.R., Liu, L., Porterfield, D.M., Smith, P.J., and Keefe, D.L. (2000). Oxidative phosphorylation-dependent and -independent oxygen consumption by individual

preimplantation mouse embryos. Biology of reproduction 62, 1866-1874.

Wales, R.G., and Hunter, J. (1990). Participation of glucose in the synthesis of glycoproteins in preimplantation mouse embryos. Reproduction, fertility, and development 2, 35-50.

Wales, R.G., and Whittingham, D.G. (1970). Incorporation of substrate carbon into mouse embryos during culture in media containing sodium pyruvate. Journal of reproduction and fertility 21, 374.

Watson, J.G., Wright, R.W., Jr., and Chaykin, S. (1977). Collection and transfer of preimplantation mouse embryos. Biology of reproduction 17, 453-458.

Weaver, J.R., Susiarjo, M., and Bartolomei, M.S. (2009). Imprinting and epigenetic changes in the early embryo. Mamm Genome 20, 532-543.

Williams, E.G., Wu, Y., Jha, P., Dubuis, S., Blattmann, P., Argmann, C.A., Houten, S.M., Amariuta, T., Wolski, W., Zamboni, N., et al. (2016). Systems proteomics of liver mitochondria function. Science 352, aad0189.

Williamson, J.R., Walajtys-Rode, E., and Coll, K.E. (1979). Effects of branched chain alpha-ketoacids on the metabolism of isolated rat liver cells. I. Regulation of branched chain alpha-ketoacid metabolism. The Journal of biological chemistry 254, 11511-11520.

Xiao, M., Yang, H., Xu, W., Ma, S., Lin, H., Zhu, H., Liu, L., Liu, Y., Yang, C., Xu, Y., et al. (2012). Inhibition of alpha-KG-dependent histone and DNA demethylases by fumarate and succinate that are accumulated in mutations of FH and SDH tumor suppressors. Genes Dev 26, 1326-1338.

Xue, Z., Huang, K., Cai, C., Cai, L., Jiang, C.Y., Feng, Y., Liu, Z., Zeng, Q., Cheng, L.,

Sun, Y.E., et al. (2013). Genetic programs in human and mouse early embryos revealed by single-cell RNA sequencing. Nature 500, 593-597.

Zheng, W., Gorre, N., Shen, Y., Noda, T., Ogawa, W., Lundin, E., and Liu, K. (2010). Maternal phosphatidylinositol 3-kinase signalling is crucial for embryonic genome activation and preimplantation embryogenesis. EMBO reports 11, 890-895.

2.7 Figures

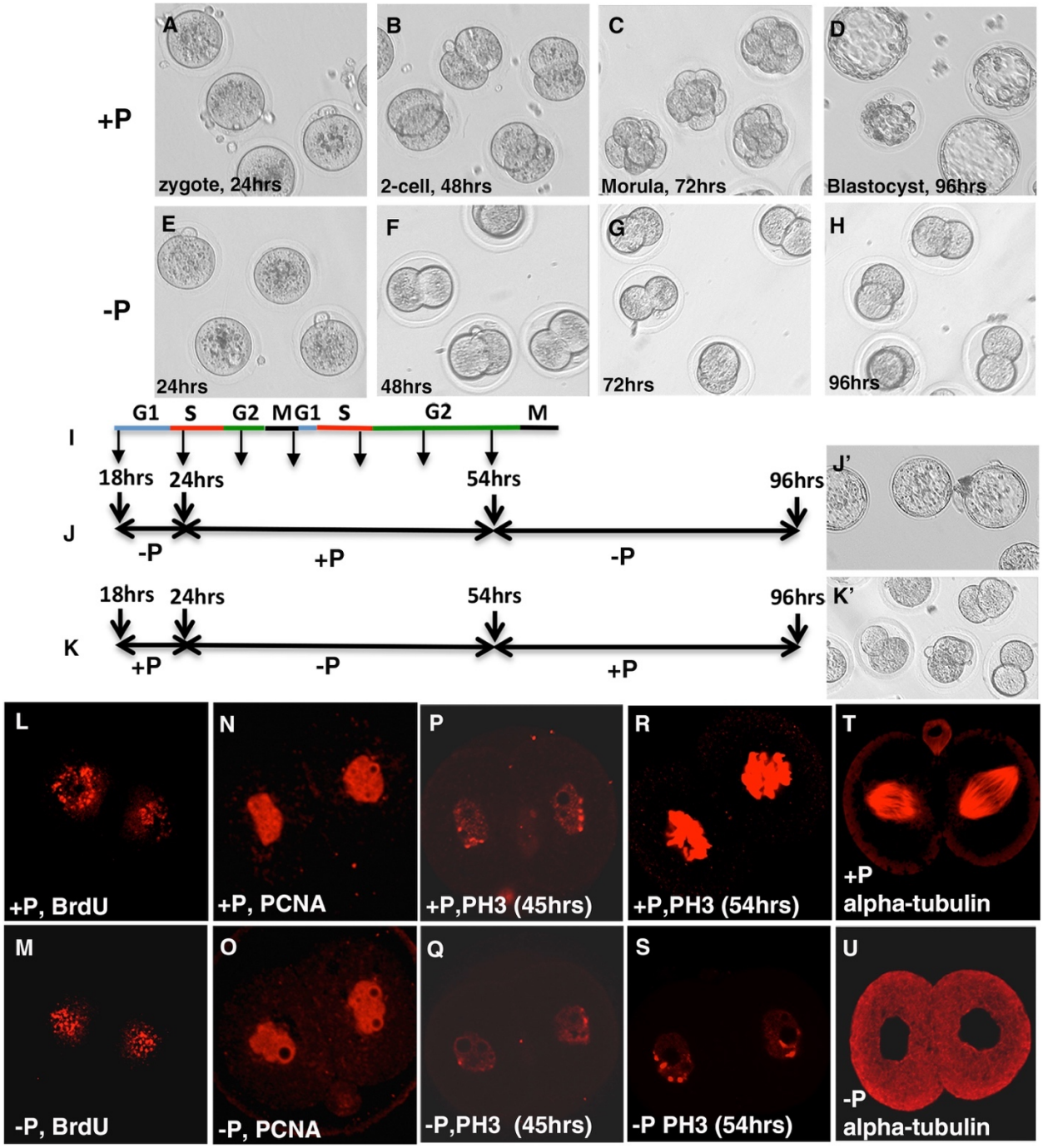
+P
-P
A
zygote, 24hrs
B
2-cell, 48hrs
C
Morula, 72hrs
D
Blastocyst, 96hrs
E
24hrs
F
48hrs
G
72hrs
H
96hrs
I
G1 S G2 M G1 S G2 M
18hrs 24hrs 54hrs 96hrs
J
-P +P -P
J'
18hrs 24hrs 54hrs 96hrs
K
+P -P +P
K'
L
+P, BrdU
N
+P, PCNA
P
+P,PH3 (45hrs)
R
+P,PH3 (54hrs)
T
+P
alpha-tubulin
M
-P, BrdU
O
-P, PCNA
Q
-P,PH3 (45hrs)
S
-P PH3 (54hrs)
U
-P
alpha-tubulin

Fig. 2-1. Role of Pyruvate in Early Development.

All timings are in hours elapsed following hCG injection. Zygotes are isolated at 18 hr post-hCG and cultured until the specified time post-hCG.

(A–D) Embryos cultured in +P medium as controls at (A) 24-, (B) 48-, and (C) 72-hr morula and (D) 96-hr blastocyst.

(E–H) Embryos cultured in –P medium at (E) 24-hr zygote; (F) 48-hr 2-cell embryo; (G) 72-hr 2-cell arrested, and (H) 96-hr 2-cell arrested.

(I) Cell-cycle phases in 1- and 2-cell embryos (adapted from Aoki et al., 1997).

(J and J') Zygotes cultured in –P (until 24 hr) and then shifted to +P (from 24 to 54 hr) and then shifted back to –P (54-hr blastocyst); these embryos develop normally and form blastocysts.

(K and K') In the converse experiment, zygotes cultured in –P medium (24–54 hr) and in +P (before 24 hr and after 54 hr) are arrested at the 2-cell stage.

(J–K') 30-hr window (24–54 hr) as necessary and sufficient for pyruvate dependence.

(L-O) Embryos at 38 hr cultured in +P (L) or –P (M) show identical 2-hr BrdU incorporation marking S phase. Similarly, PCNA staining, also marking S phase, is unchanged in +P (N) and –P (O) cultured embryos.

(P–S) G2 phase monitored by PH3 staining shows entry into this phase (at 45 hr) with very faint PH3 staining in both +P (P) and –P (Q) embryos. However at 54 hr, progression through G2 in +P (R) is marked by high PH3 staining, not seen in –P (Q).

(T–U) At 60 hr, tubulin expression highlights spindle assembly in +P (T) and the lack of it in –P (U).

See also Figure S2-1.

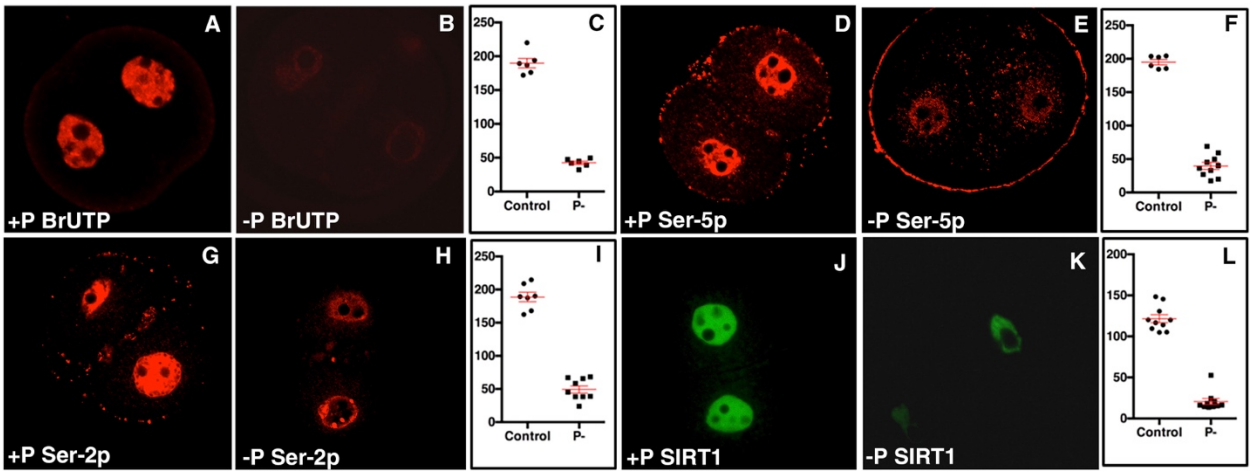

Fig. 2-2: Pyruvate Dependence of Zygotic Genome Activation.

All times are in hours post-hCG injection; embryos are isolated at 18 hr and cultured in either +P or –P media until 54 hr post-hCG.

(A–C) +P (A) but not –P (B) grown embryos incorporate BrUTP that marks synthesis of nascent transcripts. (C) $p < 0.0001$ (nuclei n = 6).

(D–I) Phosphorylation of serine moieties at positions 5 and 2 of Pol II is essential for transcription. Both sites are phosphorylated in +P embryos (D and G) but not in –P medium (E and H). $p < 0.0001$ (nuclei n = 10 for 5P and n = 9 for 2P) (F and I).

(J–L) SIRT1 is an early zygotic gene expressed in +P (J) but not in embryos cultured in –P medium (K). $p < 0.0001$ (nuclei n = 10) (L).

Data are presented as the means ± SEM. See also Figure S2-2.

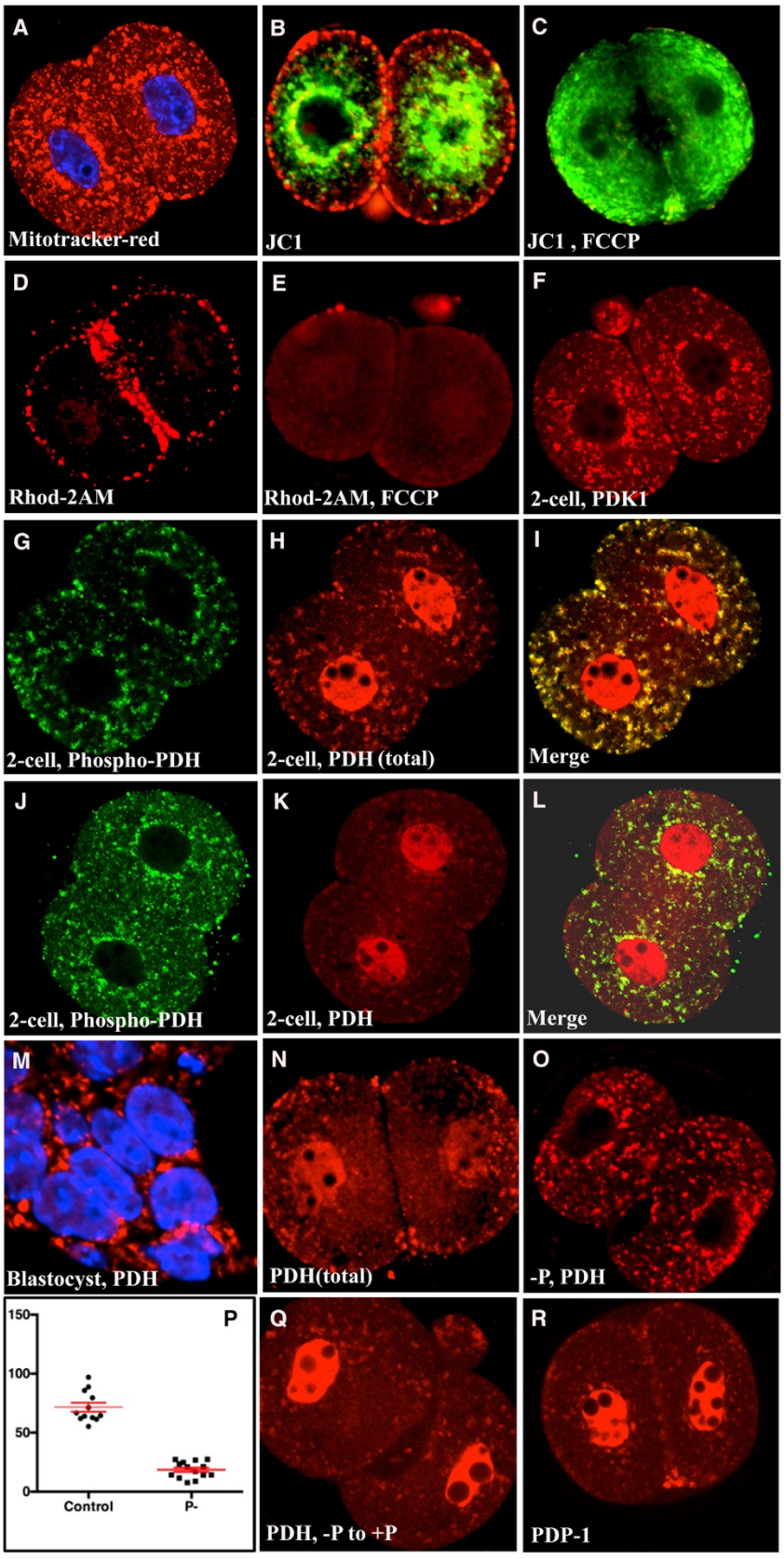
A
Mitotracker-red
B
JC1
C
JC1 , FCCP
D
Rhod-2AM
E
Rhod-2AM, FCCP
F
2-cell, PDK1
G
2-cell, Phospho-PDH
H
2-cell, PDH (total)
I
Merge
J
2-cell, Phospho-PDH
K
2-cell, PDH
L
Merge
M
Blastocyst, PDH
N
PDH(total)
O
-P, PDH
P
150
100
50
0
Control
P-
Q
PDH, -P to +P
R
PDP-1

Fig. 2-3: Sub-cellular Distribution of Pyruvate Dehydrogenase Complex.

All embryos are at 54 hr post-hCG except where noted.

(A) Mitochondria identified by Mitotracker staining (red).

(B) JC1 dye identifies mitochondria with high (red) and low (green) membrane potential. Low activity and membrane potential for the majority of mitochondria is also revealed by calcium sensing dye (Figure S3A) staining.

(C–E) A 30-min FCCP treatment causes loss of active (red) JC1 staining (C) and a corresponding increase in inactive (green) mitochondria. Similarly, FCCP significantly reduces uptake of the calcium-sensitive mitochondrial dye, Rhod-2AM (compare (D) and (E).

(F) PDK1 (inhibitor of PDH) is first detected in single cell embryos (also, Figures S2-3D and S2-3E), rising to high levels at 54 hr.

(G) α-phospho-PDH antibody staining shows that $PDH^{inactive}$ is exclusively mitochondrial.

(H) α-PDH^{total} shows staining in the mitochondrion and the nucleus.

(I) A merge of the images in (H) and (I) establishes that the nuclear component is PDH^{active} (red not green) and the mitochondrial component is $PDH^{inactive}$ (red and green).

(J) Mitochondrial localization of $PDH^{inactive}$.

(K) The PDH antibody Ab110334 exclusively recognizes the nuclear component.

(L) Merge of images in (J) and (K) indicates that Ab110334 specifically recognizes PDH^{active}.

(M) 96-hr blastocyst, no PDH is detected in the nucleus, and α-PDH^{total} specifically marks mitochondria. This is also true for somatic cell lines (Figure S2-4A). To-Pro (blue) marks the nucleus.

(N) α-PDH^{total} (Control +P medium) shows dual nuclear and mitochondrial staining.

(O) Nuclear localization is lost in –P medium.

(P) $p < 0.0001$(nuclei n = 14) comparing nuclear signal intensity.

(Q) 66 hr (until 54 hr in –P, then shifted to +P for 12 hr) rescues nuclear localization.

(R) PDP-1 is nuclear and presumably activates PDH.

Data are presented as the means ± SEM. See also Figure S2-3.

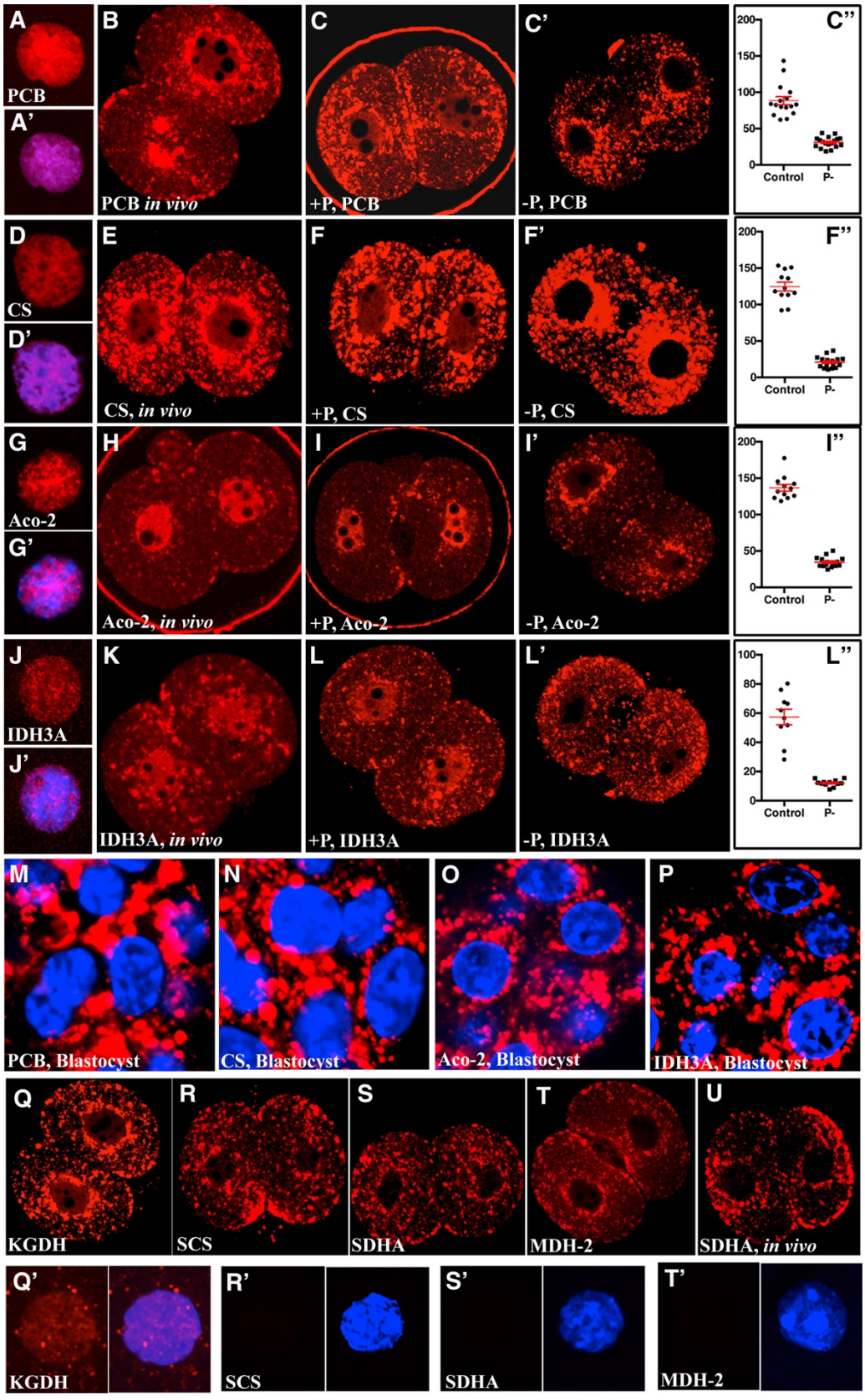
A
PCB
A'
B
PCB *in vivo*
C
+P, PCB
C'
-P, PCB
C''
200
150
100
50
0
Control
P-
D
CS
D'
E
CS, *in vivo*
F
+P, CS
F'
-P, CS
F''
G
Aco-2
G'
H
Aco-2, *in vivo*
I
+P, Aco-2
I'
-P, Aco-2
I''
J
IDH3A
J'
K
IDH3A, *in vivo*
L
+P, IDH3A
L'
-P, IDH3A
L''
100
80
60
40
20
M
PCB, Blastocyst
N
CS, Blastocyst
O
Aco-2, Blastocyst
P
IDH3A, Blastocyst
Q
KGDH
R
SCS
S
SDHA
T
MDH-2
U
SDHA, *in vivo*
Q'
R'
S'
T'

Fig. 2-4: Sub-cellular Localization of TCA Cycle Proteins.

(A–L'') Nuclear localization of a subset of TCA-cycle-related (class 1) enzymes.

(A, D, G, and J) Nuclei isolated from 54-hr +P embryos, fixed, and then stained with indicated antibodies.

(A', D', G', and J') The same nuclei are shown, including the To-pro channel (blue).

(B, E, H, and K) Embryos allowed to develop in vivo during the preimplantation phase until late 2-cell stage and stained with the indicated antibodies without any in vitro culture.

(C, F, I, and L) Embryos cultured in medium containing pyruvate (+P).

(C', F', I', and L') Embryos cultured in medium lacking pyruvate (–P).

(C", F", I", and L") Quantitation of data comparing intensity of nuclear staining in (+P) and (–P) grown embryos.

In all four instances, p value is <0.0001(nuclei n = 18 PCB, n = 16 for CS, n = 16 for Aco-2, and n = 12 for IDH3A). Clear evidence for pyruvate-dependent nuclear localization is evident for the enzymes pyruvate carboxylase (PCB) (A–C"), citrate synthase (CS) (D–F"), mitochondrial aconitase-2 (Aco-2) (G–I"), and mitochondrial isocitrate dehydrogenase 3A (IDH3A) (J–L").

(M–P) Embryos cultured to the blastocyst stage in +P medium and stained with antibodies against, PCB (M), CS (N), Aco-2 (O), and IDH3A (P). In each case, the respective TCA-cycle-related, class I enzyme is exclusively mitochondrial with no

nuclear component detected at this late developmental stage. Nuclei (blue) are marked with To-Pro.

(Q–T') Sub-cellular and nuclear localization of the next series of TCA enzymes in +P cultured embryos. None of these enzymes is seen in the nucleus: α-ketoglutarate-dehydrogenase (KGDH) (Q and Q'), succinyl Co-A synthetase (SCS) (R and R'), succinate dehydrogenase A (SDHA) (S and S'), and mitochondrial malate dehydrogenase-2 (MDH-2) (T and T') are exclusively localized to the mitochondria with no detectable staining seen in the nucleus.

(U) SDHA expression is specifically mitochondrial in late 2-cell stage allowed to develop in vivo until this later time and stained with no ex vivo culture of the embryos.

Data are presented as the means ± SEM. See also Figure S2-4.

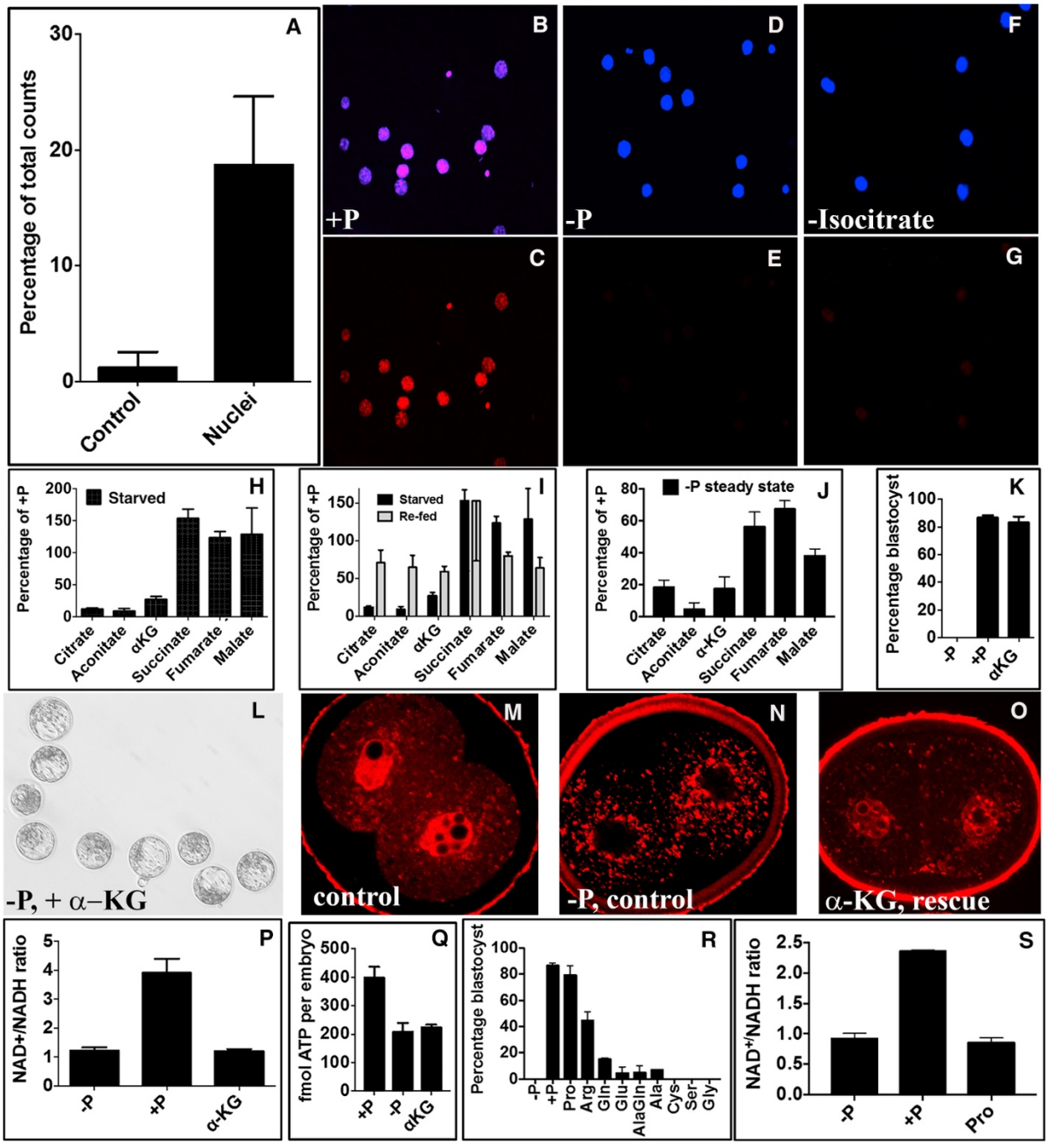
A
Percentage of total counts
30
20
10
0
Control
Nuclei
B
+P
C
D
-P
E
F
-Isocitrate
G
H
Percentage of +P
200
150
100
50
0
Starved
Citrate
Aconitate
αKG
Succinate
Fumarate
Malate
I
Starved
Re-fed
J
-P steady state
α-KG
K
Percentage blastocyst
-P
+P
αKG
L
-P, + α–KG
M
control
N
-P, control
O
α-KG, rescue
P
NAD+/NADH ratio
-P
+P
α-KG
Q
fmol ATP per embryo
+P
-P
αKG
R
Pro
Arg
Gln
Glu
AlaGln
Ala
Cys
Ser
Gly
S
NAD+/NADH ratio
Pro

Fig. 2-5: Functional Characterization of Pyruvate Metabolism in Early Embryos.

(A) Generation of $^{14}CO_2$ from 1-^{14}C-pyruvate by nuclei isolated from two-cell embryos ($p = 0.04$, $n = 3$, each biological replicate comprises 200 nuclei).

(B–G) Isocitrate dehydrogenase activity in nuclei isolated from 2-cell embryos. DAPI (blue) identifies individual nuclei, fluorescence generated by reduction of cyano-tetrazolium dye is indicative of IDH activity and is shown in red.

(B and C) Nuclei ($n = 76$) from +P embryos assayed in complete assay solution are positive for IDH activity (red).

(D and E) Nuclei ($n = 86$) from –P embryos assayed in complete assay solution; absence of signal in (E) confirms pyruvate dependence.

(F and G) Nuclei ($n = 72$) from +P embryos evaluated in assay solution without isocitrate; absence of signal in (F) shows specificity of the assay for IDH that converts isocitrate to α-KG.

(H) 2-cell embryos are starved for 30 min in medium lacking pyruvate, lactate, and glucose. Metabolite levels are compared to control embryos moved for 30 min to a fresh medium including pyruvate but lacking glucose and lactate. Citrate ($p = 0.021$), aconitate ($p = 0.0056$), and alpha-ketoglutarate ($p = 0.0098$) levels in starved samples are significantly lower than in control. In contrast, succinate levels increase ($p = 0.0087$) and malate ($p = 0.35$) and fumarate levels do not change ($p = 0.25$). Data are presented as the means ± SD; $n = 3$; each biological replicate contains more than 200 embryos.

(I) Starved embryos are re-fed with pyruvate for 20 min. Citrate ($p = 0.0039$), aconitate ($p = 0.0038$), and alpha-ketoglutarate ($p = 0.0026$) levels recover (increase) significantly following re-feeding. In contrast, re-feeding has little effect on succinate ($p = 0.99$) and malate ($p = 0.061$) and even caused a significant drop for fumarate ($p = 0.002$). Data are presented as the means ± SD; n = 3; each biological replicate contains more than 200 embryos.

(J) Pyruvate dependence of TCA cycle metabolite levels at 48 hr. The steady-state levels of all metabolites are lower in –P compared with +P control. However, the drop in citrate, aconitate, and α-KG levels is more substantial than that seen for succinate, fumarate, and malate. Data are presented as the means ± SD, n = 3, with each replicate containing at least 100 embryos.

(K–O) Percentage of 120-hr embryos forming blastocysts in a –P medium supplemented with a membrane permeable form of 1 mM α-KG. n = independent isolations with each isolation containing least ten embryos. –P n = 10, +P n = 24, α-KG n = 9 (K). Representative examples of α-KG rescued 96-hr blastocysts (L). (M–O) A fraction of PDH is nuclear in +P (M) but not –P (N) cultured embryos. Nuclear localization is restored in –P medium supplemented with α-KG (O).

(P and Q) Neither the lowered NAD^+/NADH ratio (n = 5 cycling assays) (P) nor the lowered ATP concentration (Q) in pyruvate-deprived embryos is rescued by α-KG supplementation of –P medium even as developmental and nuclear localization defects

(K–O) are completely rescued. p values: +P to –P (p = 0.0199). +P to α-KG (p = 0.0125). –P to α-KG (p = 0.6355). n = 3 independent isolations of embryos.

(R) The percentage of 120-hr embryos forming blastocysts following culture in –P medium supplemented with each indicated amino acid (1 mM). Proline fully and arginine partially rescue the pyruvate defect. n = independent isolations, with each isolation containing least ten embryos. –P n = 10, +P n = 24, proline n = 8, arginine n = 6.

(S) The lowered NAD^+/NADH ratio upon pyruvate deprivation is not rescued by proline supplementation (n = 4 cycling assays). Thus, pyruvate-deprived embryos continue to be under energetic and redox stress with supplemented α-KG, even as the 2-cell block and ZGA are rescued.

Data are presented as the means ± SEM, unless otherwise stated. See also Figure S5.

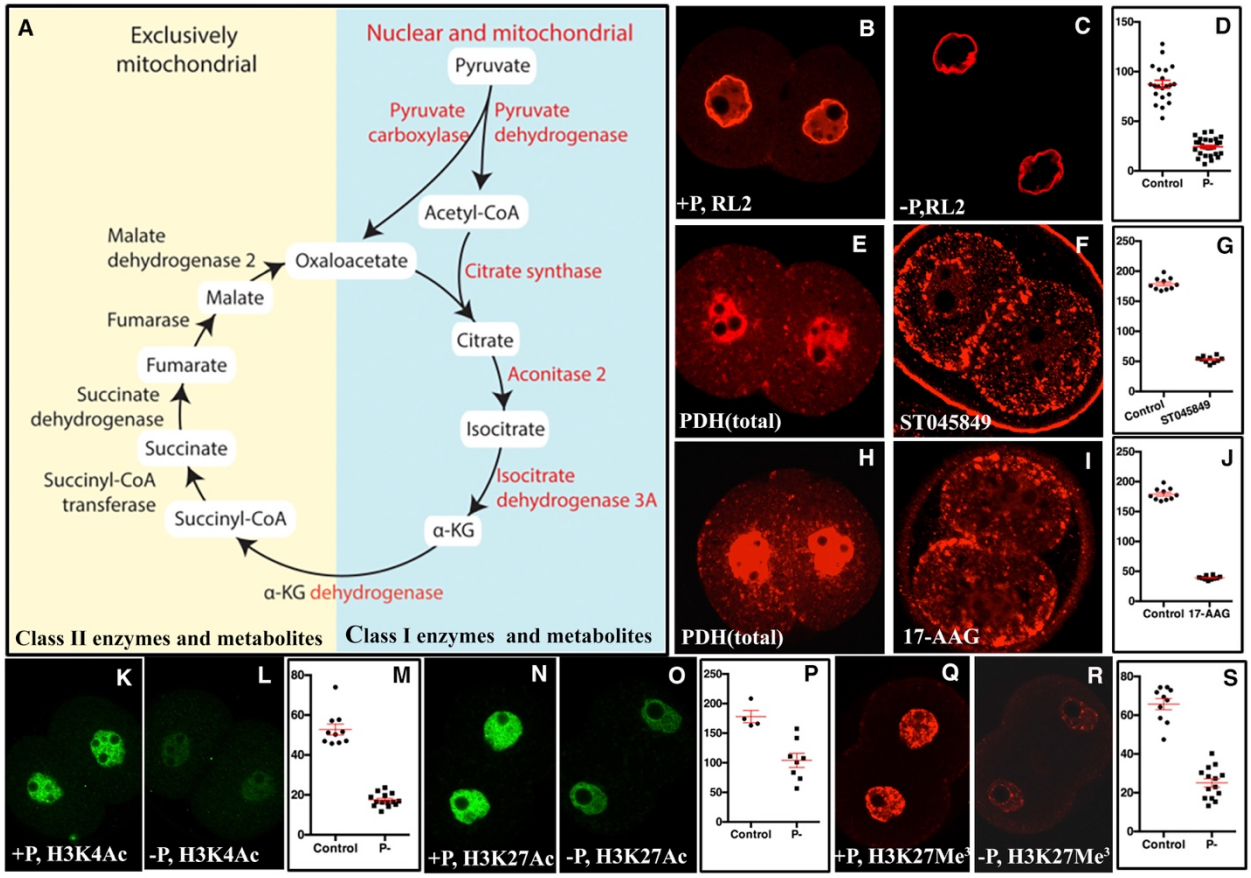

Fig. 2-6: Regulation of Nuclear Import and Its Role in Epigenetic Reprogramming.

(A) Schematic representation of the TCA-cycle-related enzymes (blue background) that are detected in the nucleus (class I enzymes), and their corresponding metabolites (class I metabolites) are essential for ZGA and development beyond 2-cell embryo. Contrasted in yellow background are class II enzymes that are never nuclear, and therefore class II metabolites are less dynamic in their response to starvation and low pyruvate.

(B–D) *O*-linked glycosylation assayed by RL2 antibody in +P shows intra-nuclear and nuclear membrane staining (B). –P embryos (C) show a significant reduction of *O*-glycosylation in the nucleoplasmic component. $p < 0.0001$(nuclei n = 27) (D).

(E–G) The OGT inhibitor, STO45849, blocks nuclear accumulation of PDH (E and F). $p < 0.0001$(nuclei n = 10) (G).

(H–J) 17-AAG specifically blocks HSP90 function and causes loss of nuclear PDH (H and I). $p < 0.0001$(nuclei n = 10) (J). Consequently, both inhibitors cause a 2-cell block (Figures S2-5M–T).

(K–M) Robust H3K4 acetylation is seen in +P (K) but not in –P (L) embryos. $p < 0.0001$ (nuclei n = 14) (M).

(N–P) H3K27 acetylation (N) is partially suppressed in –P medium (O), $p = 0.0027$ (nuclei n = 8) (P).

(Q–S) H3K27 trimethylation in embryos cultured in +P (Q) is significantly reduced in –P (R) medium. $p < 0.0001$ (nuclei n = 14) (S). All other acetylation and trimethylation marks tested remain unchanged (Figures S2-6U–X').

Data are presented as the means ± SEM. See also Figure S2-6.

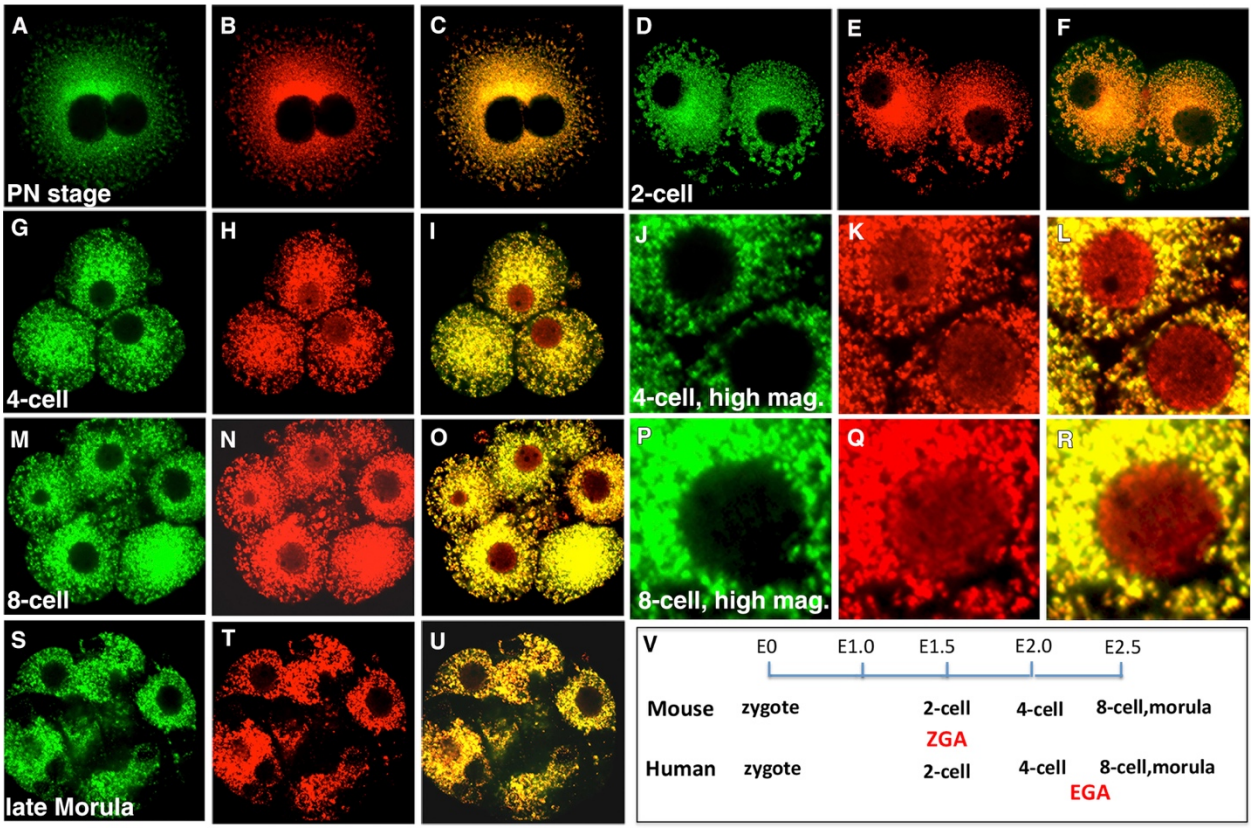

Fig. 2-7: PDH Localization in Preimplantation Human Embryos.

α-PDH^{inactive} staining is shown in green, and α-PDH^{total} staining is in red. In the merged images, overlap (yellow) represents PDH^{inactive} and any non-overlap (red) demarcates PDH^{active}.

(A–F) Unlike in mice (Figure S2-3Q), no nuclear PDH is detected in the human embryo at either the late 1-cell pro-nuclear fusion stage (A-C) or at the 2-cell stage (D–F). PDH is mitochondrial and largely inactive (yellow).

(G–R) At the 4-cell stage (G–L) and 8-cell stage (M–R), embryos show clear evidence for active PDH in the nucleus (red not green), while $PDH^{inactive}$ (red and green) is restricted to the mitochondrion.

(S–U) A single stage later, in the morula, there is no trace of PDH left in the nucleus.

(V) Nuclear localization of PDH, initiating at the late 1-cell stage in mouse and 4-cell stage in humans, closely correlates with the timing of zygotic/embryonic genome activation: 2-cell stage in mouse, 8-cell stage in humans.

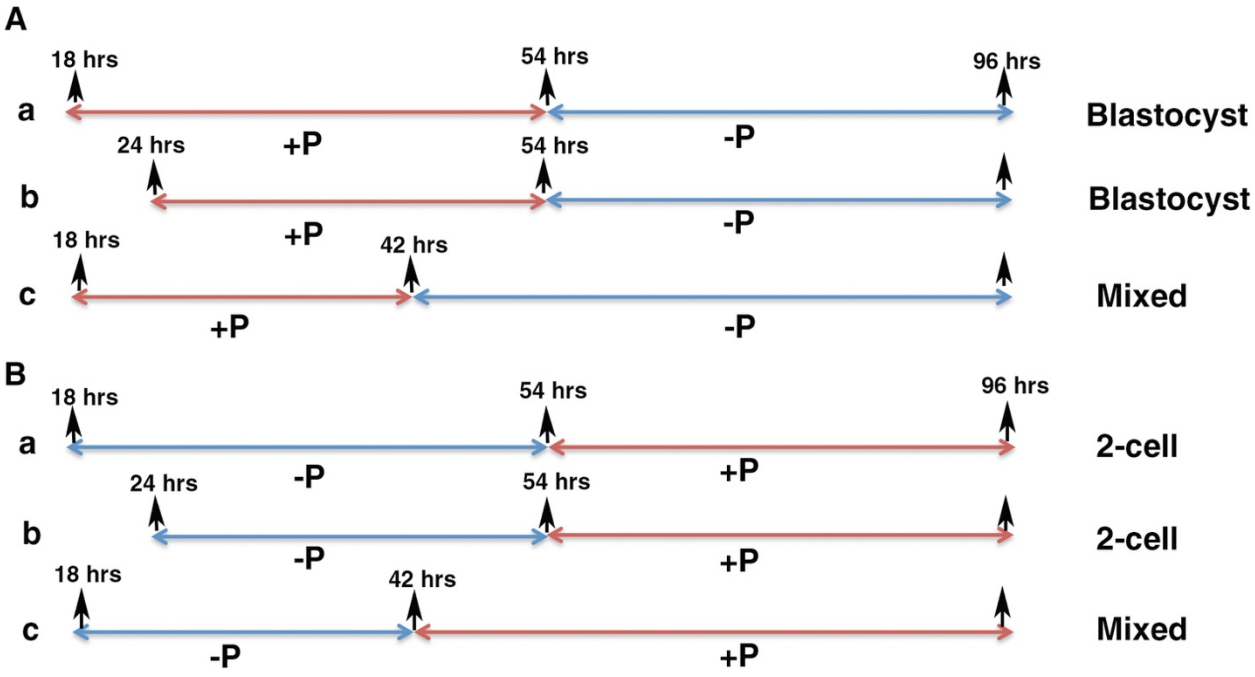

Fig. S2-1: Defining the Critical Period for Pyruvate Requirement, Related to Figure 2-1.

The 30 hr critical time window for pyruvate requirement is shown in Figures 1J and 1K. This interval was determined by transferring embryos from +P to –P culture media (A) and vice versa (B), at the indicated times, shown in this figure.

The following was the distribution of embryos at different stages, for each experiment between 70-80 embryos were used and were cultured for 96 hr.

(A) (a) For the 18-54 hr +P to –P experiment, 70 embryos developed to the blastocysts, 3 were blocked at the 2-cell stage. (b) For the 24-54hrs +P to –P experiment, 72 embryos developed to the blastocyst stage, 6 were arrested at the 1-cell stage and 1-

embryo at the 2-cell stage. (c) For the 18-42 hr +P to –P experiment, 26 embryos were blocked at the 2-cell stage and 44 embryos developed to blastocysts.

(B) (a) 18-54hrs –P to +P experiment, 48 were blocked at 2-cell stage, 14 embryos were blocked at 1-cell stage and 3 embryos at 3-cell stage. (b) For 24-54 hr –P to +P experiment, 54 were blocked at 2-cell stage, 11 embryos were blocked at the 1-cell stage and 6 embryos at the 3-cell stage. (c) for the 18-42hrs –P to +P experiment, 36 embryos were blocked at the 2-cell stage and 44 embryos eventually developed to the blastocysts.

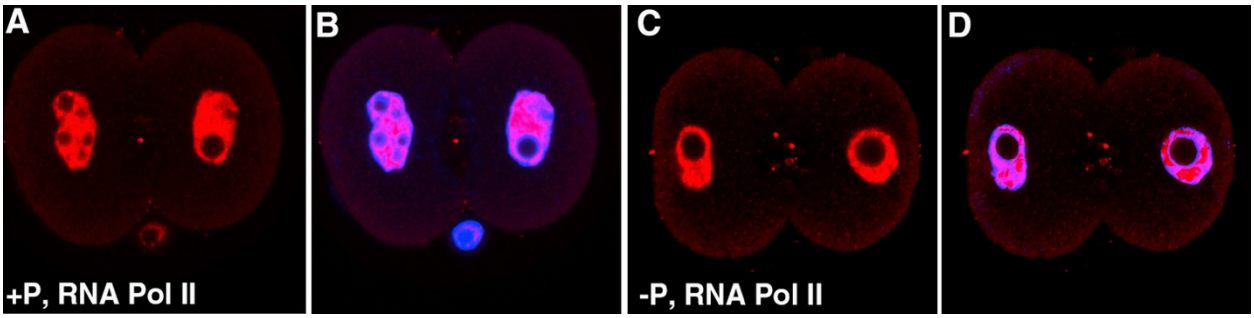

Fig. S2-2: Role of Pyruvate in ZGA, Related to Figure 2-2.

Total RNA Pol II in the nucleus (A-D) is not dependent on exogenously provided pyruvate (Compare with Figures 2-2C-F and 2-2I-N).

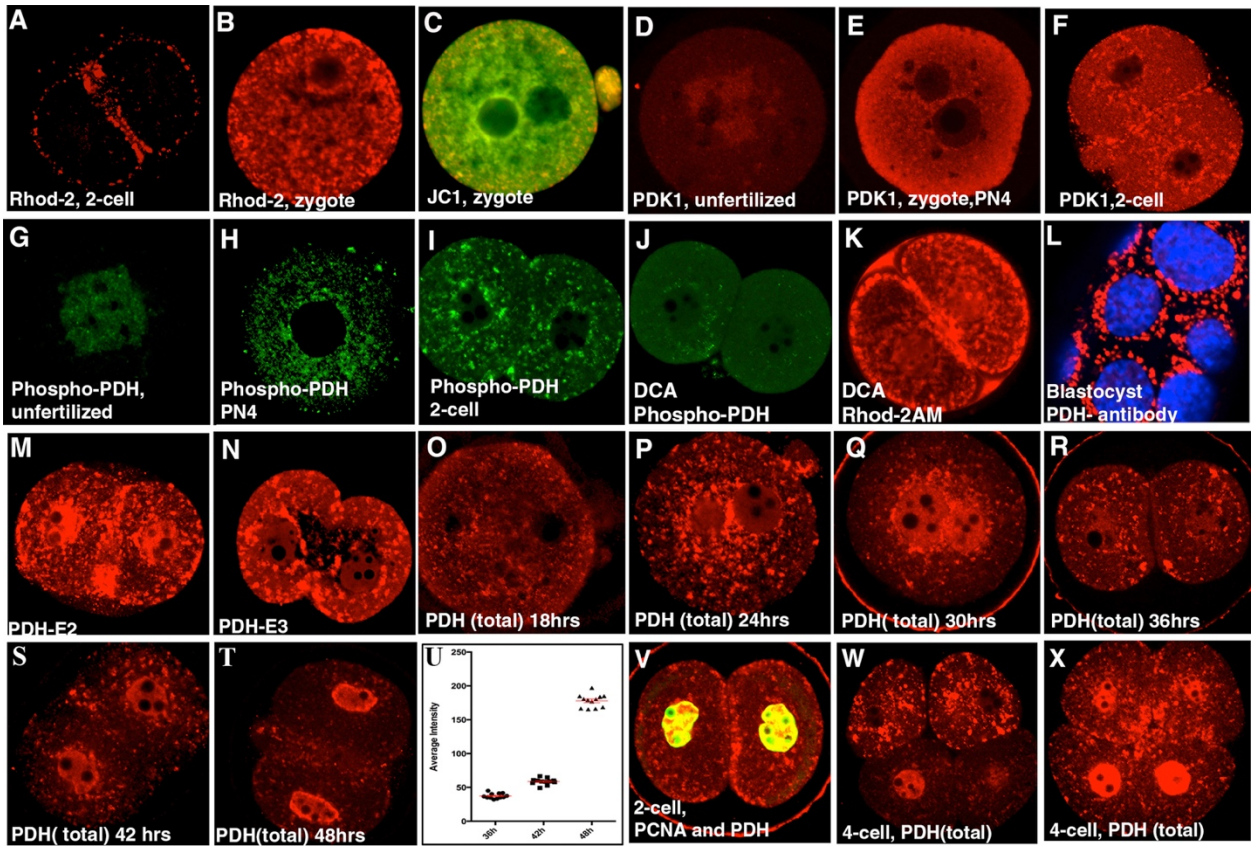

Fig. S2-3: Mitochondrial Activity and Developmental Regulation of PDK and PDH, Related to Figure 2-3.

(A) 2-cell embryo cultured in +P medium stained for Rhod-2AM shows only some small number mitochondria near the plasma membrane have increased levels of Ca2+, hence higher in activity than the ones deeper inside the embryo.

(B) In contrast, in an earlier pro-nuclear stage zygote (PN2), Rhod-2 staining extends to mitochondria throughout the zygote.

(C) JC1 staining of a zygote at PN3 stage (compare with 2-cell stage, Figure 2-3B).

(D–F) PDK1 expression and localization.

PDK1 expression is marginally detectable in unfertilized oocytes (D), becomes more prominent in PN4 zygotes (E) and is prominently mitochondrial at the 2-cell stage (F) At all stages, PDK1 is excluded from the nucleus.

(G–I) Phospho-PDH (inactive) closely parallels PDK1 expression.

p-PDH is first detected in the unfertilized oocyte (G), upregulated in the one cell (PN4) embryo (H), and seen at high levels in the mitochondrion of 2-cell embryos (I). At no stage of development is inactive PDH detected in the nucleus.

(J and K) DCA (Dichloroacetate), a PDK inhibitor causes significant reduction in p-PDH staining in the mitochondria (J) and an increase in Rhod-2AM staining (K).

(L) α-PDH antibody (ab110334) that does not recognize the inactive form of PDH, and is nuclear at the 2-cell stage (Figure 2-3H), is nevertheless, mitochondrial at the later, blastocyst stage. Nuclei are marked with To-Pro.

(M and N) PDH-E2 (M) and PDH-E3 (N), the two subunits of PDH other than the PDH-E1 subunit (shown in Figures 2-3E and 2-3H) are also detected in the nucleus.

(O–U) Developmental profile of PDH^{total} expression. (O) at 18 hr post-HCG PDH expression is exclusively mitochondrial with no visible nuclear staining. (P) at 24 hr post-hCG (PN3), low levels of PDH is visible in the nucleus, but majority of the staining is still in the mitochondria. (Q) at 30 hr post-hCG (PN5) strong nuclear staining is visible with a concomitant decrease of the staining in the mitochondria. (R) 36 hr post-hCG, a just formed 2-cell shows high levels of PDH staining in the mitochondria with very low levels in the nucleus. (S) at 42 hr post-hCG, PDH staining is observed both in the mitochondria and the nucleus. (T) 48 hr post-hCG, PDH staining is high in the nucleus with reduced levels in the mitochondria. (U) Quantitation of the nuclear signal of PDH from 2-cell embryos at 36 (n = 12), 42(n = 8), 48 hr (n = 12) respectively.

(V) 42 hr post-hCG, the 2-cell embryos are in S-phase of cell cycle. PDH staining (red) colocalizes with PCNA (green, S-phase marker) in the nucleus.

(W and X) 4-cell embryos from in vivo collection often show two sister cells with exclusively mitochondrial PDH while the two sister cells, slightly asynchronous with the first pair show significant nuclear staining (W). In other 4-cell embryo example (X) from the same collection, all four cells show dual nuclear and mitochondrial localization of PDH. Data is presented as the means ± SEM.

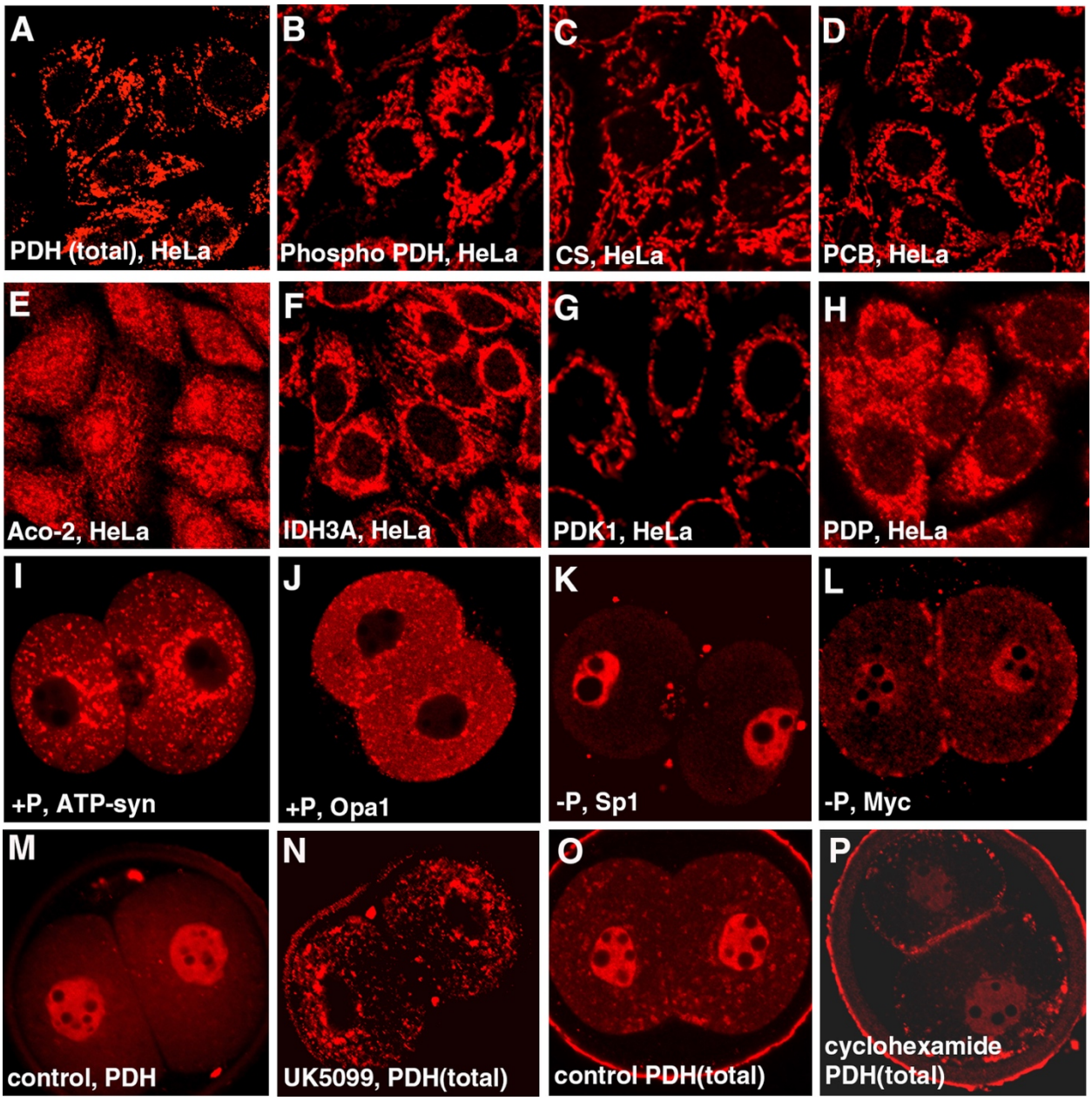

Fig. S2-4: Staining Controls for Figure 4, Related to Figure 2-4.

(A–H) Localization of PDH, PCB and TCA cycle proteins in HeLa cells. confluent HeLa cells were stained for PDHtotal (A) PDHinactive (B), CS (C), PCB (D), Aco-2 (E), IDH3A (F), PDK1 (G) and PDP (H)). With the exception of Aco-2, all other TCA enzymes and

associated proteins are exclusively localized to the mitochondria and not detected in the nucleus.

(I–J) Canonical mitochondrial proteins ATP-Syn (I) and OPA1 (J) are not detected in the nucleus after culture to 54hrs post-hCG.

(K–L) Canonical nuclear proteins, Sp1 (K) and Myc (L) do not lose their nuclear localization when cultured in a –P medium until 54hrs post-hCG.

(M and N). A block in the pyruvate import to the mitochondria by UK5099 which targets specifically mitochondrial pyruvate import blocks nuclear translocation of PDH (N).

(O and P) Blocking protein translation using Cyclohexamide treatment of embryos reduces the level of total PDH in the cell but nuclear PDH is observed under these conditions (P).

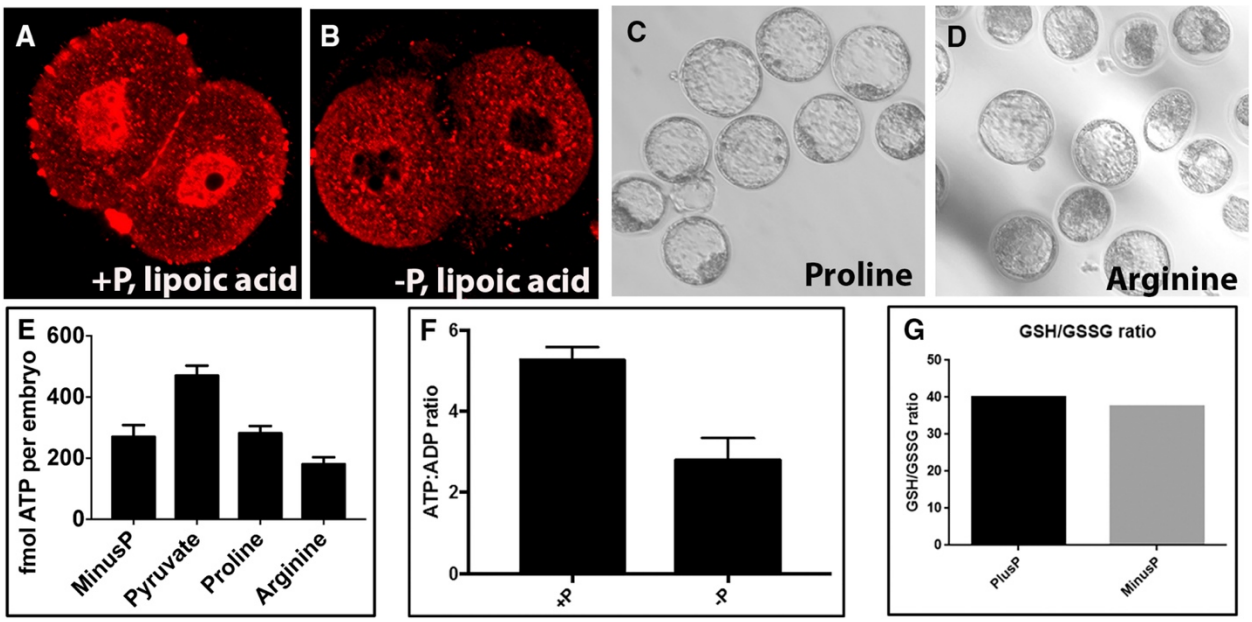

Fig. S2-5: Nuclear Localization and Rescue Experiments, Related to Figure 2-5.

(A and B) Localization of proteins containing a conjugated lipoic acid moiety (A) embryos cultured +P media, (B) embryos in –P media.

(C and D) Representative images of embryos cultured from the zygote stage to the blastocyst in medium containing 1 mM proline or 1 mM arginine.

(E) The ATP levels relative to +P embryos, in two-cell embryos cultured in –P medium or –P medium supplemented with 1 mM proline or 1 mM arginine, respectively. ATP levels are significantly lower in –P, proline and arginine cultured embryos compared to control ($p = 0.0343$, $p = 0.0005$, $p < 0.0001$, respectively, $n = 6$).

(F) The ATP/ADP ratio in embryos cultured in +P and –P media. The ATP/ADP ratio is significantly lower in –P media ($p = 0.0002$, $n = 4$).

(G) The GSH/GSSG ratio in embryos cultured in +P and –P media. The ratio is not significantly different in +P or –P media (n = 4). Data is presented as the means ± SEM.

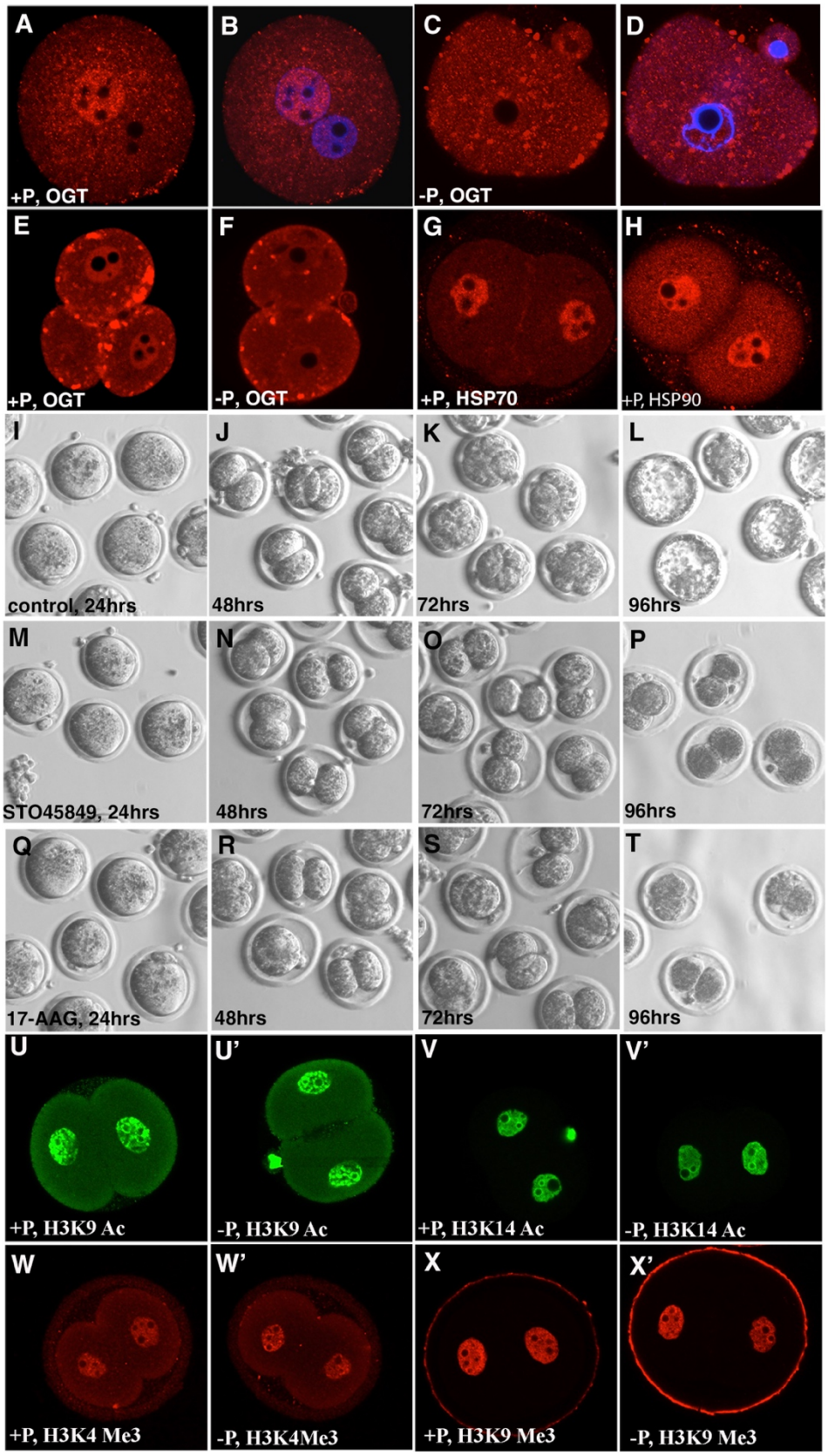
A
+P, OGT
B
C
-P, OGT
D
E
+P, OGT
F
-P, OGT
G
+P, HSP70
H
+P, HSP90
I
control, 24hrs
J
48hrs
K
72hrs
L
96hrs
M
STO45849, 24hrs
N
48hrs
O
72hrs
P
96hrs
Q
17-AAG, 24hrs
R
48hrs
S
72hrs
T
96hrs
U
+P, H3K9 Ac
U'
-P, H3K9 Ac
V
+P, H3K14 Ac
V'
-P, H3K14 Ac
W
+P, H3K4 Me3
W'
-P, H3K4Me3
X
+P, H3K9 Me3
X'
-P, H3K9 Me3

Fig. S2-6: O-glycosylation and Pyruvate-Dependent Nuclear Transport, Related to Figure 2-6.

(A–F) Subcellular localization of OGT in +P and –P medium. OGT is localized to the male pro-nucleus and in the cytoplasm in PN4 zygotes cultured in +P medium (A, B). In –P medium the nuclear localization to the male pro-nucleus is lost (C, D). In the 2-cell stage, OGT is localized to the nucleus and the cytoplasm (E) and its nuclear localization is lost in embryos cultured in –P medium (F).

(G and H) HSP70 (G) and HSP90 (H) are expressed at high levels in 2-cell embryos.

(I–L) Control embryos at different stages of developmental progression.

(M–T) Drug induced blockage of OGT by 1 μM STO45849 (M-P,) and HSP90 function by 10 μM 17-AAG (Q-T), results in 2-cell block. (Compare M-T with control I-L).

(U–X′) Acetylation levels of histone H3K9 and H3K14 (U-V′) and trimethylation levels of H3K4 and H3K8 (W-X′) are not dependent on exogenously provided pyruvate.

Chapter 3: Glycolysis independent glucose metabolism distinguishes TE from ICM fate during mammalian embryogenesis

3.1 Abstract

The mouse embryo undergoes compaction at the 8-cell stage and its transition to 16 cells generates polarity such that the outer apical cells are trophectoderm (TE) precursors and the inner cell mass (ICM) gives rise to the embryo. We report here, that this first cell fate specification event is controlled by glucose. Glucose does not fuel mitochondrial ATP generation and glycolysis is dispensable for blastocyst formation. Furthermore, glucose does not help synthesize amino acids, fatty acids, and nucleobases. Instead, glucose metabolized by the hexosamine biosynthetic pathway (HBP) allows nuclear localization of YAP1. In addition, glucose dependent nucleotide synthesis by the pentose phosphate pathway (PPP), along with sphingolipid (S1P) signaling, activates mTOR and allows translation of *Tfap2c*. YAP1, TEAD4 and TFAP2C interact to form a complex that controls TE-specific gene transcription. Glucose signaling has no role in ICM specification, and this process of developmental metabolism specifically controls TE cell fate.

3.2 Introduction

Following fertilization, the single-cell mouse zygote undergoes three cleavages to generate eight totipotent blastomeres. The 8-cell embryo then undergoes compaction,

which generates tightly connected cells that have barely distinguishable boundaries. As this “compacted morula” transitions to the 16-cell stage, the outer cells acquire an apical (facing outward) and a basal surface, while the resulting inner cells, surrounded by other cells are non-polar. The first cell-specification event that creates two distinct lineages is now evident and the apical blastomeres ultimately differentiate to form the extraembryonic trophectoderm (TE) while the inner cells remain nonpolar and largely contribute to the pluripotent inner cell mass (ICM) at the blastocyst stage (Chazaud and Yamanaka, 2016; Leung et al., 2016; Rossant, 2018; White et al., 2018).

The nutritional requirements of the preimplantation embryo are minimal and are largely derived from the oviductal fluid in which it floats. An in vitro culture medium with only pyruvate, lactate, and glucose as nutrients, but lacking any amino acids, fats or proteins supports normal development through the 4.5 days of preimplantation stages (Biggers et al., 1997; Nagaraj et al., 2017). Growth factors or cytokines from the local environment are not crucial for development as early embryogenesis occurs normally without any proteins added to the medium. In this Chapter, we demonstrate that developmental cues are instead generated by cooperative interactions between metabolite uptake and internal signaling events. The embryo is self-sufficient in producing all necessary components to sustain all early developmental events. We find that this combined metabolic and developmental strategy is different in many respects, and similar in others, to that seen in differentiated cells, stem cells and cancer tissues.

A growth medium lacking pyruvate is unable to support progression beyond the 2-cell stage (Biggers et al., 1965; Biggers et al., 1967; Brown and Whittingham, 1991; Whittingham and Biggers, 1967). In a previous study we showed that pyruvate is essential for initiating zygotic genome activation (ZGA) and also for the selective translocation of key mitochondrial TCA cycle proteins to the nucleus. This unusual process allows epigenetic remodeling and ZGA (Nagaraj et al., 2017). Glucose is not required during this 2-cell stage. Rather, Whittingham and co-workers established a specific requirement for glucose during the compacted morula to blastocyst transition (Brown and Whittingham, 1991). This requirement for glucose is absolute, and glucose cannot be substituted by pyruvate and lactate that fully support the earlier developmental stages (Martin and Leese, 1995). While this might suggest a bioenergetic role of glucose at this stage, early studies reported minimal oxidation of glucose in the mitochondria (Fridhandler, 1961; Fridhandler et al., 1967). Our data support, extend and unify these empirical observations as we investigate how the three major arms of glucose metabolism, glycolysis, pentose phosphate pathway (PPP) and hexosamine biosynthetic pathway (HBP) control developmental signals that allow transition to the blastocyst stage.

3.3 Results

3.3.1 Glucose is Essential for the Morula to Blastocyst Transition

In the absence of glucose, zygotes proceed normally through early cleavage stages, and undergo the compaction process (Figure 3-1A-M), but then block in their development precisely at the compacted 8-cell morula stage (Figure 3-1N). These arrested embryos eventually de-compact and fragment. The term “morula” in this chapter refers to embryos cultured until 78h post injection of hCG injection, which promotes ovulation. In normal media, 78h embryos are at the post-compaction 8-16 cell stage.

2-cell embryos that are mechanically split into single cell components and allowed to develop, proceed through all preimplantation development stages and give rise to a smaller than normal blastocyst (Casser et al., 2017). We confirm that split embryos grown with glucose compact at the 4-cell stage, before progressing to the 8-cell and blastocyst stages (Figure 3-1O, Q). Split embryos grown without glucose also undergo compaction at the 4-cell stage, however they fail to develop beyond 4 cells (Figure 3-1P, Q). Thus reaching the 8-cell stage per se is not an absolute requirement for the arrest caused by a lack of glucose.

To investigate if the process of compaction itself is causal to the morula block, we utilized earlier observations that showed that embryos fail to compact in a Ca2+ free medium (Shirayoshi et al., 1983), and that WGA (wheat germ agglutinin) confers compaction within 1-2 hours at any developmental stage (Johnson, 1986; Watson and Kidder, 1988). We find that while a calcium-free medium with glucose prevents compaction, the embryos proceed past the 8-cell stage (Figure 3-1R, T). In contrast, in

medium that is both glucose and calcium free, the uncompacted embryos also exhibit an 8-cell developmental block (Figure 3-1S, T). Similarly, while WGA applied to a 4-cell embryo always causes rapid compaction (Figure 3-1U, V), such prematurely compacted embryos continue to develop beyond the 8-cell stage only when glucose is added to the medium (Figure 3-1W-Y). We conclude that compaction does not determine the timing of the glucose requirement. The requirement for glucose seems to follow a counting process that follows ZGA, the mechanism for which is as yet unclear.

3.3.2 Glucose Supports Anabolic Processes but not Energy Production

Based on the observation that glucose uptake increases rapidly from the 8-cell to the blastocyst stage (Leese and Barton, 1984), it is tempting to speculate (Johnson et al., 2003) that the 8-cell block is due to lowered energy levels in the absence of glucose. To track the breakdown products of glucose through metabolomic analysis, we incubated embryos throughout their developmental stages in the presence of uniformly-labeled (U-^{13}C) glucose and unlabeled pyruvate/lactate. In a parallel experiment, the medium contained unlabeled (^{12}C) glucose and labeled, U-^{13}C pyruvate/lactate. The two metabolites, pyruvate and lactate, are labeled together since they interconvert rapidly with the carbon on lactate contributing to pyruvate (Brinster, 1967; Landau and Wahren, 1992; Lane and Gardner, 2005). Embryos are allowed to develop until the compacted morula stage and are then analyzed for metabolites by MS. Two different platforms are utilized to separate the metabolites. When properly optimized, the HPLC-MS method combined with the more sensitive ion chromatography system (ICS-MS) detects approximately 100 metabolites from 250 embryos per sample. Each sample is run in

three biological replicates. In spite of the limitations of tissue availability, this technique enables us to map the distribution of glucose and pyruvate/lactate derived carbons with a high degree of confidence. The MS analysis identifies metabolites that derive carbons from glucose as opposed to pyruvate/lactate and also those that are not labeled with either, indicating that they are either maternally derived from the oocyte or endogenously generated from the breakdown of other stored metabolites.

Surprisingly, we find that glucose does not contribute significant levels of carbon to pyruvate as would be expected in cells with active glycolysis (Figure 3-2A, B). More importantly, metabolites derived from the TCA cycle are not labeled by glucose carbons either. Instead, it is exogenously derived-carbons provided by pyruvate/lactate, that solely populate TCA cycle metabolites (Figure 3-2B). For instance, 82% of citrate carbons are derived from pyruvate/lactate, the contribution from glucose, less than 0.5%, is close to our limit of detection. The remaining unlabeled citrate is not derived from exogenously added nutrients. Since citrate carbons are not acquired from glucose, citrate-derived fatty acids, cholesterol and several other lipids would not acquire glucose carbons either.

The TCA cycle metabolite alpha-ketoglutarate (α-KG) shows a labeling pattern that is similar to citrate with 57% of α-KG carbons obtained from pyruvate/lactate, but < 0.05% from glucose (Figure 3-2B). Pyruvate and TCA cycle intermediates, such as α-KG, are the precursors of the four abundant amino acids, alanine, glutamate, glutamine, and aspartate that are extensively labeled by carbons from pyruvate/lactate, but not by

carbons from glucose (Figure 3-2C). The rest of the amino acids are endogenous as they are not labeled by either glucose or pyruvate/lactate (Figure 3-2C). Similarly, neither glucose nor pyruvate/lactate contributes to glutathione, and thus, the entire pool of glutathione in the compacted morula stage is maternally derived. (Figure 3-2C).

The labeling data show that PPP is one of the limited numbers of metabolic pathways that is sourced by glucose at this stage of development. Labeling experiments, including isotopologue analyses, provide evidence that ribose-5-phosphate (R5P) is generated from glucose, but not from pyruvate/ lactate (Figure 3-2D, E). R5P is generated by either the oxidative (via G6P) or the non-oxidative (via F6P) arm of the PPP. The metabolic data suggest no significant contribution of glucose to the base components of purine nucleotides (Figure 3-2F, G; Figure S3-1A). Pyruvate and lactate make some contribution to the carbons used to synthesize pyrimidine bases (uracil 37%, cytosine 19%), while glucose does not label any of the detectable nucleobases (uracil < 0.02%, adenine < 0.05%, cytosine < 0.01% and thymine < 0.03%) (Figure 3-2G, H; Figure S3-1A). The lack of glucose contribution to purine bases is consistent with amino acid labeling data that finds glycine and serine are neither labeled by glucose (both < 0.2%) nor by pyruvate/lactate (both < 0.3%) (Figure 3-2C). In systems with proven contribution of glucose carbons to serine, this amino acid is converted to glycine which in turn contributes to purine bases (Mattaini et al., 2016).

The contribution of exogenous glucose to the ribose group is extensive. For instance, 89% of the UTP in the embryo contains ribose that is derived from glucose,

while pyruvate/lactate do not provide any carbon to UTP ribose (< 0.1%) (Figure 3-2F-H). Thus, much of the UTP, and other uridine containing nucleotides acquire carbons from glucose (Figure 3-2F, G). Adenine and cytidine nucleotides have a larger unlabeled component (indicating maternal origin) compared to the uridine nucleotides (~35 % unlabeled vs ~10 % for uridine, Figure 3-2G). The low maternal contribution of uridine likely reflects a combination of its small pool size and increased turnover (Clegg and Piko, 1977; Hsieh et al., 1979).

Pyrimidine nucleotides contain carbons derived from pyruvate/lactate (Figure 3-2F, H). Given that pyruvate/lactate do not contribute to R5P, we infer that the donated carbons belong to the base and not the ribose sugar. Thus, both glucose and pyruvate/lactate contribute to nucleotide formation at this stage, but they do so by very different pathways. In addition to the PPP, glucose derived carbons are incorporated into HBP related metabolites such as GlcNAc-1P that is labeled by U-^{13}C glucose (Figure S3-1B). To identify the metabolic pathways that are most sensitive to glucose omission, embryos are cultured with and without glucose present in the medium. Metabolites are extracted at the compacted morula stage and analyzed by MS following separation by the two platforms described above. Twenty-four metabolites (of total 106) are highly glucose sensitive and their levels decrease by more than 4-fold in the absence of glucose (Figure 3-2I). Notable examples include direct or indirect derivatives of the upper arm of glycolysis (e.g. G6P), or PPP (e.g. R5P, UTP), or the HBP (e.g. glucosamine and UDP-GlcNAc). Also notable is the observation that pyruvate and lactate remain unaffected in the metabolomic experiments that are discussed above

(Figure 3-2I). In summary, the compacted morula does not use glucose to fuel mitochondrial ATP generation, or provide carbon to synthesize amino acids, fatty acids, and nucleobases. These processes are fueled by pyruvate and lactate or by endogenous sources. Glucose contributes to the synthesis of metabolites derived from HBP and PPP.

3.3.3 Glycolysis, PPP and HBP Play Distinct Roles in Developmental Progression

Loss of function analysis of metabolic enzymes poses a significant challenge in the context of the preimplantation embryo since enzymes involved in glucose metabolism are maternally deposited as proteins and RNA based knockdowns are therefore ineffective. Zygotic null alleles (such as for PDH) often bypass early phenotypes (Johnson et al., 2001), and as essential genes, we expect that maternal nulls in metabolic enzymes will affect prezygotic stages (Johnson et al., 2007). We use two independent strategies to generate loss of function. The first is to use multiple enzyme inhibitors for each pathway. The second and more definitive method is to use the “Trim-Away” (Clift et al., 2017) method, that directly eliminates both maternally deposited and newly synthesized proteins (see STAR methods).

Glycolysis and generation of energy: The inhibitor YZ9 (Figure 3-2A) blocks glycolysis at the level of PFK and therefore inhibits the cascade that generates pyruvate. PPP and HBP are not affected by YZ9 (Seo et al., 2011). Strikingly, continuous inhibition of glycolysis from the 1-cell stage onward has no adverse effect on

progress to the blastocyst stage (Figure 3-3A). While counterintuitive and surprising, this finding of glucose independence of bioenergetics is completely consistent with the 13C-glucose labeling results (Figure 3-2B). In those experiments, we find that it is exogenous pyruvate and not glucose that contributes to the TCA cycle. Consistent with these requirements, addition of YZ9 blocks blastocyst formation if the growth medium lacks pyruvate (Figure 3-3A). A mere lack of pyruvate with no added YZ9 has no effect on blastocyst formation (not shown). Thus, YZ9 indeed functions as a specific inhibitor of glycolysis, but its block at the level of PFK is bypassed when pyruvate feeds into the pathway further downstream and provides carbons to the TCA cycle. We also used a second inhibitor, shikonin, which selectively blocks the function of the embryonic pyruvate kinase M2 (PKM2) (Chen et al., 2011). Similar to the results with YZ9, shikonin has no phenotypic consequence for blastocyst development, but a medium lacking pyruvate but with shikonin added is unable to sustain growth beyond the morula stage even when glucose is present (Figure S3-2A).

Depletion of PKM2 using Trim-Away both establishes the efficacy of the method and validates the inhibitor experiment. We find that the procedure eliminates all of the detectable PKM2 protein (Figure 3-3B, C), and yet PKM2-depleted embryos form blastocysts with the same efficiency as in controls (Figure 3-3D). However, as predicted by the inhibitor analysis, in a medium lacking pyruvate, PKM2 depleted embryos are unable to transition to blastocysts (Figure 3-3D). Taken together, the metabolomic, inhibitor and protein loss data unambiguously establish that core glycolysis, the conversion of glucose to pyruvate, is not essential for the morula to blastocyst transition.

The insensitivity of embryos to the inhibition of PFK or PKM contrasts with the morula block that is caused by treatment with 2-deoxyglucose (2-DG), an inhibitor that blocks early enzymes in glycolysis, including hexokinase (Chen and Gueron, 1992). In addition to glycolysis, 2-DG treatment is expected to affect HBP and the PPP, which are not affected by PFK or PKM inhibition.

Hexosamine biosynthetic pathway (HBP) Treatment of embryos with the commonly used inhibitors of the HBP, such as azaserine and DON that target GFPT1, results in a developmental arrest at the compacted morula stage (Figure S3-2A). However, these inhibitors can, under some circumstances, have off-target effects. More convincingly, we recall from the metabolomic data that UDP-GlcNAc, the critical product generated by HBP, is labeled by ^{13}C-glucose and that its levels decrease in the absence of exogenously added glucose (Figure 3-2I). UDP-GlcNAc facilitates both *N*- and *O*-linked glycosylation. Experiments with tunicamycin that blocks *N*-glycosylation have suggested a role for this protein modification in the morula to blastocyst transition (Surani,1979). However, we later show that although *N*-glycosylation plays a role in the proper localization of apical-domain proteins, its role in cell fate determination is minor, especially in comparison to that of *O*-glycosylation in this process. ST045849 is a widely used, and very specific inhibitor of OGT (*O*-linked *N*-acetyl glucosamine transferase) function (Gross et al., 2005). When added to post ZGA 2-cell embryos, ST045849 causes a developmental arrest at the compacted morula stage (Figure 3-3E). The morphological phenotype of *O*-glycosylation inhibited embryos is indistinguishable from those cultured without glucose. Also, glucosamine (GlcN) is able to bypass and rescue

the morula block caused by lack of glucose (Figure 3-3E) (Pantaleon et al., 2008). These data convincingly show that glucose metabolism by HBP and its role in protein *O*-glycosylation are critically important for the progression to the blastocyst stage.

To be absolutely sure of this important conclusion, we used the Trim-Away method with a specific GFPT1 antibody. This process completely eliminates the protein and also causes a compacted morula block (Figure 3-3F-H). Importantly, GFPT1 protein depleted embryos are rescued to form blastocysts if the growth medium is supplemented with GlcN (Figure 3-3H) that directly generates glucosamine-6-phosphate (GlcN-6P), bypassing the need for an active GFPT1 enzyme.

Pentose phosphate pathway (PPP): ^{13}C labeling by glucose demonstrates that carbons from glucose contribute extensively towards nucleotide ribose sugar biosynthesis suggesting an influx of glucose into the PPP at this stage. Furthermore, the level of nucleotides and PPP metabolites decrease substantially in embryos that are cultured without glucose. We assessed the role of PPP by inhibiting the pathway using 6-aminonicotinamide (6-AN) that is a well-established competitive inhibitor of 6-phosphogluconate dehydrogenase (PGD), the last enzyme of the oxidative PPP (Downs SM, 1998; Kohler et al., 1970; Lange and Proft, 1970). With PPP thus blocked, embryos proceed normally to the 8-cell stage, undergo compaction, but arrest in development at the compacted morula stage and fail to form blastocysts (Figure 3-3I). The terminal product of the PPP pathway includes ribose sugars that contribute to nucleotide

formation. We find that uridine, which is a source of ribose for all nucleotides, added to a medium lacking glucose restores blastocyst formation (Figure 3-3I).

Phenotypically, 6-AN treatment closely recapitulates the developmental block caused by glucose omission. Nevertheless, 6-AN activity could, in principle, extend to other $NADP^+$ dependent enzymes, although within the bounds of glucose metabolism, the PPP arm is heavily impacted. 6-phosphogluconate is an upstream metabolite of 6-AN inhibition in the PPP. We find that it is undetectable in control embryos, but accumulates to very high levels when 6-AN is added (Figure 3-3N).

In order to verify results from inhibitor and metabolomic analyses, we specifically depleted G6PD, the first enzyme in the oxidative branch of the PPP using Trim-Away. A monoclonal antibody that specifically recognizes G6PD is used in these experiments and we find that the G6PD protein becomes undetectable following the procedure (Figure 3-3J, K). Importantly, this manipulation also causes a specific developmental block at the compacted morula stage. To test the specificity of the depletion, we asked if restoring PPP activity downstream of G6PD rescues the phenotype. Partial rescue is observed when the metabolite uridine is used to supplement the culture medium of embryos with depleted G6PD (Figure 3-3L). This rescue is much improved when antioxidants are used along with uridine to remove the extra ROS accumulated when this enzyme function is blocked (Figure 3-3L).

Remarkably, of the metabolites detected in our assay, only 6 decrease substantially (more than 4-fold with $P < 0.05$) upon 6-AN treatment, and these metabolites all contain a nucleotide group (Figure 3-3M). 6-AN treatment almost completely abolishes the synthesis of nucleotide ribose. And also, pyrimidine nucleotides and their derivatives are particularly affected, which may reflect the smaller sizes of these pools and/or increased turnover at this stage of development (Clegg and Piko, 1977; Hsieh et al., 1979). The high sensitivity of UTP production to 6-AN explains why the HBP component UDP-GlcNAc is eliminated when PPP is blocked, while other metabolites belonging to the HBP pathway remain unaffected. This result highlights one of the important mechanisms of cross-talk between PPP and HBP (see below). In summary, the PPP is absolutely critical for the transition from the morula to the blastocyst stage and additionally, these data provide the first hints of a cross-talk between the different arms of the glucose metabolism pathways.

3.3.4 Cross-talk Between PPP and HBP

In the experiments described above we show that exogenously added GlcN or uridine overcomes the morula block seen upon HBP or PPP inhibition respectively (Figure 3-3H, L). However, we also find that both GlcN and uridine can independently overcome the phenotype resulting from glucose depletion (Figure 3-3E, I). Without glucose, both PPP and HBP are nonfunctional and it is puzzling how such an overall deficit in glucose metabolism is rescued by separately adding either GlcN or uridine to the medium.

To investigate this question, we started with a glucose-free medium and supplemented it with fully ^{13}C-labeled glucosamine (U-^{13}C-GlcN). Embryos are allowed to grow to the compacted morula stage, and metabolites are then extracted and the flow of labeled carbons to other metabolites is tracked using MS. We find that GlcN carbons not only populate HBP metabolites (such as GlcN-6P, GlcNAc-P, UDP-GlcNAc), but interestingly, they also populate metabolites associated with the PPP (such as ribose-phosphate) and glycolytic intermediates (such as G6P) in a manner similar to that seen upon glucose labeling (Figure 3-3O, P). Also, similar to glucose, GlcN does not contribute carbons to the TCA cycle, to amino acid synthesis, or to nucleobases (Figure 3-3O, S3-2B-C).

In a similar vein, when uridine whose 5 ribose-ring carbons are labeled with ^{13}C [1',2',3',4',5'-$^{13}C_5$] uridine (the base is not labeled and is ^{12}C) is used instead in the above labeling experiment, carbons from the ribose ring also populate metabolites in a pattern that is virtually identical to that seen when glucose is used for isotope labeling (Figure 3-3O, P). For instance, as with glucose, nucleotide containing metabolites, derived from the PPP, are labeled with uridine, and importantly, so are the intermediates of glycolysis and the HBP (Figure 3-3O, P). We conclude that uridine is metabolized and fed into glycolysis by non-oxidative PPP. As with glucose, TCA cycle intermediates, amino acids and nucleobases are not labeled by uridine (Figure 3-3O, Figure S3-2B-C). In summary, the labeling data show that either uridine or GlcN can supply carbons to all the metabolites that G6P generates and provides evidence for extensive cross-talk between these two arms of the glucose metabolism pathways.

3.3.5 Glucose Metabolism and TE Specification

The first lineage specification event in the developing embryo is later than but not far in time from when glucose becomes essential for further development leading us to investigate whether lineage specification might be causally linked to glucose utilization. We find that the canonical TE specification and maturation transcription factor CDX2 (Strumpf et al., 2005), is not expressed in embryos cultured in a glucose deprived medium or those in which either the HBP or the PPP pathway is specifically inhibited (Figure 3-4A-E). To our surprise, the expression of ICM markers such as OCT4 and NANOG remain entirely unaffected in the absence of glucose, and their expression also remains normal when HBP derived glycosylation or PPP is inhibited (Figure 3-4F-O).

The timing of the 8-cell morula block is earlier than that of the first expression of CDX2 (16-cell stage). To determine if the results above merely represent the fact that glucose deprived embryos simply do not reach the stage that corresponds to CDX2 expression, we decided to cause a cell cycle block by alternative means. The drug aphidicolin inhibits DNA replication, and cytochalasin D inhibits the cleavage of blastomeres. When added to early 8-cell embryos they both cause a compacted 8-cell morula block. In contrast to glucose deprived embryos, however, these 8-cell blocked embryos express normal levels of CDX2 at 78h post hCG (Figure S3-3A, A', D, D'') showing that CDX2 expression does not require the embryos be at the 16-cell stage or later.

A morula blocked embryo never reaches the blastocyst stage which is when the fates of the TE and ICM cells become obvious, not only by markers but also by their cell position and shape. To address whether glucose is important for this later process of TE determination, rather than simply for the expression of a few isolated markers, we developed a chimera assay for our system. In these experiments, two embryos grown independently until the 8-cell stage are mechanically aggregated together to form one larger embryo that is competent to develop further to form “chimeric” blastocysts (Spindle, 1982; Tarkowski, 1961). For fate mapping purposes, one of the embryos is injected at the 1-cell stage with GFP mRNA that is efficiently translated into the green protein and marks all progeny to the blastocyst stage (Figure 3-4P, P’). As control, both the green and the non-green embryos are grown in normal medium containing glucose, fused at the 8-cell stage, and then further grown to the blastocyst stage in a medium lacking glucose. As expected, we find in this control that the blastomeres from the GFP and non-GFP embryos are equally competent to generate ICM and TE lineages (Figure 3-4Q-S, 3-4T-V). For the experimental group, the GFP labeled embryo is allowed to mature from the 1-cell to the early 8-cell stage in a glucose-free medium while an unlabeled embryo is grown in the normal glucose containing medium. The two embryos are aggregated and the resulting chimera is grown in a glucose-free medium until the blastocyst stage (Figure. 3-4Q’-S’, 3-4T’-V’). We find a very significant decrease ($P < 0.0001$) in the propensity of labeled (glucose deprived) vs the unlabeled (glucose supplemented) cells to be CDX2 positive (Figure 3-4Q’-S’, W). There is no significant difference in the total number of ICM or TE cells (regardless of GFP status) in chimeric blastocysts ($P = 1.0$). A few green cells are CDX2 positive and these are often found

directly abutted to an unlabeled neighbor (Figure 3-4Q'-S'), and the simplest explanation is that these cells exchange a glucose derived metabolite with the neighboring cell. The proportion of glucose deprived blastomeres in the TE and ICM are shown in Figure 3-4W, X. Overall, these results provide a strong basis in favor of the hypothesis that the presence of glucose is required for TE fate. The loss of TE related markers is seen at a stage earlier than the actual establishment of the fate. The chimera allows us to grow the embryo until the blastocyst stage when the fate choices are clearly discernible.

3.3.6 Molecular Mechanisms Linking Glucose Metabolism to CDX2 Expression

The next step in this analysis is to probe the molecular mechanism that links CDX2 expression to PPP and HBP, since expression of CDX2 is critically dependent on the proper functioning of these two arms of glucose metabolism. The transcription factors that control CDX2 expression are well characterized in past studies (Cao et al., 2015; Rayon et al., 2014). Principal amongst these are pre-TE specification factors YAP1 and TFAP2C. The active YAP1 (Sasaki, 2017) is nuclearly localized within the pre-TE, but not in the ICM cells. TFAP2C is widely expressed in the 8-cell morula, but is later an important factor in controlling CDX2 in the TE (Auman et al., 2002; Cao et al., 2015; Kuckenberg et al., 2012). We focused on nuclear YAP1 and TFAP2C since they are dramatically affected in the absence of glucose (Figure 3-5A-F) and because these two transcription factor complexes are implicated in the direct control of CDX2 (Cao et al., 2015; Nishioka et al., 2009). Interestingly, TEAD4, the binding partner of YAP1, is also reduced in the absence of glucose, and this low TEAD4 level also likely contributes

to prevent TE fate (Figure S3-4D'-G'). Other transcription factors such as GATA3 and SBNO1 have also been linked to TE fate initiation (Home et al., 2009; Ralston et al., 2010; Watanabe et al., 2017), but since they do not show glucose dependent expression (Figure S3-4A-D), we have not studied these further. The expression of TFAP2C and YAP1 remains high in embryos that are arrested at the 8-cell stage following treatment with aphidicolin or cytochalasin D, and, thus, their expression is not affected by cell cycle arrest at this stage, allowing them to activate CDX2 (Figure S3-3A-F; D"-F").

Loss of HBP and PPP manifest themselves in distinct ways in affecting YAP1 vs TFAP2C. For blocking either pathway, once again, we used the reliable and specific Trim-Away technique. Loss of GFPT1 protein (HBP) using this method blocks nuclear localization of YAP1 (Figure 3-5G, H) but has no effect on TFAP2C expression (Figure 3-5K, L). Whereas, G6PD (PPP) loss by Trim-Away causes complete elimination of TFAP2C expression and YAP1 nuclear localization is also affected (Figure 3-5I, M). We conclude that PPP plays an important role in causing TFAP2C expression, while HBP does not (Figure 3-5K-M). YAP1 nuclear localization is affected when either HBP or PPP is perturbed (Figure 3-5G-I). These data are quantified in (Figure 3-5J, N).

The nuclear localization of YAP1 is severely compromised in embryos in which O-glycosylation is inhibited (Figure S3-4E, G). Recent studies have shown that nuclear localization of YAP1 requires *O*-linked glycosylation at 1-4 specific sites on the protein (Peng et al., 2017; Zhang et al., 2017). This is a likely explanation for loss of YAP1

localization when this protein modification is blocked. However, with technology currently available to us, combined with the limited availability of tissue, we cannot rule out the possibility that loss of *O*-glycosylation affects an unrelated protein that in turn affects YAP1 localization. In either case, it remains clear that HBP related *O*-glycosylation is essential for producing active nuclear YAP1 which is necessary for CDX2 expression. Phosphorylation at serine-127 also correlates with YAP1 activity (Zhao et al., 2007) but is not altered in response to glucose in our assay (Figure 3-6E). Consistent with the Trim-Away data, expression of TFAP2C is not at all altered when HBP-related glycosylation is inhibited (Figure S3-4H, J). The impact of glucose on YAP1, TFAP2C, and CDX2 expression, but not ICM markers, is phenocopied when embryos are treated with 2-DG (Figure S3-3D-F'), which is expected to inhibit glycolysis, PPP and HBP.

Tunicamycin, a drug that blocks the HBP-related process of *N*-linked glycosylation affects the localization of apical membrane proteins (Olden et al., 1979) such as PARD6B (Figure S3-4K, L). However, this perturbation has no effect on either YAP1 nuclear localization or TFAP2C expression (Figure S3-4K-N) suggesting parallel and perhaps a more minor contribution of N-glycosylation compared to its *O*-glycosylation counterpart in the process of TE fate determination. Finally, it is interesting that YAP1 nuclear localization is affected by PPP. Our metabolomic analysis shows a high sensitivity of UDP-GlcNAc levels to PPP inhibition (Figure 3-3B). UTP is one of the most strongly affected metabolites upon PPP loss and is critically important for the generation of UDP-GlcNAc. We propose that the link between PPP and *O*-glycosylation

is through this pathway's ability to generate precursors for UDP-GlcNAc. We are able to demonstrate this to be the likely scenario by supplementing PPP inhibited embryos with uridine, a source of ribose that bypasses the PPP block to replenish UTP levels. However, we note that uridine can also rescue the levels of other nucleotides (Figure 3-3P). Addition of uridine to PPP inhibited embryos fully restores YAP1 nuclear localization (Figure 3-5O-Q), but not TFAP2C expression (Figure 3-5R-T). This further demonstrates the independent regulation of TFAP2C and YAP1. Finally, although we are not yet able to measure the level of *O*-glycosylation on any individual protein, we can demonstrate that bulk *O*-glycosylation levels in the embryo are not only sensitive to HBP, but also to PPP inhibition (Figure S3-4O-R). This supports our hypothesis that UDP-GlcNAc generation is critically dependent on the PPP.

We next investigated the mechanism for the control of TFAP2C by PPP. From ongoing RNA-seq profiling across developmental stages we find that Tfap2c mRNA level reaches a relatively high plateau that remains virtually unchanged between the 4-cell and blastocyst stages (not shown). Importantly, this mRNA expression pattern is not dependent on the presence of glucose in the medium (Figure S3-4A'). Moreover, EU incorporation results demonstrate that global transcription is not abolished in embryos cultured without glucose (Figure S3-4B', C'). In contrast, the TFAP2C protein, barely detectable until the early 8-cell stage, rises abruptly and dramatically at the compacted morula stage (Figure S3-4S-V). Also, the TFAP2C protein is eliminated upon deprivation of glucose (Figure 3-5D-F). These results first suggested to us that the control of TFAP2C expression is likely to be post-transcriptional. To test this hypothesis,

early 8-cell embryos were treated with α-amanitin to inhibit transcription or with cycloheximide to inhibit translation. We find that TFAP2C protein expression remains unaffected in the presence of α-amanitin but is eliminated by cycloheximide (Figure S3-4W-Z). This suggests that glucose metabolism is involved in translational control of Tfap2c at the compacted morula stage.

In search of a mechanism, we turned to an analysis of the mTOR pathway that regulates protein translation in response to nutrients (Kim and Guan, 2019). To determine if mTOR activity is sensitive to glucose availability, embryos are cultured in a glucose deprived medium from the zygote stage and the level of several mTOR targets assayed in the compacted morulae. In addition to immunofluorescence analysis, we also used western blots against several components of the mTOR pathway. A key phosphorylation target of mTOR is 4E-BP1, which enables CAP-dependent translation (Sonenberg and Hinnebusch, 2009). In embryos cultured without glucose, phospho-4E-BP1 expression is abolished (Figure 3-6A-E) as is a second target, phospho-ULK1 (Kim et al., 2011b) (Figure S3-5A, B). Finally, another critical target in the mTOR-related translational cascade is the ribosomal protein S6 (RPS6), and we find that its phosphorylation level is also highly glucose sensitive (Figure 3-6E, S3-5C, D). The sensitivity of mTOR activity to glucose is not related to HBP and is traced entirely to the PPP arm of glucose metabolism (Figure 3-6D).

Four independent mTOR inhibitors, Torin2 and INK128 (Figure 3-6L), as well as rapamycin and PP242 (not shown) cause a block in the transition from the compacted

morula to the blastocyst (Figure 3-6L). Importantly, these mTOR inhibitors abolish TFAP2C (Figure 3-6G-I, K) and CDX2 (Figure S3-5E-G) expression, but OCT4 (Figure S3-5I-K) and YAP1 (Figure S3-5M-O) remain unaffected. The fact that YAP1 nuclear localization is not mTOR dependent lends further support to the idea that the PPP dependence of YAP1 is secondarily related to its role in UDP-GlcNAc generation.

Together, our analysis shows that PPP, but not HBP, is necessary to maintain TFAP2C protein levels, and glucose metabolism does not control *Tfap2c* transcription. PPP inhibition also causes a decrease in the activity of mTOR. Given the well described role of mTOR in translational control, and the data showing that mTOR inhibition also decreases TFAP2C protein levels, we propose a model in which glucose is metabolized through PPP and generates an as yet unidentified metabolite that activates mTOR and thereby translation of Tfap2c. Such a metabolite would represent a nutritional signal for mTOR activation. In this context, we note that amino acids that are typically associated with mTOR activation, or the metabolite SAM, are not glucose dependent (Figure 3-2I) and also that the PI3K/RTK/AKT dependent regulation of mTOR is not involved in this pathway at the 8-cell stage (Figure 3-6L).

The most sensitive set of metabolites to PPP inhibition are nucleotides, and there is precedence in the published literature on unrelated systems of mTOR inhibition upon attenuation of de novo nucleotide biosynthesis in general (Hoxhaj et al., 2017), and guanine nucleotides in particular (Emmanuel et al., 2017). De novo purine synthesis inhibitors (LTX, MTX, Miz, or AVN944), added to the culture medium at the 2-cell stage

cause developmental arrest at the compacted morula stage (8-16 cells). LTX and MTX block early stages of purine synthesis and are expected to decrease both adenine and guanine nucleotide pools. Miz and AVN944 block only the synthesis of guanine nucleotides, and so will specifically deplete the guanine nucleotide pool (GMP, GDP, GTP) (Hoxhaj et al., 2017).

Importantly, the pan-purine nucleotide synthesis inhibitors and the specific inhibitors of guanine nucleotide synthesis also reduce mTOR activity and TFAP2C expression, but do not influence YAP1 nuclear localization (Figure S3-5Q-Y). The pyrimidine synthesis inhibitor leflunomide also causes a morula block, and a modest decrease in TFAP2C expression. Taken together the most parsimonious explanation is that glucose metabolism, via the PPP, is necessary for nucleotide synthesis, and that a decrease in purine nucleotides is sensed by the mTOR pathway that controls the translation of Tfap2c.

3.3.7 Activation of mTOR by a Signaling Lipid

The mechanism linking depletion in GTP and other purines to mTOR activity is likely to be complex and subject to a variety of stress response systems. We focused on defining other mechanisms of mTOR activation during normal development. A non-RTK driven mechanism for mTOR activation involves G-protein coupled receptors (GPCRs) (Puertollano, 2019; Wauson et al., 2013). Expression analysis reveals that a small but specific class of GPCRs that bind the signaling lipid sphingosine-1-phosphate (S1P) is highly represented in the transcriptome across preimplantation stages. These attracted

our attention since S1P receptors are involved in mTOR activation (Liu et al., 2009; Liu et al., 2010; Maeurer et al., 2009; Taniguchi et al., 2012). Of the several S1P receptors expressed in the embryo, the receptor S1PR2 follows a profile that reaches peak expression level at the morula stage.

S1P binds the extracellular domain of S1PR2 and activates its intracellular signaling cascade (Pyne and Pyne, 2010). The compound JTE-013, is a specific antagonist that exclusively prevents S1P binding to S1PR2 (Ohmori et al., 2003; Osada et al., 2002; Parrill et al., 2004). When included in the culture medium at the late 2-cell stage and beyond, JTE-013 causes a compacted morula block, and a marked decrease in phospho-4E-BP1 (Figure S3-5Z) and phospho-RPS6 levels (Figure 3-6F). Moreover, S1PR2 inhibition causes loss of TFAP2C (Figure 3-6J, K) and CDX2 expression (Figure S3-5H), without affecting ICM markers (OCT4 shown in Figure S3-5L), or the nuclear localization of YAP1 (Figure S3-5P). We conclude that in addition to being downstream of the PPP, the mTOR/4E-BP1/RPS6/TFAP2C cascade is also downstream of the S1P/S1PR2 pathway.

Although S1P binds the extracellular domain of the receptor, no lipid is exogenously provided in the medium to initiate such a signal. We therefore reasoned that S1P is synthesized within the embryo, and locally transported out of the cell. Once extruded, this lipid is able to bind the cell-surface receptor. Beyond a threshold ligand concentration, this complex would engage an intracellular signal. Several genes involved in salvage or de novo synthesis of sphingosine as well as sphingosine kinase

(SPHK that phosphorylates sphingosine to form S1P) are all very well represented in the transcriptome at this stage of development. Inhibition of SPHK causes phenotypes that are identical to those seen upon loss of S1PR2 and includes a morula block (Figure 3-6L), loss of p-4E-BP1 (Figure S3-5Z), and TFAP2C (Figure 3-6K). Thus, like glucose, the sphingolipid pathway also regulates mTOR to control TFAP2C.

The molecular details of the link between GPCRs and mTOR are not fully understood, although several past studies have placed Rac1 as an actin cytoskeleton based downstream target of S1P/S1PRs (Gonzalez et al., 2006; Kim et al., 2011a; Reinhard et al., 2017; Zhao et al., 2009). Furthermore, a biochemical analysis has proposed that Rac1 activates mTOR by altering its localization within the cell (Saci et al., 2011). The exact activation mechanism is not the central goal of our study and we focus here instead on testing whether Rac1 is a possible link between lipid signaling and mTOR activation in our system. Following our standard assays we determined that inactivation of Rac1 function (using the Rac1-GEF inhibitor NSC23766) leads to loss of p-RPS6 (Figure 3-6F), p-4E-BP1 (Figure S3-5Z), and TFAP2C (Figure 3-6K) and a failure to make the compact morula to blastocyst transition (Figure 3-6L).

The active, GTP bound form of Rac1 is detected at the apical surface of the 8-cell embryo cultured in the presence of glucose (Figure 3-6M) and as a control we demonstrate that Rac1-GTP staining is lost when the interaction between Rac1 and its GEF is inhibited (Gao et al., 2004) (Figure 3-6N). Rac1-GTP localization is unchanged when mTOR is inhibited (Figure 3-6O). Importantly however, expression of Rac1-GTP is

completely lost when either S1PR2 or SPHK is inhibited (Figure 3-6P, Q). These results place Rac1 upstream of mTOR and as a downstream target of S1P/S1PR2.

Interestingly, in sharp contrast to the dependence of Rac1 on lipid signaling, absence of glucose, or inhibition of either PPP or HBP has no effect on Rac1-GTP expression (Figure 3-6R-T). In other words, Rac1-GTP expression is S1P signaling dependent and glucose signaling independent. Yet, loss of either S1P or glucose (PPP) generated signal causes loss of mTOR function and prevents mTOR-induced downstream translational control. We conclude that S1P/S1PR2/Rac1 and glucose/PPP provide parallel inputs into mTOR. Dual inputs usually regulate mTOR (Gonzalez and Hall, 2017). For the 8-cell embryo, these are the signals generated by a lipid and an unidentified glucose (PPP) metabolism byproduct.

3.3.8 Functional Integration of HBP and PPP Inputs through YAP1/TEAD4 and TFAP2C

The TE specific marker CDX2 is downstream of YAP1 and TFAP2C and published literature has shown that these two proteins participate in the direct transcriptional activation of Cdx2. Consistent with these results, the proposed promoter and enhancer regions of *Cdx2* contain both TEAD4 and TFAP2C binding sites (Cao et al., 2015; Rayon et al., 2014). TEAD4 is the DNA binding component of the YAP1/TEAD4 transcription complex (Li et al., 2010), and we wondered if TFAP2C functions separately or as part of a larger complex with YAP1/TEAD4. This question was addressed using co-immunoprecipitation assays. Due to the very limited availability

of embryos, these experiments are performed in extracts of HEK293T cells that are transfected with and express uniquely tagged YAP1, TFAP2C and TEAD4 proteins. The results from the co-immunoprecipitation assays support a physical association between YAP1/TEAD4 and TFAP2C that would result in the formation of a larger transcription complex (Figure 3-7A-C). Interactions between proteins over-expressed in HEK293T cells are not always physiologically relevant. Therefore, we used a proximity ligation assay (PLA) as a reporter ((Bedzhov and Stemmler, 2015); see STAR methods) for an *in situ* interaction inside the normal embryo. As a control, we establish that the PLA assay can detect known heterodimer formation between YAP1 and TEAD4 and that this interaction is restricted to the TE but not the ICM cell population (Figure 3-7D-F). In the experimental set up, a PLA assay using antibodies against YAP1 and TFAP2C demonstrates that a similar protein level interaction is seen between YAP1 and TFAP2C, also restricted to the TE cells (Figure 3-7G-I).

3.4 Acknowledgments

We thank members of our laboratory for suggestions and support. Yonggang Zhou for RNA seq and Daniel Braas, Johanna ten Hoeve-Scott, Tom Graeber and the UCLA Metabolomics Center for help in metabolomic analysis. Heather Christofk and Hilary Coller provided reagents and advice. We thank Huachun Liu, Wei Liao, Qin An and Wanlu Liu for help with molecular techniques, sequencing and bioinformatic analyses. Bin Gu at Sick Kids, Toronto and Bin Zhao at Zhejiang University provided valuable input.

This work was supported by the NIH Director's Pioneer Award to U.B. (DP1DK098059). U.B. is supported by MOD (1-FY17-788). and NCI (R01CA217608). F.C. by a China Scholarship Council Award and a California Institute for Regenerative Medicine pre-doctoral fellowship. We are grateful to Owen Witte and the Broad Stem Cell Research Center for several innovation awards and for continued support.

3.5 Materials and methods

3.5.1 Mouse embryo culture

All animal care and procedures used in this study are approved by the Animal Regulatory Committee (ARC) of the University of California at Los Angeles (UCLA).

Mouse zygotes and preimplantation embryos were collected from super-ovulated 4-week old C57BL/6J X C3He (Jackson Labs) F1 females. Mice were super-ovulated by peritoneal injection of 7.5 IU of PMSG (Pregnant Mare Serum Gonadotropin) to

stimulate egg production, followed by 7.5 IU of hCG (human Chorionic Gonadotropin) 48h after PMSG. Embryos were obtained by mating the super-ovulated females with C57BL/6 X C3He F1 males. Mating was confirmed by the presence of the vaginal plug. For isolation of fertilized 1-cell zygotes, super-ovulated females were euthanized 18h post hCG and zygotes were dissected out of the ampulla in the oviduct. The embryo cumulus complexes were treated with 300µg/ml of hyaluronidase to disperse the cumulus cells, washed in mKSOM medium without pyruvate/glucose and transferred to the appropriate culture medium (+G or –G) and cultured at 37°C in 5% CO_2. All mouse embryos used in this study were cultured in a modified KSOM medium whose composition is identical to KSOM in salts, glucose, lactate and pyruvate (95mM NaCl, 2.5mM KCl, 0.35mM KH_2PO_4, 0.20mM $MgSO_4$, 25mM $NaHCO_3$, 1.71mM $CaCl_2$, 0.01 mM EDTA, 0.20mM glucose, 10mM lactate, 0.20mM pyruvate) but was devoid of all amino acids and BSA. The medium also contained 0.01% PVA (polyvinyl alcohol). At the 72h post hCG, an embryos growing in our mKSOM medium compacts and contains 8 cells. When grown in –G, the embryos are blocked at 8-cell stage. Most of the staining were performed at 78h post hCG, at which stage the embryos contains 12-16 cells.

3.5.2 Antibody staining for immunofluorescence

Embryos were fixed in 4% paraformaldehyde for 30 min at room temperature, permeabilized for 30 min in PBS with 0.4% Triton (PBST), blocked in PBST with 3% albumin (PBSTA) for 30 min and incubated with the desired primary antibody in PBSTA overnight at 4°C. The following day the embryos were washed in PBST 4 times for 10 min each, blocked with PBSTA, incubated with the appropriate secondary antibody

(1:500 dilution) and DAPI overnight at 4°C. Embryos were washed again 3 times for 10 min each in PBST, deposited on glass slides and mounted in Vectashield (Vector Laboratories) medium. Images were captured using Zeiss LSM700 or LSM880 confocal microscopes.

3.5.3 Inhibitor experiments

Most of the inhibitors were used to treat the embryos in the oil-free condition to avoid the oil absorption at the late 2-cell stage (at 50h post hCG). Early 4-cell stage embryos (56h post hCG) were treated with 20μg/ml WGA for 2 hours to induce premature compaction. Early 8-cell stage embryos (66h post hCG) were treated with 10μM of aphidicolin, 100μg/ml of α-amanitin, or 10μg/ml of cycloheximide for 12 hours (until 78h post hCG) in the oil-free condition. Cytochalasin D (CCD, 500nM) was added to the embryos at the early 8-cell stage (66h) for 8 hours to inhibit cleavage, then transferred to normal medium, allowing them compaction for 4 hours. The embryos treated with different drugs were fixed in 4% paraformaldehyde for 30 min for immunofluorescence.

3.5.4 Measurement of metabolite levels

The metabolites are measured using the procedure described previously (Nagaraj et al., 2017; Sullivan et al., 2018). For samples analyzed under different conditions, embryos were very briefly washed in ice-cold 150mM ammonium acetate, and transferred into 80% methanol. Dried metabolites were re-suspended in 20μl 50% ACN and 5μl was injected for chromatographic separation on the UltiMate 3000 RSLC

(Thermo Scientific) UHPLC system which is coupled to a Thermo Scientific Q Exactive that is run in polarity switching mode. For the UHPLC separation, the mobile phase comprised (A) 5mM NH4AcO, pH 9.9, and (B) ACN. A Luna 3mm NH2 100A (150 × 2.0mm) (Phenomenex) column was used with a 300 µL/min flow-rate. The gradient ran from 15% A to 95% A in 18 min, followed by an isocratic step for 9 min and re-equilibration for 7 min. The remainder of the sample was diluted 2.67-fold and 10µl were applied to a Thermo Scientific Ion Chromatography System (ICS) 5000 that is also coupled to a Thermo Scientific Q Exactive run in negative polarity mode. The gradient ran from 10mM to 90mM KOH over 25 min with a flow rate of 350µl/min. The settings for the HESI-II source were: S-lens 50, Sheath Gas 18, Aux Gas 4, spray heater 320°C, and spray voltage −3.2 kV. Metabolites were identified based on accurate mass (±3 ppm) and retention times of pure standards. Relative amounts of metabolites and contribution of 13C labeled nutrients (following correction for natural abundance) were quantified using TraceFinder 3.3. The data were analyzed using the Prism software package.

3.5.5 Trim-Away Experiment

The Trim-Away procedure was performed as previously described in the published literature with minor modifications (Clift et al., 2018). mCherry-Trim21 mRNA was in vitro transcribed using the HiScribe™ T7 ARCA mRNA Kit according to the manufacturer's instructions. Specific antibodies in carrier-free solution (PBS) were purchased from CST or Abcam as listed above, with the stock concentration 2mg/ml. Then the mCherry-Trim21 mRNA (final concentration: 400ng/µl) and specific antibody

(final concentration: 1mg/ml) were mixed with each other, and the detergent NP-40 so that the final concentration of NP-40 is 0.01%. The mixture is then microinjected into 1-cell (20h hCG) and 2-cell stage (46h hCG) embryos using a FemtoJet microinjector. A negative capacitance is generated using micro-ePORE (World Precision Instruments) to assist the 2-cell microinjection (Gu et al., 2018; Zernicka-Goetz et al., 1997). The developmental progression of these Trim-Away embryos was monitored until 114h post hCG or the embryos were fixed at the morula stage for further immunofluorescence analysis.

3.5.6 Aggregation of chimeric embryos

Embryos were labeled by microinjecting 100ng/µl GFP mRNA at 1-cell stage (20h hCG), and then cultured in +G or –G medium until the morula stage (76h hCG). Unlabeled embryos were cultured in +G medium until the compacted morula stage (76h hCG) as aggregation partners. The zona pellucida was removed by incubating each group of embryos in pre-warmed acidic tyrode's solution for 30 seconds at 37°C. Zona-free embryos from GFP labeled (–G, or +G in the control group) and unlabeled (+G in both control and experimental) groups were immediately aggregated and cultured in small drops (10µl) of –G medium. The drops were covered with mineral oil. Each small drop of the –G medium contains a tiny well that is created by pressing and rotating the tip of a ball-point pen on the surface of the tissue culture dishes. The significance of the difference in the propensity to form TE and ICM cells was determined using a 2X2 contingency table that contained the number GFP labeled and unlabeled cells in each population and was analyzed using Fisher’s exact test.

3.5.7 Cell culture, transfection, immunoprecipitation

HEK293T cells were cultured in DMEM (Invitrogen) containing 10% FBS (Invitrogen) and 50 μg/ml penicillin/streptomycin (P/S). Transfection with Lipofectamine (Invitrogen) was performed according to the manufacturer's instructions.

For immunoprecipitation, HEK293T cells were transfected with the indicated plasmids when cells reached 60%–80% confluence. 48h post-transfection, cells were lysed with mild lysis buffer (50mM HEPES at pH 7.5, 150mM NaCl, 1mM EDTA, 1% NP-40, 10mM pyrophosphate, 10mM glycerophosphate, 50mM NaF, 1.5mM Na3VO4, protease inhibitor mixture (Roche), 1mM DTT, 1mM PMSF). Anti-Flag or anti-Myc antibodies were added to the cell lysate and incubated at 4°C for 2h to bind Flag-YAP1 or Myc-TEAD4, and then Pierce Protein A/G agarose beads were added to precipitate the antibody-substrate complex at 4°C for 2h. GFP-Trap agarose beads were directly added to the cell lysis to precipitate GFP-TFAP2C. The immuno-precipitates were washed three times with mild lysis buffer and boiled with SDS sample buffer before analysis by western blot.

3.5.8 Duolink Proximity Ligation Assay (PLA)

A proximity ligation assay was performed by using the Duolink In Situ Red Starter Kit (Millipore Sigma) to detect the binding between YAP1 and TFAP2C proteins according to the manufacturer's instructions. YAP1/TEAD4 antibodies were used as a positive control. Blastocyst embryos were fixed with 4% paraformaldehyde for 30 min at room temperature, permeabilized for 30 min in PBST, and blocked in pre-heated Duolink blocking solution for 60 min at 37°C. YAP1/TEAD4 or YAP1/ TFAP2C primary

antibodies were diluted at 1:50 in the Duolink antibody diluent, and embryos were incubated in these primary antibodies solution at overnight at 4°C. Then, PLA probe incubation, ligation, amplification processes were performed following the manufacturer's protocol. Finally, embryos were deposited on glass slides and mounted in Vectashield (Vector Laboratories) medium. Images were captured using a Zeiss LSM880 confocal microscope.

3.5.9 Quantification and Statistical Analysis

Statistical parameters are reported in the figures and figure legends. Data is considered significant if $p < 0.05$. Statistical analysis was performed using GraphPad Prism software.

3.5.10 Data and Code Availability

This study did not generate datasets or code.

3.5.11 Key Resources Table

REAGENT or RESOURCE	SOURCE	IDENTIFIER
Antibodies		
Rabbit monoclonal anti-PKM2 (D78A4)	Cell Signaling	Cat #4053
Rabbit monoclonal anti-G6PD (D5D2)	Cell Signaling	Cat #12263
Rabbit monoclonal anti-GFPT1 (EPR4854)	Abcam	Cat #ab236053
Mouse IgG1 monoclonal isotype control (MG1-45)	Abcam	Cat #ab18447
Rabbit IgG monoclonal isotype control (EPR25A)	Abcam	Cat #ab199376
Mouse monoclonal anti-CDX2 (CDX2-88)	Biogenex	Cat #MU392A-UC
Goat anti-OCT4	Santa Cruz	Cat #sc-8628
Rabbit anti-NANOG	ReproCELL	Cat #RCAB0002P-F
Goat anti-SOX2	R&D Systems	Cat #AF2018
Mouse monoclonal anti-YAP (2F12)	Abnova	Cat #H00010413-M01
Mouse monoclonal anti-TFAP2C (6E4/4)	Santa Cruz	Cat #sc-12762
Rabbit anti-TFAP2C	Santa Cruz	Cat #sc-8977

Rabbit anti-p-Ezrin (T567)/Radixin (T564)/Moesin (T558)	Cell Signaling	Cat #3141
Rabbit anti-SBNO1	Abcam	Cat #ab122789
Rabbit anti-GATA3	Santa Cruz	Cat #sc-9009
Rabbit anti-PARD6B	Santa Cruz	Cat #sc-67393
Mouse monoclonal anti-O-Linked N-Acetylglucosamine (RL2)	Abcam	Cat #ab2739
Rabbit monoclonal anti-pT37/46-4E-BP1 (236B4)	Cell Signaling	Cat #2855S
Rabbit monoclonal anti-pS235/236-RPS6 (D57.2.2E)	Cell Signaling	Cat #4858
Rabbit monoclonal anti-mTOR (7C10)	Cell Signaling	Cat #2983
Rabbit monoclonal anti-Tuberin/TSC2 (D93F12)	Cell Signaling	Cat #4308
Rabbit monoclonal anti-pS473-AKT (Ser473) (D9E)	Cell Signaling	Cat #4060
Rabbit anti-pS127-YAP	Cell Signaling	Cat #4911
Rabbit anti-pS757-ULK1	Cell Signaling	Cat #6888
Mouse monoclonal anti-active Rac1-GTP	NewEast	Cat #26903
Chemicals, Peptides, and Recombinant Proteins		
Lectin from Triticum vulgaris (wheat)–WGA (20µg/ml)	Sigma-Aldrich	Cat # L0636
YZ9 (1µM)	Cayman Chemical	Cat #15352
ST045849 (0.8µM)	TimTec	Cat #ST045849
Tunicamycin (5µM)	Sigma-Aldrich	Cat #T7765
6-Aminonicotinamide (6-AN) (2µM)	Sigma-Aldrich	Cat #A68203
N-Acetylcysteine (NAC) (1mM)	Sigma-Aldrich	Cat #A7250
Hypotaurine (1mM)	Sigma-Aldrich	Cat #H1384
Shikonin (1µM)	Cayman Chemical	Cat #14751
Azaserine (5µM)	Sigma-Aldrich	Cat #A4142
6-Diazo-5-oxo-L-norleucine (DON) (20µM)	Sigma-Aldrich	Cat #D2141
2-Deoxy-D-glucose (1µM)	Sigma-Aldrich	Cat #D8375
Aphidicolin (10µM)	Cayman Chemical	Cat #14007
Cytochalasin D (500nM)	Cayman Chemical	Cat #11330
α-Amanitin (100µg/ml)	Cayman Chemical	Cat #17898
Cycloheximide (10µg/ml)	Cayman Chemical	Cat #14126
Torin2 (10nM)	Cayman Chemical	Cat #14185
INK128 (100nM)	Cayman Chemical	Cat #11811
JTE013 (1µM)	Tocris	Cat #2392
SKI-II (0.8µM)	Echelon	Cat #B-0024
NSC26722 (100µM)	Tocris	Cat #2161
BYL719 (1µM)	Cayman Chemical	Cat #16986
BKM120 (0.5µM)	Cayman Chemical	Cat #11587
GDC0941 (0.5µM)	Cayman Chemical	Cat #11600
TGX221 (0.5µM)	Cayman Chemical	Cat #10007349
BX912 (100nM)	Cayman Chemical	Cat #14708
GSK2334470 (50nM)	Cayman Chemical	Cat #18095
MK2206 (200nM)	Cayman Chemical	Cat #11593
Lometrexol (250-500nM)	Cayman Chemical	Cat #18049
Methotrexate (200nM)	Cayman Chemical	Cat #13960
Mizoribine (1µM)	Cayman Chemical	Cat #23128
AVN-944 (50nM)	Cayman Chemical	Cat #21284
Leflunomide (5µM)	Cayman Chemical	Cat #14860

U-$^{13}C_6$-D-Glucose (200μM)	Cambridge Isotope Laboratories	Cat #CLM-1396-PK
U-$^{13}C_3$-Pyruvic Acid Sodium Salt (200μM)	Toronto Research Chemicals	Cat #P998904
U-$^{13}C_3$-L-(+)-Lactic Acid Sodium Salt (5mM)	Toronto Research Chemicals	Cat #L113507
[1', 2', 3', 4', 5'-$^{13}C_5$]-Uridine (200μM)	Omicron	Cat #NUC-034
U-$^{13}C_6$-D-Glucosamine hydrochloride	Omicron	Cat #GLC-091
Pregnant Mare Serum Gonadotropin (PMSG)	ProSpec	Cat #hor-272
Chorionic gonadotropin human (hCG)	Sigma-Aldrich	Cat #CG10
Critical Commercial Assays		
Click-iT™ RNA Alexa Fluor™ 594 Imaging Kit	Thermo Scientific	Cat #C10330
Duolink® In Situ PLA® Probe Anti-Rabbit PLUS	Sigma-Aldrich	Cat #DUO92002
Duolink® In Situ PLA® Probe Anti-Mouse MINUS	Sigma-Aldrich	Cat #DUO92004
Duolink® In Situ Detection Reagents Red	Sigma-Aldrich	Cat #DUO92008
Duolink® In Situ Wash Buffers, Fluorescence	Sigma-Aldrich	Cat #DUO82049
Experimental Models: Cell Lines		
HEK293T	This lab	N/A
Mouse: embryo culture	This lab	N/A
Experimental Models: Organisms/Strains		
Mouse: B6C3F1/J	Jackson Laboratory	Stock No: 100010
Oligonucleotides		
CleanCap EGFP mRNA (5moU)	TriLink	Cat #L-7201
mCherry-mTrim21 mRNA	This lab	N/A
Recombinant DNA		
pGEMHE-mCherry-mTrim21	Addgene	Cat #105522
pCMV6-*Yap1*	OriGene	Cat #MR226049
pCMV6-*Tead4* (ATT)	OriGene	Cat #MR219506
pCMV6-*Tfap2c*	OriGene	Cat #MR207174
pCMV6-Flag-*Yap1*	This lab	N/A
pCMV6-Myc-*Tead4* (ATG)	This lab	N/A
pQCMV-GFP-*Tfap2c*	This lab	N/A
Software and Algorithms		
Graphpad Prism 7	GraphPad	http://www.graphpad.com/
TraceFinder 3.3	Thermo Scientific	N/A
ImageJ	NIH	https://imagej.nih.gov/ij/
MetaboAnalyst	(Xia and Wishart, 2011)	https://www.metaboanalyst.ca/
Other		
WPI MICRO-ePORE	World Precision Instruments	N/A

3.6 References

Auman, H.J., Nottoli, T., Lakiza, O., Winger, Q., Donaldson, S., and Williams, T. (2002). Transcription factor AP-2γ is essential in the extra-embryonic lineages for early postimplantation development. Development 129, 2733.

Bedzhov, I., and Stemmler, M.P. (2015). Applying the proximity ligation assay (PLA) to mouse preimplantation embryos for identifying protein-protein interactions in situ. Methods Mol Biol 1233, 57-64.

Biggers, J.D., Summers, M.C., and McGinnis, L.K. (1997). Polyvinyl alcohol and amino acids as substitutes for bovine serum albumin in culture media for mouse preimplantation embryos. Hum Reprod Update 3, 125-135.

Brinster, R.L. (1967). Carbon dioxide production from glucose by the preimplantation mouse embryo. Experimental cell research 47, 271-277.

Brown, J.J., and Whittingham, D.G. (1991). The roles of pyruvate, lactate and glucose during preimplantation development of embryos from F1 hybrid mice in vitro. Development 112, 99-105.

Cao, Z., Carey, T.S., Ganguly, A., Wilson, C.A., Paul, S., and Knott, J.G. (2015a). Transcription factor AP-2gamma induces early Cdx2 expression and represses HIPPO signaling to specify the trophectoderm lineage. Development 142, 1606-1615.

Casser, E., Israel, S., Witten, A., Schulte, K., Schlatt, S., Nordhoff, V., and Boiani, M. (2017). Totipotency segregates between the sister blastomeres of two-cell stage mouse embryos. Scientific reports 7, 8299-8299.

Chazaud, C., and Yamanaka, Y. (2016). Lineage specification in the mouse

preimplantation embryo. Development 143, 1063-1074.

Chen, J., Xie, J., Jiang, Z., Wang, B., Wang, Y., and Hu, X. (2011). Shikonin and its analogs inhibit cancer cell glycolysis by targeting tumor pyruvate kinase-M2. Oncogene 30, 4297-4306.

Chen, W., and Gueron, M. (1992). The inhibition of bovine heart hexokinase by 2-deoxy-D-glucose-6-phosphate: characterization by 31P NMR and metabolic implications. Biochimie 74, 867-873.

Clegg, K.B., and Piko, L. (1977). Size and specific activity of the UTP pool and overall rates of RNA synthesis in early mouse embryos. Dev Biol 58, 76-95.

Clift, D., McEwan, W.A., Labzin, L.I., Konieczny, V., Mogessie, B., James, L.C., and Schuh, M. (2017). A Method for the Acute and Rapid Degradation of Endogenous Proteins. Cell 171, 1692-1706.e1618.

Clough, J.R., and Whittingham, D.G. (1983). Metabolism of [14C]glucose by postimplantation mouse embryos in vitro. J Embryol Exp Morphol 74, 133-142.

Downs SM, H.P., Leese HJ (1998). Meiotic induction in cumulus cell-enclosed mouse oocytes: involvement of the pentose phosphate pathway. Biol Reprod 58, 1084-1094.

Emmanuel, N., Ragunathan, S., Shan, Q., Wang, F., Giannakou, A., Huser, N., Jin, G., Myers, J., Abraham, R.T., and Unsal-Kacmaz, K. (2017). Purine Nucleotide Availability Regulates mTORC1 Activity through the Rheb GTPase. Cell Reports 19, 2665-2680.

Faubert, B., Li, K.Y., Cai, L., Hensley, C.T., Kim, J., Zacharias, L.G., Yang, C., Do, Q.N., Doucette, S., Burguete, D., et al. (2017). Lactate Metabolism in Human Lung

Tumors. Cell 171, 358-371 e359.

Fridhandler, L. (1961). Pathways of glucose metabolism in fertilized rabbit ova at various pre-implantation stages. Experimental cell research 22, 303-316.

Fridhandler, L., Wastila, W.B., and Palmer, W.M. (1967). The Role of Glucose in Metabolism of the Developing Mammalian Preimplantation Conceptus. Fertility and Sterility 18, 819-830.

Gao, Y., Dickerson, J.B., Guo, F., Zheng, J., and Zheng, Y. (2004). Rational design and characterization of a Rac GTPase-specific small molecule inhibitor. Proc Natl Acad Sci U S A 101, 7618-7623.

Gonzalez, A., and Hall, M.N. (2017). Nutrient sensing and TOR signaling in yeast and mammals. EMBO J 36, 397-408.

Gonzalez, E., Kou, R., and Michel, T. (2006). Rac1 modulates sphingosine 1-phosphate-mediated activation of phosphoinositide 3-kinase/Akt signaling pathways in vascular endothelial cells. The Journal of biological chemistry 281, 3210-3216.

Gross, B.J., Kraybill, B.C., and Walker, S. (2005). Discovery of O-GlcNAc transferase inhibitors. J Am Chem Soc 127, 14588-14589.

Home, P., Ray, S., Dutta, D., Bronshteyn, I., Larson, M., and Paul, S. (2009). GATA3 is selectively expressed in the trophectoderm of peri-implantation embryo and directly regulates Cdx2 gene expression. The Journal of biological chemistry 284, 28729-28737.

Hoxhaj, G., Hughes-Hallett, J., Timson, R.C., Ilagan, E., Yuan, M., Asara, J.M., Ben-Sahra, I., and Manning, B.D. (2017). The mTORC1 Signaling Network Senses

Changes in Cellular Purine Nucleotide Levels. Cell reports 21, 1331-1346.

Hsieh, B., Chi, M.M., Knor, J., and Lowry, O.H. (1979). Enzymes of glycogen metabolism and related metabolites in preimplantation mouse embryos. Dev Biol 72, 342-349.

Hui, S., Ghergurovich, J.M., Morscher, R.J., Jang, C., Teng, X., Lu, W., Esparza, L.A., Reya, T., Le, Z., Yanxiang Guo, J., et al. (2017). Glucose feeds the TCA cycle via circulating lactate. Nature 551, 115-118.

Johnson, L.V. (1986). Wheat germ agglutinin induces compaction- and cavitation-like events in two-cell mouse embryos. Dev Biol 113, 1-9.

Johnson, M.T., Freeman, E.A., Gardner, D.K., and Hunt, P.A. (2007). Oxidative Metabolism of Pyruvate Is Required for Meiotic Maturation of Murine Oocytes In Vivo1. Biology of Reproduction 77, 2-8.

Johnson, M.T., Mahmood, S., Hyatt, S.L., Yang, H.-S., Soloway, P.D., Hanson, R.W., and Patel, M.S. (2001). Inactivation of the Murine Pyruvate Dehydrogenase (Pdha1) Gene and Its Effect on Early Embryonic Development. Molecular Genetics and Metabolism 74, 293-302.

Johnson, M.T., Mahmood, S., and Patel, M.S. (2003). Intermediary metabolism and energetics during murine early embryogenesis. The Journal of biological chemistry 278, 31457-31460.

Kim, E.S., Kim, J.S., Kim, S.G., Hwang, S., Lee, C.H., and Moon, A. (2011a). Sphingosine 1-phosphate regulates matrix metalloproteinase-9 expression and breast cell invasion through S1P3-Galphaq coupling. J Cell Sci 124, 2220-2230.

Kim, J., and Guan, K.-L. (2019). mTOR as a central hub of nutrient signalling and cell

growth. Nature Cell Biology 21, 63-71.

Kim, J., Kundu, M., Viollet, B., and Guan, K.L. (2011b). AMPK and mTOR regulate autophagy through direct phosphorylation of Ulk1. Nat Cell Biol 13, 132-141.

Kohler, E., Barrach, H., and Neubert, D. (1970). Inhibition of NADP dependent oxidoreductases by the 6-aminonicotinamide analogue of NADP. FEBS Lett 6, 225-228.

Kuckenberg, P., Kubaczka, C., and Schorle, H. (2012). The role of transcription factor Tcfap2c/TFAP2C in trophectoderm development. Reproductive BioMedicine Online 25, 12-20.

Landau, B.R., and Wahren, J. (1992). Nonproductive exchanges: the use of isotopes gone astray. Metabolism 41, 457-459.

Lane, M., and Gardner, D.K. (2005). Mitochondrial malate-aspartate shuttle regulates mouse embryo nutrient consumption. The Journal of biological chemistry 280, 18361-18367.

Lange, K., and Proft, E.R. (1970). Inhibition of the 6-phosphogluconate dehydrogenase in the rat kidney by 6-aminonicotinamide. Naunyn Schmiedebergs Arch Pharmakol 267, 177-180.

Leese, H.J., and Barton, A.M. (1984). Pyruvate and glucose uptake by mouse ova and preimplantation embryos. Journal of reproduction and fertility 72, 9-13.

Leung, C.Y., Zhu, M., and Zernicka-Goetz, M. (2016). Polarity in Cell-Fate Acquisition in the Early Mouse Embryo. Curr Top Dev Biol 120, 203-234.

Li, Z., Zhao, B., Wang, P., Chen, F., Dong, Z., Yang, H., Guan, K.L., and Xu, Y. (2010). Structural insights into the YAP and TEAD complex. Genes Dev 24, 235-240.

Liu, G., Burns, S., Huang, G., Boyd, K., Proia, R.L., Flavell, R.A., and Chi, H. (2009). The receptor S1P1 overrides regulatory T cell-mediated immune suppression through Akt-mTOR. Nat Immunol 10, 769-777.

Liu, G., Yang, K., Burns, S., Shrestha, S., and Chi, H. (2010). The S1P(1)-mTOR axis directs the reciprocal differentiation of T(H)1 and T(reg) cells. Nat Immunol 11, 1047-1056.

Maeurer, C., Holland, S., Pierre, S., Potstada, W., and Scholich, K. (2009). Sphingosine-1-phosphate induced mTOR-activation is mediated by the E3-ubiquitin ligase PAM. Cell Signal 21, 293-300.

Martin, K.L., and Leese, H.J. (1995). Role of glucose in mouse preimplantation embryo development. 40, 436-443.

Mattaini, K.R., Sullivan, M.R., and Vander Heiden, M.G. (2016). The importance of serine metabolism in cancer. The Journal of cell biology 214, 249-257.

Nagaraj, R., Sharpley, M.S., Chi, F., Braas, D., Zhou, Y., Kim, R., Clark, A.T., and Banerjee, U. (2017). Nuclear Localization of Mitochondrial TCA Cycle Enzymes as a Critical Step in Mammalian Zygotic Genome Activation. Cell 168, 210-223 e211.

Nishioka, N., Inoue, K.-i., Adachi, K., Kiyonari, H., Ota, M., Ralston, A., Yabuta, N., Hirahara, S., Stephenson, R.O., Ogonuki, N., et al. (2009). The Hippo Signaling Pathway Components Lats and Yap Pattern Tead4 Activity to Distinguish Mouse Trophectoderm from Inner Cell Mass. Developmental Cell 16, 398-410.

Ohmori, T., Yatomi, Y., Osada, M., Kazama, F., Takafuta, T., Ikeda, H., and Ozaki, Y. (2003). Sphingosine 1-phosphate induces contraction of coronary artery smooth

muscle cells via S1P2. Cardiovasc Res 58, 170-177.

Olden, K., Pratt, R.M., Jaworski, C., and Yamada, K.M. (1979). Evidence for role of glycoprotein carbohydrates in membrane transport: specific inhibition by tunicamycin. Proc Natl Acad Sci U S A 76, 791-795.

Osada, M., Yatomi, Y., Ohmori, T., Ikeda, H., and Ozaki, Y. (2002). Enhancement of sphingosine 1-phosphate-induced migration of vascular endothelial cells and smooth muscle cells by an EDG-5 antagonist. Biochem Biophys Res Commun 299, 483-487.

Pantaleon, M., Scott, J., and Kaye, P. (2008). Nutrient Sensing by the Early Mouse Embryo: Hexosamine Biosynthesis and Glucose Signaling During Preimplantation Development, Vol 78.

Parrill, A.L., Sardar, V.M., and Yuan, H. (2004). Sphingosine 1-phosphate and lysophosphatidic acid receptors: agonist and antagonist binding and progress toward development of receptor-specific ligands. Semin Cell Dev Biol 15, 467-476.

Peng, C., Zhu, Y., Zhang, W., Liao, Q., Chen, Y., Zhao, X., Guo, Q., Shen, P., Zhen, B., Qian, X., et al. (2017). Regulation of the Hippo-YAP Pathway by Glucose Sensor O-GlcNAcylation. Molecular Cell 68, 591-604.e595.

Puertollano, R. (2019). GPCRs join the mTORC1 regulatory network. Nat Cell Biol 21, 538-539.

Pyne, N.J., and Pyne, S. (2010). Sphingosine 1-phosphate and cancer. Nat Rev Cancer 10, 489-503.

Ralston, A., Cox, B.J., Nishioka, N., Sasaki, H., Chea, E., Rugg-Gunn, P., Guo, G.,

Robson, P., Draper, J.S., and Rossant, J. (2010). Gata3 regulates trophoblast development downstream of Tead4 and in parallel to Cdx2. Development 137, 395-403.

Rayon, T., Menchero, S., Nieto, A., Xenopoulos, P., Crespo, M., Cockburn, K., Canon, S., Sasaki, H., Hadjantonakis, A.K., de la Pompa, J.L., et al. (2014). Notch and hippo converge on Cdx2 to specify the trophectoderm lineage in the mouse blastocyst. Dev Cell 30, 410-422.

Reinhard, N.R., Mastop, M., Yin, T., Wu, Y., Bosma, E.K., Gadella, T.W.J., Jr., Goedhart, J., and Hordijk, P.L. (2017). The balance between Galphai-Cdc42/Rac and Galpha12/13-RhoA pathways determines endothelial barrier regulation by sphingosine-1-phosphate. Mol Biol Cell 28, 3371-3382.

Rossant, J. (2018). Genetic Control of Early Cell Lineages in the Mammalian Embryo. Annu Rev Genet 52, 185-201.

Saci, A., Cantley, L.C., and Carpenter, C.L. (2011). Rac1 regulates the activity of mTORC1 and mTORC2 and controls cellular size. Molecular cell 42, 50-61.

Sasaki, H. (2017). Roles and regulations of Hippo signaling during preimplantation mouse development. Development, Growth & Differentiation 59, 12-20.

Seo, M., Kim, J.-D., Neau, D., Sehgal, I., and Lee, Y.-H. (2011). Structure-based development of small molecule PFKFB3 inhibitors: a framework for potential cancer therapeutic agents targeting the Warburg effect. PLoS One 6, e24179-e24179.

Shirayoshi, Y., Okada, T.S., and Takeichi, M. (1983). The calcium-dependent cell-cell adhesion system regulates inner cell mass formation and cell surface polarization

in early mouse development. Cell 35, 631-638.

Sonenberg, N., and Hinnebusch, A.G. (2009). Regulation of translation initiation in eukaryotes: mechanisms and biological targets. Cell 136, 731-745.

Spindle, A. (1982). Cell allocation in preimplantation mouse chimeras. J Exp Zool 219, 361-367.

Strumpf, D., Mao, C.A., Yamanaka, Y., Ralston, A., Chawengsaksophak, K., Beck, F., and Rossant, J. (2005). Cdx2 is required for correct cell fate specification and differentiation of trophectoderm in the mouse blastocyst. Development 132, 2093-2102.

Taniguchi, M., Kitatani, K., Kondo, T., Hashimoto-Nishimura, M., Asano, S., Hayashi, A., Mitsutake, S., Igarashi, Y., Umehara, H., Takeya, H., et al. (2012). Regulation of autophagy and its associated cell death by "sphingolipid rheostat": reciprocal role of ceramide and sphingosine 1-phosphate in the mammalian target of rapamycin pathway. The Journal of biological chemistry 287, 39898-39910.

Tarkowski, A.K. (1961). Mouse chimaeras developed from fused eggs. Nature 190, 857-860.

Watanabe, Y., Miyasaka, K.Y., Kubo, A., Kida, Y.S., Nakagawa, O., Hirate, Y., Sasaki, H., and Ogura, T. (2017). Notch and Hippo signaling converge on Strawberry Notch 1 (Sbno1) to synergistically activate Cdx2 during specification of the trophectoderm. Scientific reports 7, 46135-46135.

Watson, A.J., and Kidder, G.M. (1988). Immunofluorescence assessment of the timing of appearance and cellular distribution of Na/K-ATPase during mouse embryogenesis. Developmental Biology 126, 80-90.

Wauson, E.M., Lorente-Rodríguez, A., and Cobb, M.H. (2013). Minireview: Nutrient sensing by G protein-coupled receptors. Molecular endocrinology (Baltimore, Md) 27, 1188-1197.

White, M.D., Zenker, J., Bissiere, S., and Plachta, N. (2018). Instructions for Assembling the Early Mammalian Embryo. Dev Cell 45, 667-679.

Whittingham, D.G., and Biggers, J.D. (1967). Fallopian tube and early cleavage in the mouse. Nature 213, 942-943.

Zhang, X., Qiao, Y., Wu, Q., Chen, Y., Zou, S., Liu, X., Zhu, G., Zhao, Y., Chen, Y., Yu, Y., et al. (2017). The essential role of YAP O-GlcNAcylation in high-glucose-stimulated liver tumorigenesis. Nature Communications 8, 15280.

Zhao, B., Wei, X., Li, W., Udan, R.S., Yang, Q., Kim, J., Xie, J., Ikenoue, T., Yu, J., Li, L., et al. (2007). Inactivation of YAP oncoprotein by the Hippo pathway is involved in cell contact inhibition and tissue growth control. Genes Dev 21, 2747-2761.

Zhao, Y.D., Ohkawara, H., Rehman, J., Wary, K.K., Vogel, S.M., Minshall, R.D., Zhao, Y.Y., and Malik, A.B. (2009). Bone marrow progenitor cells induce endothelial adherens junction integrity by sphingosine-1-phosphate-mediated Rac1 and Cdc42 signaling. Circ Res 105, 696-704, 698 p following 704.

3.7 Figures

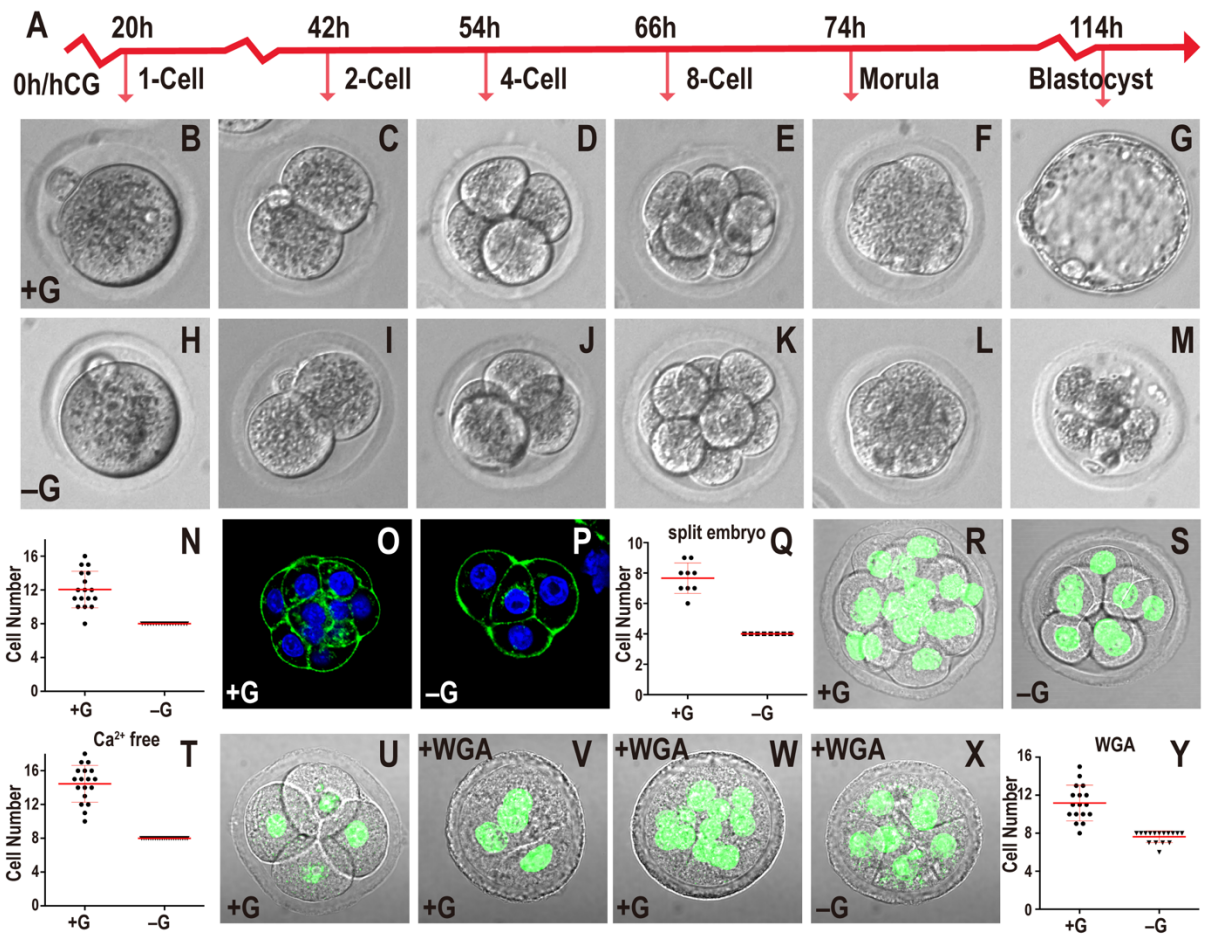

Fig. 3-1: Role of glucose in early embryonic development.

In all figures, hours (h) is following human chorionic gonadotropin (hCG) injection. Growth media including or lacking glucose indicated as +G or –G respectively. Zygotes are isolated at 18h and cultured until the specified hours (h) post hCG. All quantitative data include mean ± SD.

(A) Timeline of preimplantation development. Morula is 78h post hCG that in +G media are at post-compaction 8-16 cell stage with no hint of blastocyst cavity formation

(B-N) Embryos cultured in +G (B-G) or –G (H-M). The times and stages are as indicated in (A). In –G, the embryo fails to make a blastocyst (compare G and M). Every embryo in –G (n=17) is blocked at the 8-cell stage (N).

(O-Q) 2-cell embryos mechanically split into two individual blastomeres and grown in +G (O) or –G (P) until 78h. In both cases the embryos compact at 4-cell. In +G, split embryos proceed to 8-cells but –G embryos are blocked at 4-cell (Q). Note: As 2-cell embryos are split at 46h, they are “4-cell” at 78h.

(R-T) Ca2+ depletion prevents compaction in both +G (R) and –G (S) 78h embryos. Quantitation (T) shows +G embryos contain 10-18 cells (n=18) and –G (n=21) is blocked at 8-cells.

(U-Y) +G grown 4-cell embryos compact when WGA is added (56h; U, 58h; V) proceed to develop beyond 8-cells (n=17) (78h; W, Y). In –G, WGA treated embryos block at 8-cells (n=16) (78h; X, Y).

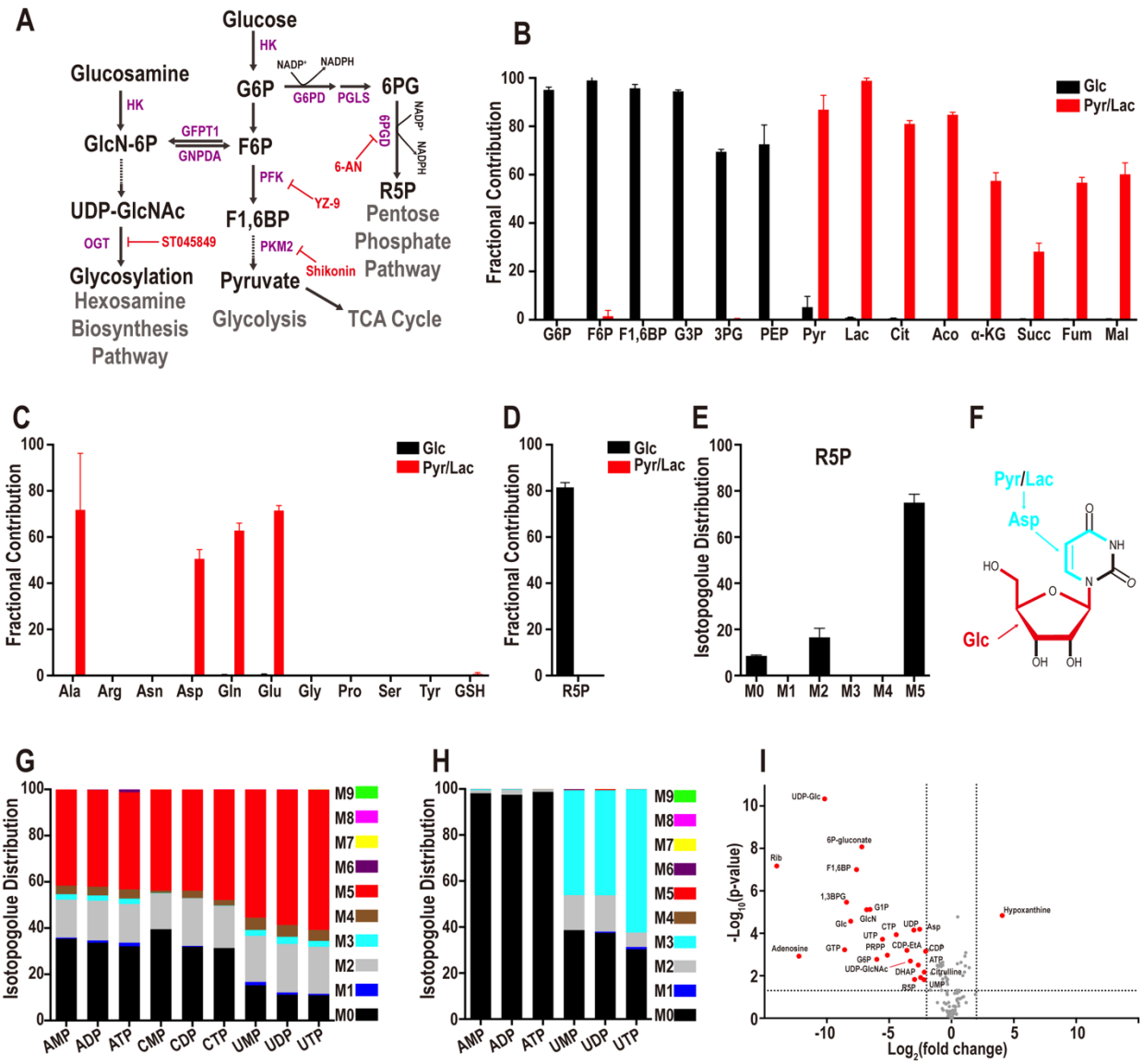

Fig. 3-2: Metabolomics analysis of the compacted morula.

(A) Representative steps in glucose metabolism.

(B) U-^{13}C glucose (black bars) contributes to glycolytic intermediates but not to TCA cycle metabolites while U-13C pyruvate+lactate (red bars) contribute to TCA intermediates.

(C) Glucose (black) does not contribute carbons to amino acids and contribution of pyruvate/lactate (red) carbons is limited to the four amino acids, Ala, Asp, Gln, and Glu.

(D, E) Fractional contribution of U-^{13}C glucose (black) and U-^{13}C pyruvate/lactate (red) (D) to the PPP metabolite ribose-5-phosphate (R5P), and glucose isotopologue distribution of R5P (E). The most abundant isotopologue is M5 in which 5 of the donated carbons are from exogenous U-^{13}C-glucose (black). M0 peak corresponds to unlabeled metabolites from internal resources. The origin of the M2 peak is unknown.

(F-H) Structural representation of uridine (F). Glucose contributes 5 carbons to the ribose sugar (red), while pyruvate/lactate contributes 3 carbons to the base (light blue), via aspartate for de novo pyrimidine biosynthesis. (G) U-^{13}C glucose contributes carbons to all nucleotides. No isotopologues greater than M5 are detected suggesting that only the ribose ring of the nucleotides is synthesized from glucose. (H) U-^{13}C pyruvate/lactate contributes 3 carbons (light blue) to pyrimidine based nucleotides (e.g. UMP, UDP, UTP), and no carbons (M0) from pyruvate/lactate are used to populate purine nucleotides (e.g. AMP, ADP, ATP).

(I) Identification of glucose sensitive metabolites. 25 metabolites (red) differ by more than 4-fold ($P < 0.05$). Metabolites that do not meet this criterion are marked in grey.

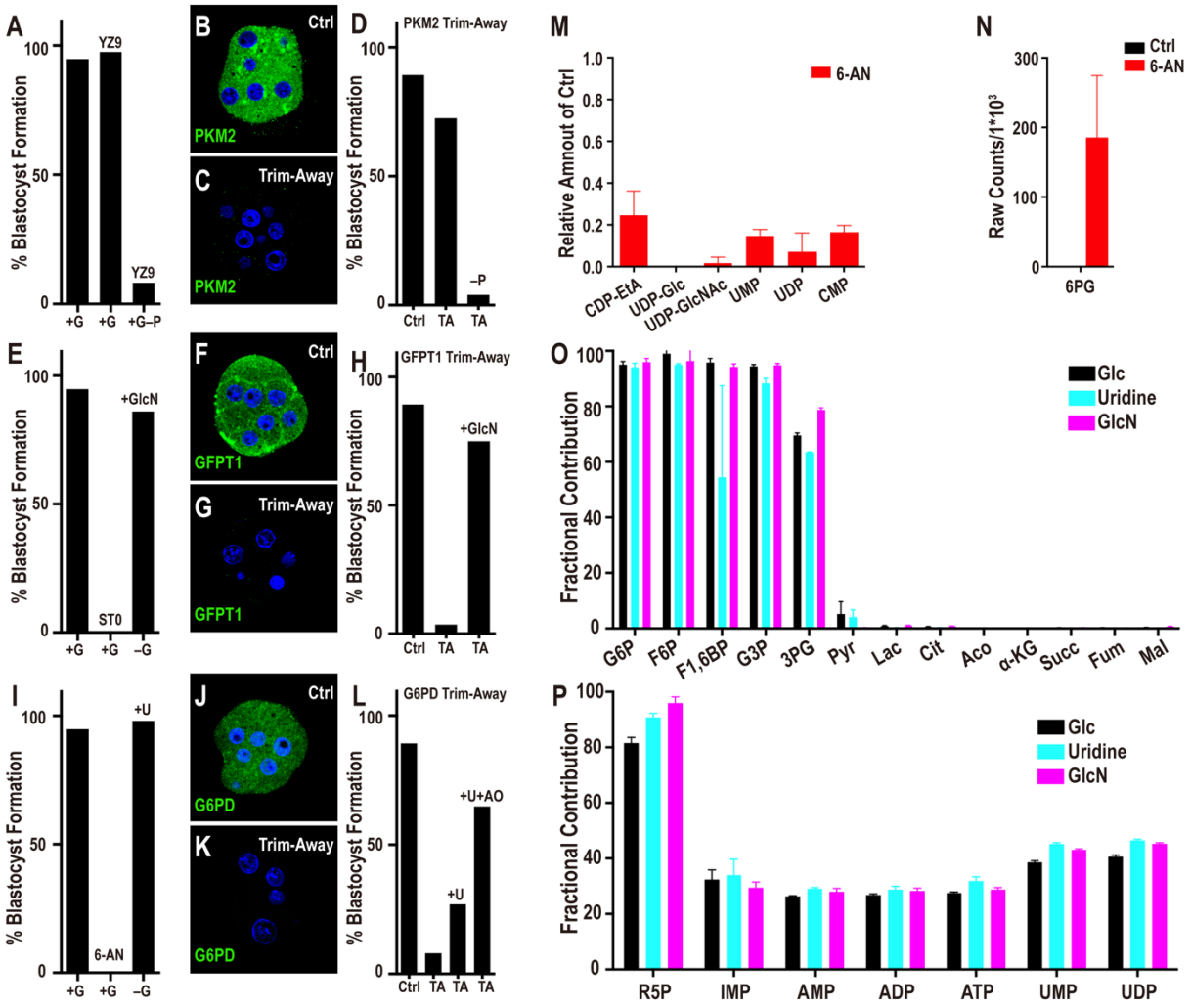

Fig. 3-3: Metabolic contribution of glycolysis, PPP and HBP.

(A) Glycolysis inhibition by YZ9 has no adverse effect on blastocyst formation unless the medium lacks pyruvate (+G–P +YZ9). (B-C) PKM2 staining at the morula stage. (B) Control injected with unrelated antibody and mCherry-Trim21 mRNA shows robust expression of PKM2. (C) Injection of mCherry-Trim21 mRNA along with an antibody against PKM2 leads to complete loss of the protein. (D) PKM2 depletion does not affect blastocyst formation unless the growth medium lacks pyruvate.

(E) Inhibition of *O*-glycosylation (by ST045849) blocks morula to blastocyst transition. Supplementation with GlcN fully rescues the morula block phenotype seen in –G. (F) Control embryo shows robust expression of GFPT1 that is lost upon Trim-Away depletion (G). This causes a morula block that is fully rescued by GlcN (H).

(I) Inhibition of PPP by 6-AN blocks the transition from morula to blastocyst. Supplementation with uridine (U) fully rescues the morula block phenotype seen in –G and restores blastocyst formation. (J-K) G6PD staining at the morula stage. (J) Control IgG shows robust expression of G6PD. (K) G6PD Trim-Away leads to complete loss of the protein. (L) Depletion of G6PD (PPP) by Trim-Away causes a morula block and prevents blastocyst formation. Uridine partially rescues G6PD loss, and this rescue is significantly better in the presence of an antioxidant (AO).
Note: experiments shown in (A, E, I) and (D, H, L) were performed together, and so the respective controls are shared between the groups.

(M) Blocking the oxidative branch of the PPP pathway with 6-AN causes a significant reduction in the levels of nucleotides and nucleotide derived metabolites. The data are normalized to the corresponding controls set at 1.0. (N) 6-PG accumulation following 6-AN treatment.

(O, P) Embryos cultured in U-^{13}C glucose (black), or in U-^{13}C GlcN (without glucose, light blue) or in 13C uridine (without glucose, purple). U-^{13}C GlcN and ^{13}C uridine show a virtually identical metabolic labeling pattern as U-^{13}C glucose.

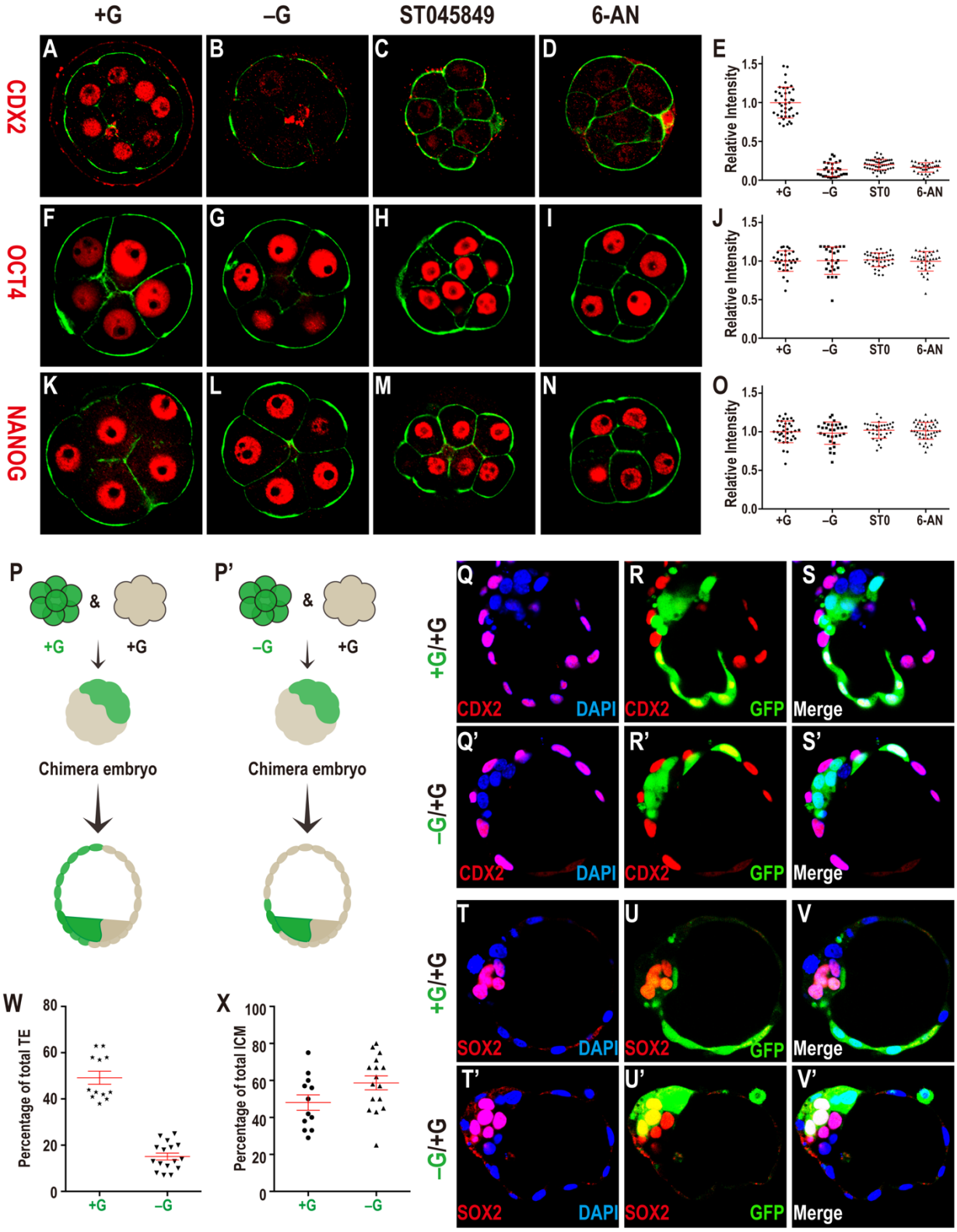
+G
–G
ST045849
6-AN
CDX2
OCT4
NANOG
A
B
C
D
E
F
G
H
I
J
K
L
M
N
O
Relative Intensity
1.5
1.0
0.5
0.0
+G
–G
ST0
6-AN
P
P'
&
+G
–G
Chimera embryo
Q
R
S
Q'
R'
S'
+G/+G
–G/+G
CDX2
DAPI
GFP
Merge
T
U
V
T'
U'
V'
SOX2
W
X
Percentage of total TE
Percentage of total ICM
80
60
40
20
0
100

Fig. 3-4: Glucose is required for TE fate initiation and specification.

CDX2 (A-E) expression is observed in outer blastomeres in +G (A), but not in –G (B), and not when O-glycosylation (HBP, C) or PPP (D) is blocked. Quantitation of CDX2 data (E).

OCT4 (F-J) and NANOG (K-O) expression in +G (F, K), –G (G, L), ST045849 (H, M), or 6-AN (I, N). Quantitation of OCT4 (J) and NANOG (O) shows that their levels are unchanged without glucose, or when PPP or O-linked glycosylation is blocked.

(P, P') Schematic representation of control (+G; P) and experimental (-G; P') derived chimeras. A GFP marked embryo (green) is cultured either in +G (P) or –G (P'). An unmarked embryo (not green) is separately grown in +G to the 8-cell stage. The green and non-green embryo are fused to make a chimera that is grown without glucose (for both P, P') to the blastocyst stage. In (P) green cells distribute equally between TE and ICM. In (P') green cells rarely take on TE fate.

(Q-X) Data supporting the scheme in (P, P'). (Q-S') CDX2 (red, purple in merge with DAPI showing nuclei, GFP green) expression in TE cells in control (Q-S) and experimental (Q'-S') chimeras. In the control, green cells populate both ICM and TE while in the experimental chimera, they are largely restricted to the ICM.

(T-V') SOX2 expression (red) is in the ICM. While green cells can be either SOX2 positive or negative in control chimera (T-V), in +G/–G chimera, the green cells are usually SOX2 positive (T'-V') (see text). (W, X) Quantitation of the chimera data.

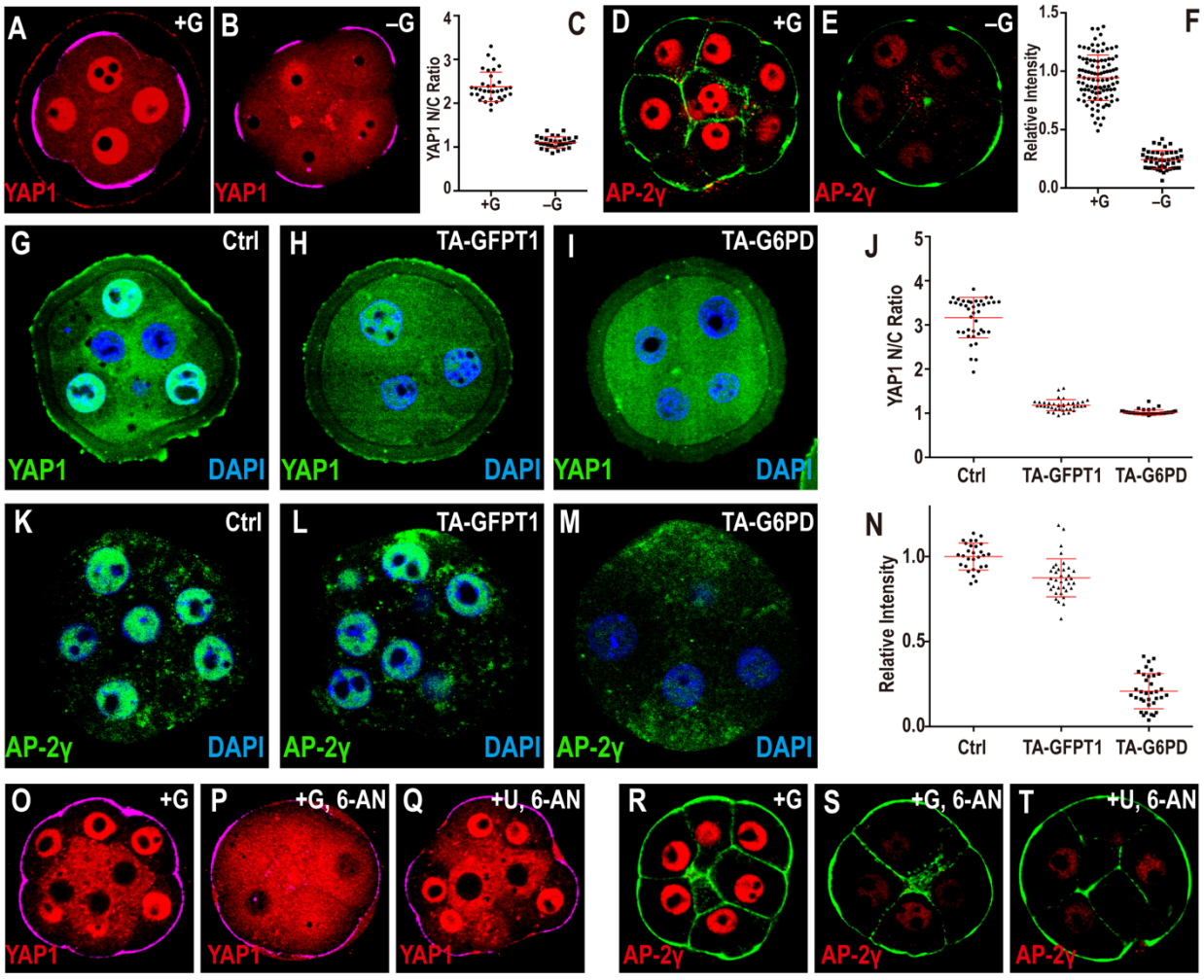

Fig. 3-5: Glucose dependent activation of transcription factors.

Cell membranes (green) are marked using phalloidin-FITC in (D, E, R, S, T), apical surfaces (purple) are marked by phospho-Ezrin/Radixin/Moesin (pERM) in (A, B, O, P, Q).

In +G control (A) YAP1 is localized to the nucleus in pERM (purple) marked polar cells (74h). This nuclear localization is significantly reduced in –G (B). (C) Quantitation of YAP1 nuclear to cytoplasmic (N/C) ratio.

(D-F) In control media TFAP2C (red) is expressed in the nuclei of all blastomeres (D) at the morula stage (78h). This expression is lost in –G (E) Quantitation shown in (F). Inhibition of PPP or HBP both give results similar to that in –G (see Figure. S3-4E-J)

(G-N) Loss of function using Trim-Away (TA).
(G) Control, morula injected with control IgG antibody. Strong nuclear YAP1 staining (green) is seen. Trim-Away (TA) with either anti-GFPT1 (HBP) (H) or anti-G6PD (PPP) (I) results in a significant reduction in nuclear YAP1. (J) Quantitation of YAP1 nuclear to cytoplasmic (N/C) ratio. (K) Control, morula injected with non-specific IgG antibody shows robust nuclear TFAP2C (green). Injection with anti-G6PD (M) causes a significant reduction in TFAP2C expression while injection with anti-GFPT1 (L) does not influence TFAP2C expression. (N) Quantitation of nuclear TFAP2C.

(O-T) Rescue experiments at morula stage (78h). YAP1 nuclear localization seen in control embryos (O) and lost in PPP blocked embryos (P) is rescued by addition of uridine (Q). In contrast, TFAP2C expression (R), also lost upon PPP inhibition (S) is not rescued by uridine (T). Quantitation for YAP1 and TFAP2C are shown in Figure S3-4G, J.

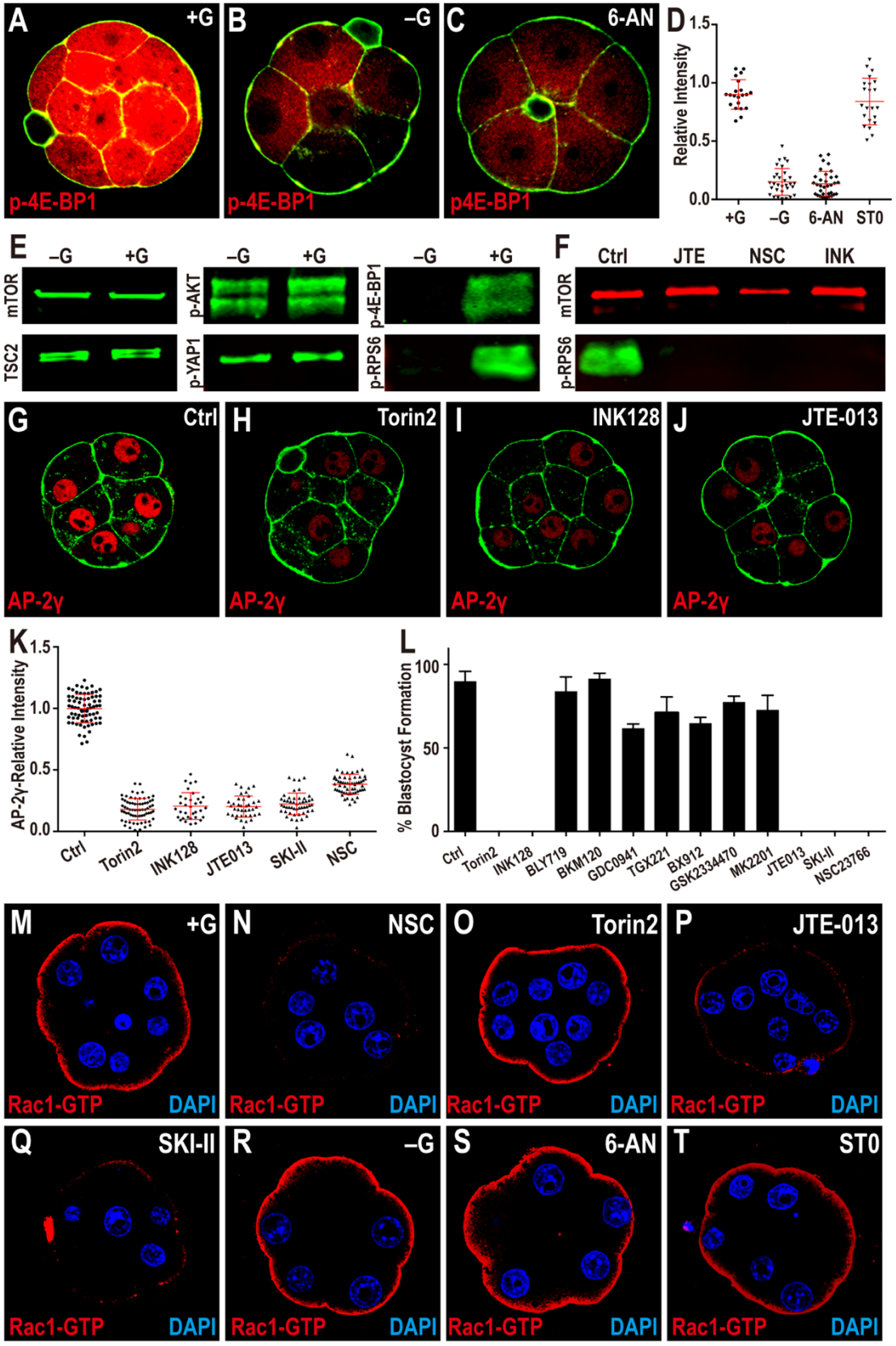
A
+G
p-4E-BP1
B
–G
p-4E-BP1
C
6-AN
p4E-BP1
D
Relative Intensity
1.5
1.0
0.5
0.0
+G
–G
6-AN
ST0
E
–G
+G
mTOR
TSC2
p-AKT
p-YAP1
p-4E-BP1
p-RPS6
F
Ctrl
JTE
NSC
INK
mTOR
p-RPS6
G
Ctrl
AP-2γ
H
Torin2
AP-2γ
I
INK128
AP-2γ
J
JTE-013
AP-2γ
K
AP-2γ-Relative Intensity
1.5
1.0
0.5
0.0
Ctrl
Torin2
INK128
JTE013
SKI-II
NSC
L
% Blastocyst Formation
100
50
0
Ctrl
Torin2
INK128
BLY719
BKM120
GDC0941
TGX221
BX912
GSK2334470
MK2201
JTE013
SKI-II
NSC23766
M
+G
Rac1-GTP
DAPI
N
NSC
Rac1-GTP
DAPI
O
Torin2
Rac1-GTP
DAPI
P
JTE-013
Rac1-GTP
DAPI
Q
SKI-II
Rac1-GTP
DAPI
R
–G
Rac1-GTP
DAPI
S
6-AN
Rac1-GTP
DAPI
T
ST0
Rac1-GTP
DAPI

Fig. 3-6: Modulation of TFAP2C Translation.

(A-D) TFAP2C translation is controlled by PPP function. Phosphorylation of threonine 37/46 on 4E-BP1 (p-4E-BP1), a target of mTOR is expressed at high levels in the 8-cell embryo (A). This expression is lost in –G (B) or when PPP is inhibited (C). Quantitation in (D) also shows that blocking HBP does not affect p-4E-BP1.

(E, F) Western blot analysis of members of mTOR signaling pathway and its activation. (E) Total mTOR, TSC2, phosphorylation level of serine 473 on AKT1/2 (p-AKT) and serine 127 on YAP1 (p-YAP1) all remain unchanged in –G embryos, but phosphorylated mTOR targets 4E-BP1 and RPS6 (p-RPS6) levels are significantly reduced. (F) p-RPS6 is eliminated when S1PR2, Rac1 or mTOR is inhibited.

(G-K) TFAP2C expression requires mTOR and S1P signaling. The expression of TFAP2C (G) is eliminated in the presence of mTOR inhibitors (H, I) and S1PR2 inhibitor JTE (J). (K) Quantitation of TFAP2C expression in embryos in which the mTOR and S1P pathways are inhibited.

(L) Quantitation shows that the morula to blastocyst transition is acutely sensitive to mTOR inhibitors, inhibitors of the S1P pathway and its downstream component Rac1, but is not affected by PI3K inhibitors.

(M-T) Role of glucose and S1P signaling in controlling Rac1 expression. In control, Rac1-GTP staining is observed only on the apical surface of the polar cells (M).

Inhibition of Rac1 (N), S1P receptor (P), and S1P biosynthesis (Q) cause a significant reduction in Rac1-GTP staining. In contrast, inhibition of mTOR (O), lack of glucose during culture (R), or inhibition of specific arms of glucose metabolism (PPP and HBP) (S-T) has no effect on Rac1-GTP levels or localization.

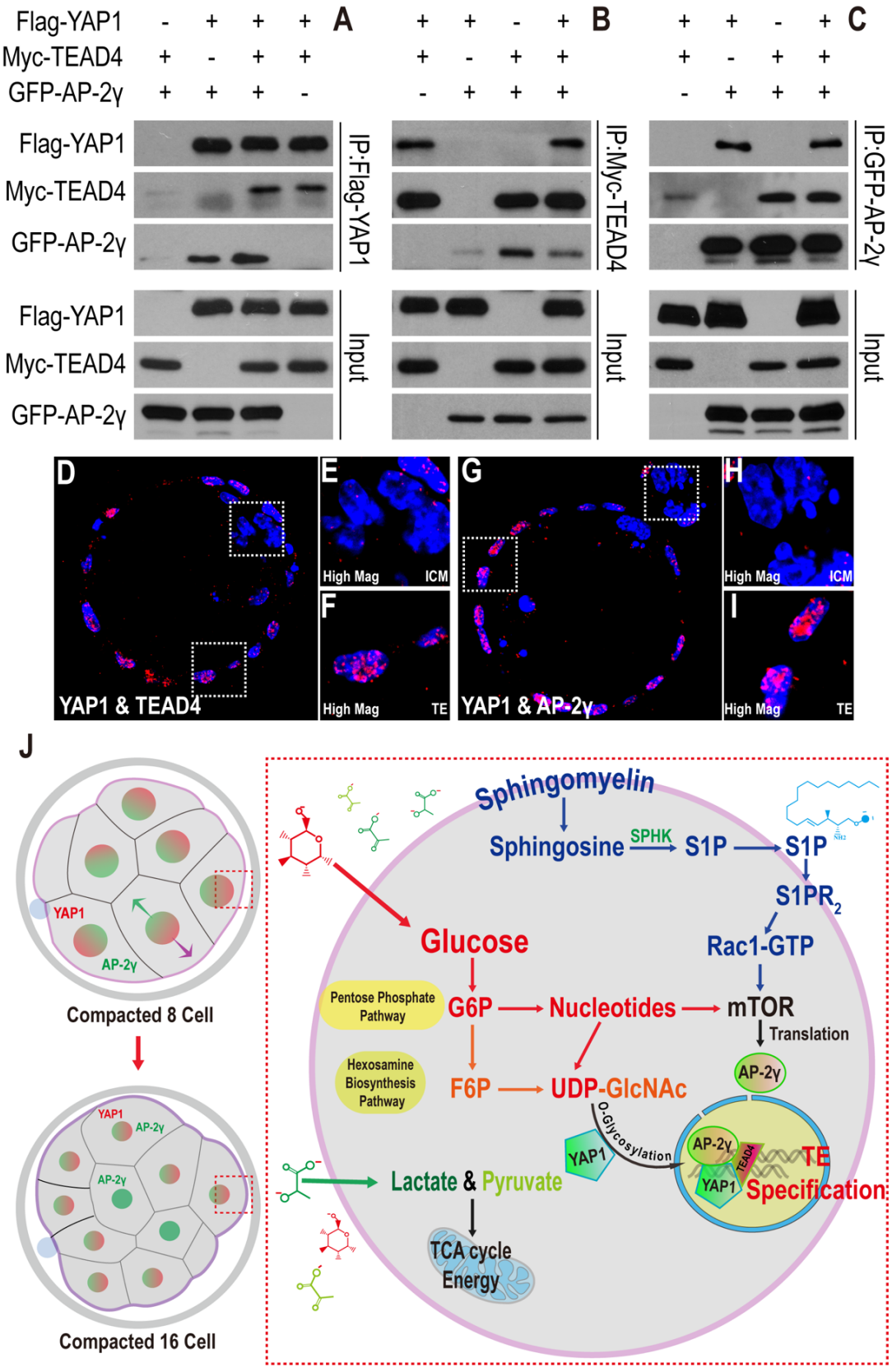
Flag-YAP1
Myc-TEAD4
GFP-AP-2γ
A
B
C
IP:Flag-YAP1
IP:Myc-TEAD4
IP:GFP-AP-2γ
Input
D
E
F
G
H
I
High Mag
ICM
TE
YAP1 & TEAD4
YAP1 & AP-2γ
J
YAP1
AP-2γ
Compacted 8 Cell
Compacted 16 Cell
Sphingomyelin
Sphingosine
SPHK
S1P
S1PR2
Rac1-GTP
Glucose
Pentose Phosphate Pathway
G6P
Nucleotides
mTOR
Translation
Hexosamine Biosynthesis Pathway
F6P
UDP-GlcNAc
O-Glycosylation
Lactate & Pyruvate
TCA cycle
Energy
TEAD4
TE Specification

Fig. 3-7: YAP1/TEAD4 and TFAP2C form a complex.

(A-C) Flag-YAP1, Myc-TEAD4, and GFP-TFAP2C are over-expressed in HEK293T cells for immunoprecipitation (IP) assay using specific antibodies as indicated. Anti-Flag antibody immunoprecipitates YAP1 (as expected) but also co-immunoprecipitates TFAP2C and TEAD4 (A). Likewise, immunoprecipitation with anti-Myc also results in the co-precipitation of TFAP2C and YAP1 (B) and anti-GFP co-precipitates both YAP1 and TEAD4 (C).

(D-I) Blastocyst embryos were harvested for Duolink PLA. (D-F) YAP1 and TEAD4 form complex in TE (E) but not in the ICM (F). (G-I) YAP1 and TFAP2C form complex in TE (H), but not in the ICM (I).

(J) A model for metabolic control of preimplantation development by glucose.

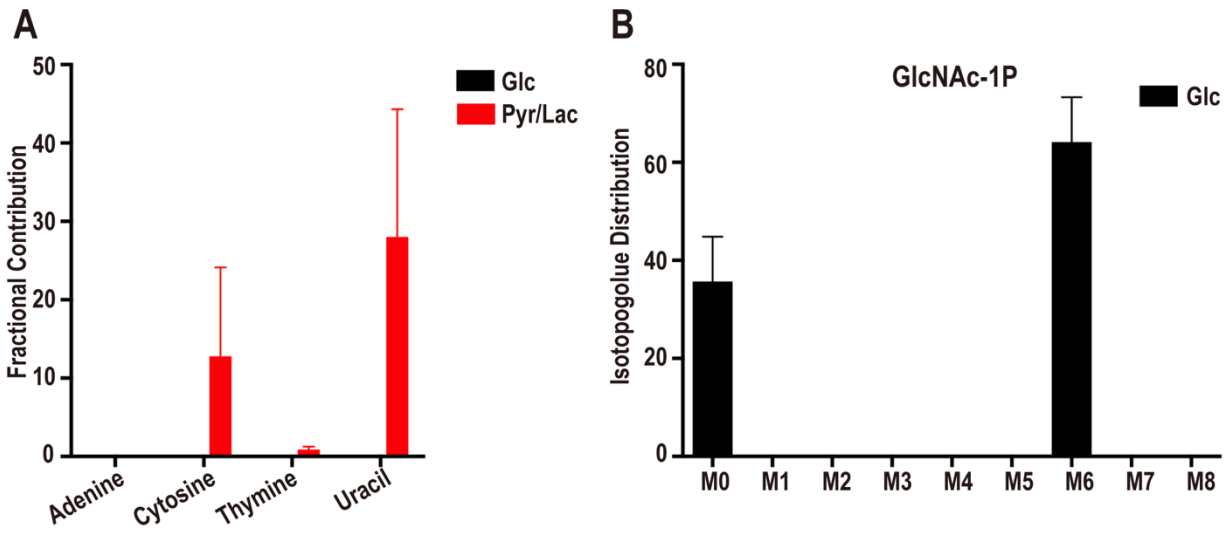

Fig. S3-1: Metabolomic analysis of the compacted morula, related to Figure 3-2.

(A) Contribution of glucose and pyruvate/lactate to nucleobases. U-^{13}C-glucose does not contribute carbon to either the purine bases (adenine) or to the pyrimidine bases (cytosine, uracil). In contrast, U-^{13}C-pyruvate/lactate contribute to the pyrimidines, but not the purine bases. The nucleobases are generated from the breakdown of nucleotides, and their labeling pattern is an indirect read-out of the labeling of bases within the nucleotides.

(B) U-^{13}C-glucose isotopologue distribution of HBP related metabolite GlcNAc-1P. The most abundant isotopologue is M6 in which 6 of the donated carbons are from exogenous (^{13}C) glucose. M0 peak corresponds to unlabeled metabolites from internal resources.

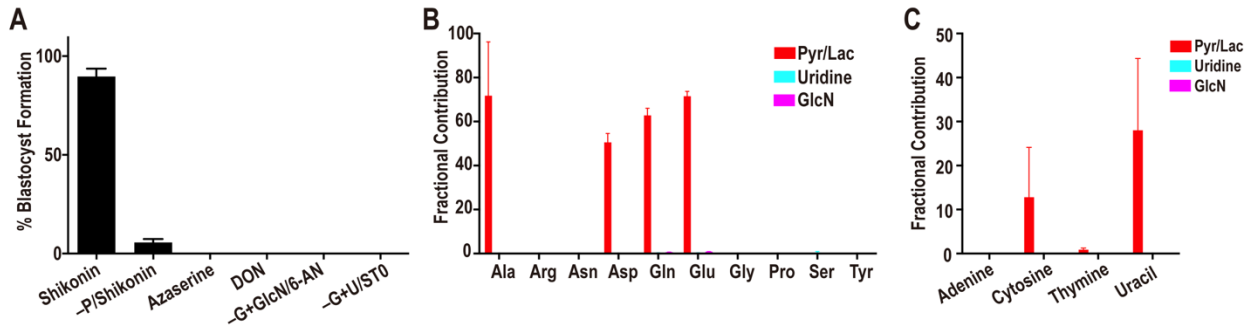

Fig. S3-2: Metabolic contribution of glycolysis, PPP and HBP, related to Figure 3-3.

(A) Percentage of embryos that form blastocysts when cultured with added inhibitors or nutrient supplements. Inhibition of glycolysis (PKM2) by shikonin in +G has no adverse effect on blastocyst formation. However, in the absence of pyruvate (+G–P), shikonin blocks blastocyst formation. Inhibition of HBP by azaserine, or DON, both block the morula to blastocyst transition. Embryos cultured in medium containing GlcN in place of glucose remain sensitive to inhibition of the PPP by 6-AN. Uridine (U) does not rescue a block caused by inhibition of OGT by ST045849 (ST0).

(B) Metabolomic analysis shows that, unlike pyruvate/lactate (red), uridine (light blue) and GlcN (purple) do not contribute carbons to non-essential amino acids.

(C) As seen with glucose, labeled uridine and GlcN do not contribute carbon to nucleobase biosynthesis. In contrast, labeled pyruvate/lactate contribute carbon to pyrimidine base biosynthesis.

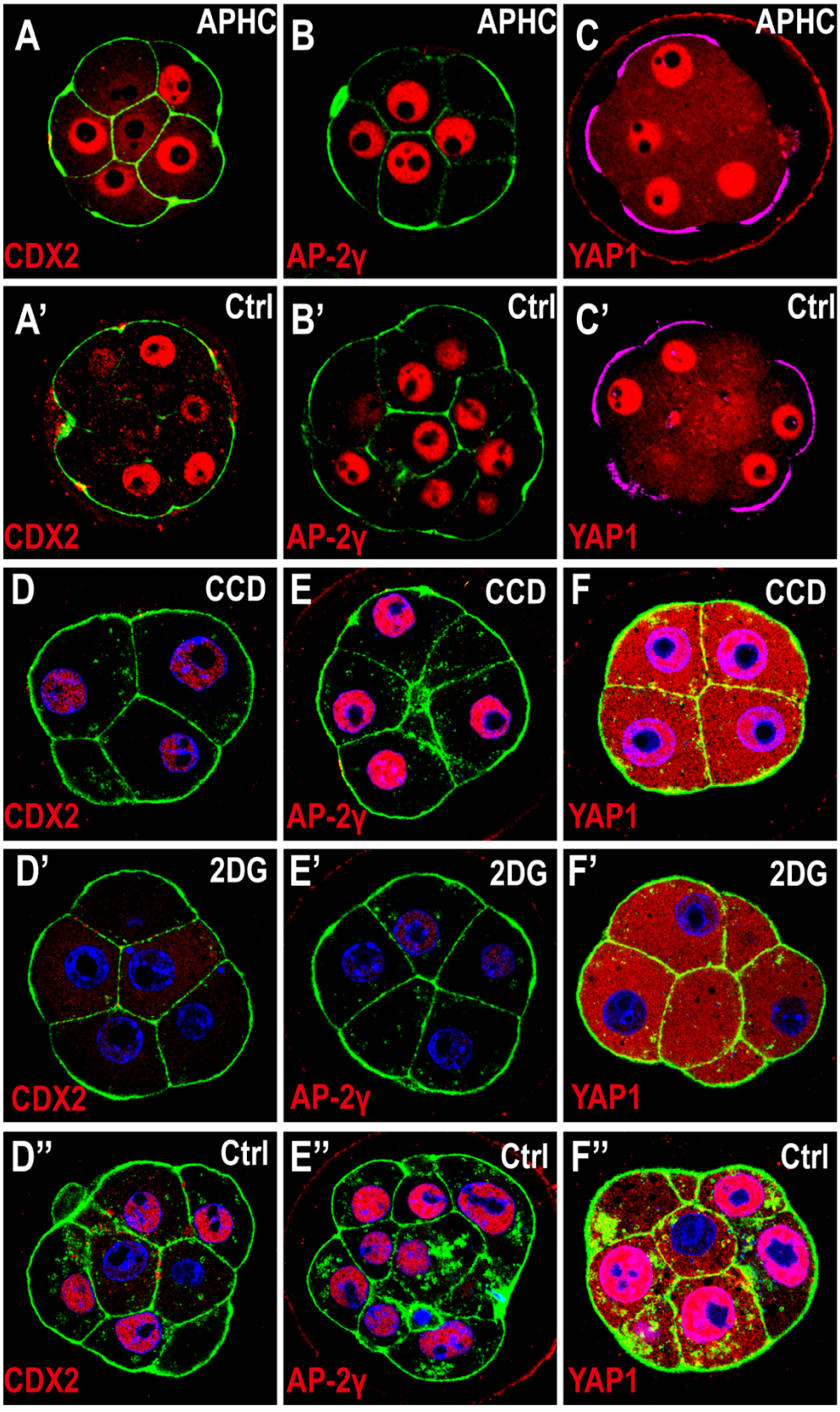
A
APHC
CDX2
B
APHC
AP-2γ
C
APHC
YAP1
A'
Ctrl
CDX2
B'
Ctrl
AP-2γ
C'
Ctrl
YAP1
D
CCD
CDX2
E
CCD
AP-2γ
F
CCD
YAP1
D'
2DG
CDX2
E'
2DG
AP-2γ
F'
2DG
YAP1
D''
Ctrl
CDX2
E''
Ctrl
AP-2γ
F''
Ctrl
YAP1

Fig. S3-3: TE fate defect is not caused by 8-cell block, related to Figures 3-4 and 3-5.

Cell membranes (green) are marked using phalloidin-FITC (A, A', B, B', D-F'), and apical surface (purple) are marked by pERM (C, C'). Aphidicolin (APHC) was added to the embryos at the early 8-cell stage (66h) to inhibit the DNA synthesis and cell cycle progression (A-C). Cytochalasin D (CCD) was added to the embryos to inhibit cleavage (D-F).

At 78h control embryos are 8-16 cells and CDX2 (red) is expressed in the polar cells (A', D''). APHC (A) and CCD (D) treated embryos are arrested at the 8-cell stage (78h), but have high levels of CDX2 expression.

APHC (B) and CCD (E) treated embryos have high levels of TFAP2C (red) that is similar to that seen in control embryos (B', E'').

YAP1 nuclear localization (red) in APHC (C) and CCD (F) treated embryos is similar to that seen in the polar cells of control embryos (C', F'').

(D'-F') CDX2, TFAP2C and YAP1 are disrupted upon 2DG treatment.

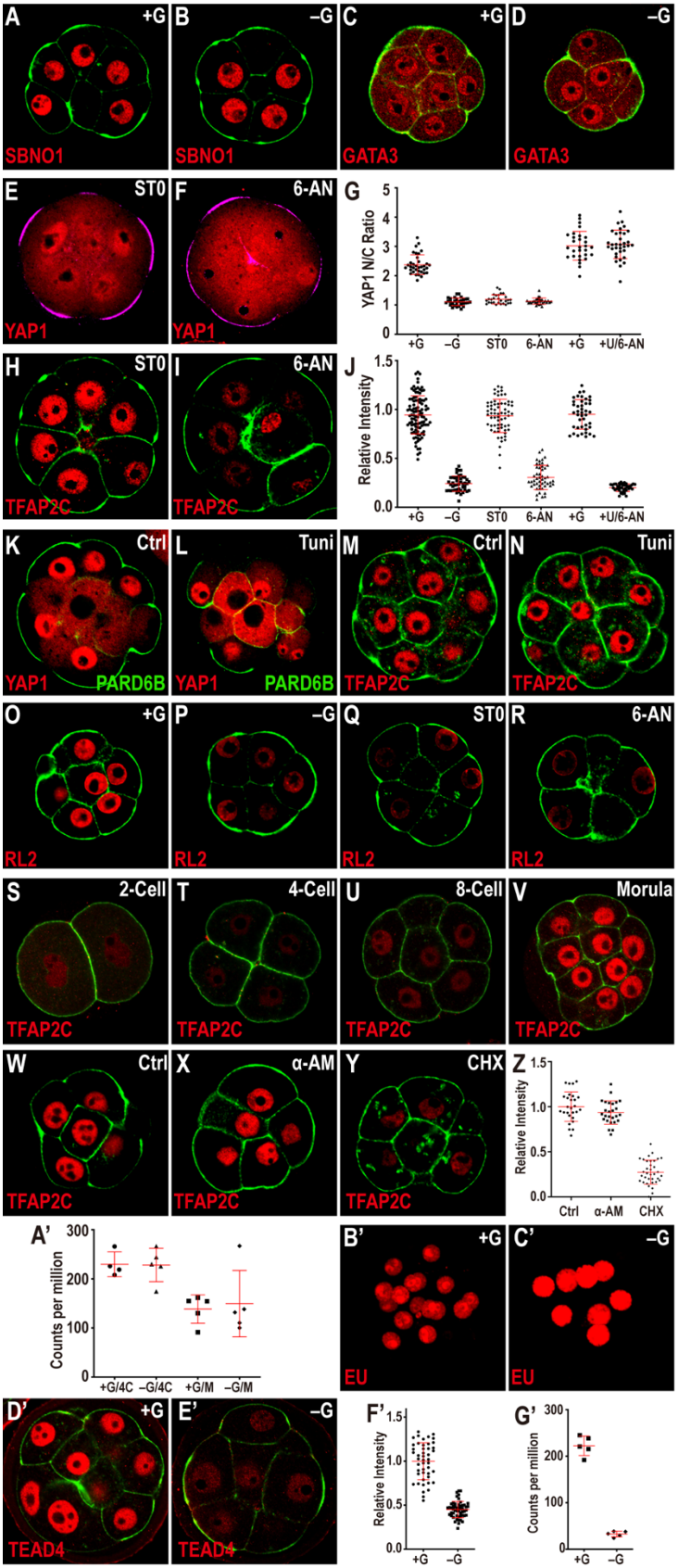
A
+G
SBNO1
B
–G
SBNO1
C
+G
GATA3
D
–G
GATA3
E
ST0
YAP1
F
6-AN
YAP1
G
YAP1 N/C Ratio
+G
–G
ST0
6-AN
+G
+U/6-AN
H
ST0
TFAP2C
I
6-AN
TFAP2C
J
Relative Intensity
K
Ctrl
YAP1
PARD6B
L
Tuni
YAP1
PARD6B
M
Ctrl
TFAP2C
N
Tuni
TFAP2C
O
+G
RL2
P
–G
RL2
Q
ST0
RL2
R
6-AN
RL2
S
2-Cell
TFAP2C
T
4-Cell
TFAP2C
U
8-Cell
TFAP2C
V
Morula
TFAP2C
W
Ctrl
TFAP2C
X
α-AM
TFAP2C
Y
CHX
TFAP2C
Z
Relative Intensity
Ctrl
α-AM
CHX
A'
Counts per million
+G/4C
–G/4C
+G/M
–G/M
B'
+G
EU
C'
–G
EU
D'
+G
TEAD4
E'
–G
TEAD4
F'
Relative Intensity
+G
–G
G'
Counts per million
+G
–G

Fig. S3-4: Glucose dependent activation of transcription factors, related to Figure 3-5.

Cell membranes (green) are marked using phalloidin-FITC, and apical surface are marked by pERM (purple in E, F) or PARD6B (green in K, L).

(A-D) Expression of SBNO1 (A, B) or GATA3 (C, D) in morula stage (78h) embryos is not dependent on exogenously provided glucose.

(E-G) PPP/HBP and YAP1 nuclear localization at compacted 8-cell stage (74h). In +G control (see Figure 3-5A) YAP1 is localized to the nucleus in pERM (purple) marked polar cells. Inhibition of O-glycosylation by ST045849 (E) or PPP by 6-AN (F) both give results similar to that of –G (see Figure 3-5B). (G) Quantitation of YAP1 nuclear to cytoplasmic (N/C) ratio at 74h, YAP1 data set at morula stage (78h) in Figure 3-5O, 3-5Q are also included.

(H-J) In control medium TFAP2C (red) is expressed in the nuclei of all blastomeres at morula stage (78h) (see Figure 3-5D). This expression is insensitive to O-linked glycosylation inhibition by ST045849 (H), but is lost when the PPP is inhibited by 6-AN (I). Quantitation shown in (J), TFAP2C quantitation in Figure 3-5R, 3-5T are also included.

(K-N) N-linked glycosylation and TE specification. Apical cells with high levels of PARD6B (green) on their membrane also show nuclear localization of YAP1 (red) (K).

Blocking N-glycosylation by tunicamycin (Tuni) treatment causes partial disruption in PARD6B apical localization (L). Apical cells that have lost apical PARD6B do not express YAP1 in the nucleus, but in other apical cells that maintain PARD6B expression YAP1 is localized in the nucleus (L). Tunicamycin treatment (N) does not influence the expression of TFAP2C (M, N).

(O-R) O-linked glycosylation is glucose, HBP and PPP dependent. O-linked glycosylation is detected using the RL2 antibody and decreases in embryos grown without glucose (P), or when O-linked glycosylation is inhibited by ST045849 (Q), or when the PPP is inhibited using 6-AN (R).

(S-V) TFAP2C expression during preimplantation development. TFAP2C expression is low at the 2-cell (S), 4-cell (T), and early 8-cell (U) stages, and then increases at the compacted morula (V) stage.
(W-Z) TFAP2C expression is sensitive to inhibition of translation. Blocking translation by cycloheximide (CHX) (Y), but not transcription inhibition by α-amanitin (α-AM) (X) causes a reduction in nuclear TFAP2C levels. (Z) Quantitation of nuclear TFAP2C.

(A') Tfap2c mRNA (counts per million) levels are unchanged at 4-cell stage and morula stage when cultured in –G condition.
(B', C') –G (C') grown embryos do not incorporate decreased amounts of EU, which marks synthesis of nascent transcripts, compared embryos grown in +G medium (B').

(D’-G’) In control medium TEAD4 protein (red) is expressed in the nuclei of all blastomeres at morula stage (78h) (D’). This expression is lost in embryos grown in –G medium (E’). Quantitation of TEAD4 protein level shown in (F’). (G’) Tead4 mRNA (counts per million) levels are significantly reduced, at the compacted 8-cell stage, in embryos grown in –G medium.

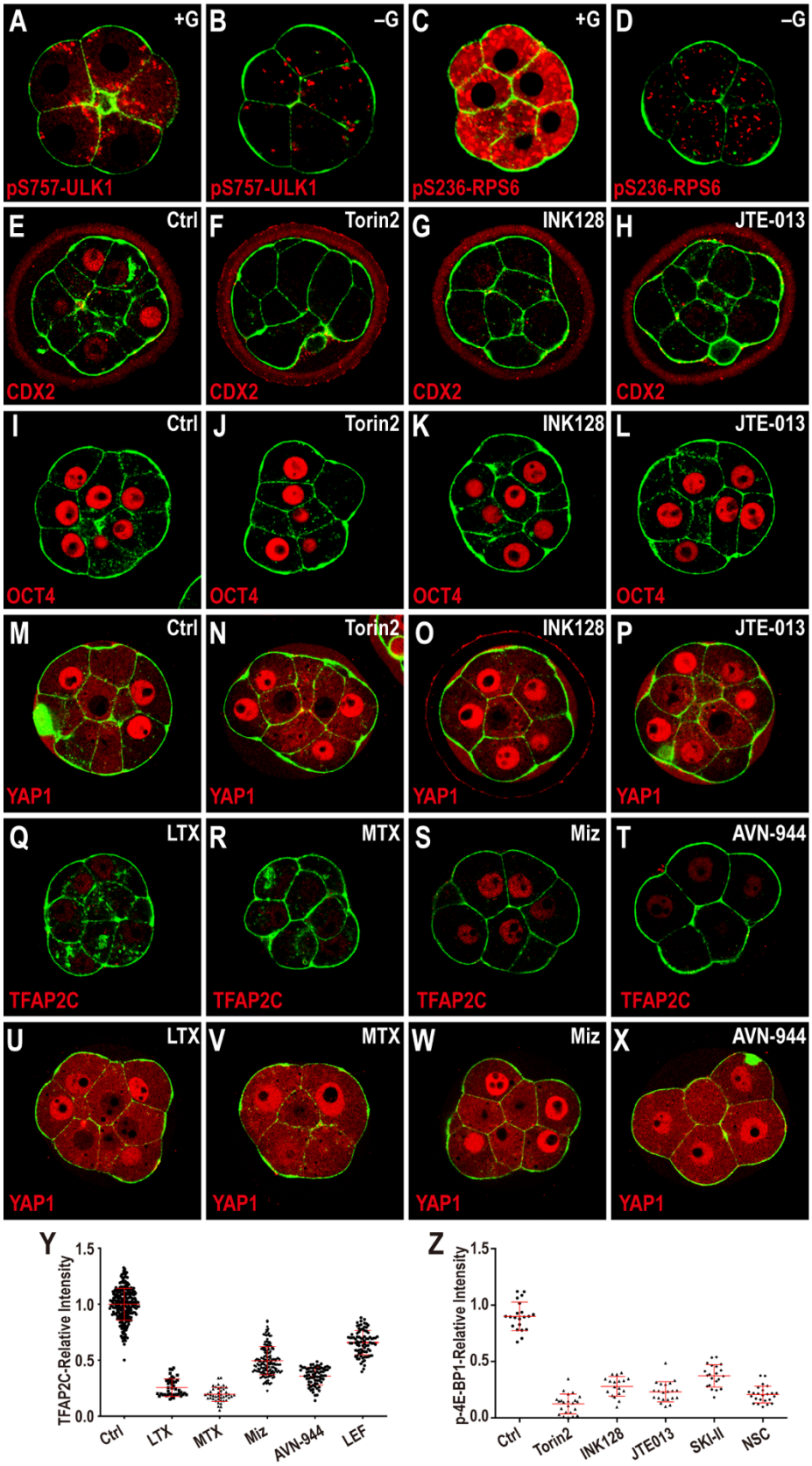
A
+G
pS757-ULK1
B
–G
pS757-ULK1
C
+G
pS236-RPS6
D
–G
pS236-RPS6
E
Ctrl
CDX2
F
Torin2
CDX2
G
INK128
CDX2
H
JTE-013
CDX2
I
Ctrl
OCT4
J
Torin2
OCT4
K
INK128
OCT4
L
JTE-013
OCT4
M
Ctrl
YAP1
N
Torin2
YAP1
O
INK128
YAP1
P
JTE-013
YAP1
Q
LTX
TFAP2C
R
MTX
TFAP2C
S
Miz
TFAP2C
T
AVN-944
TFAP2C
U
LTX
YAP1
V
MTX
YAP1
W
Miz
YAP1
X
AVN-944
YAP1
Y
TFAP2C-Relative Intensity
1.5
1.0
0.5
0.0
Ctrl
LTX
MTX
Miz
AVN-944
LEF
Z
p-4E-BP1-Relative Intensity
1.5
1.0
0.5
0.0
Ctrl
Torin2
INK128
JTE013
SKI-II
NSC

Fig. S3-5: Activation of mTOR by glucose and S1P, related to Figure 3-6.

Embryos were isolated at 18h and cultured in either +G or –G media until 78h, and inhibitors were added to the medium at 50h. Cell membranes are marked by phalloidin-FITC staining (green).

(A-D) mTOR target expression requires glucose. In control embryos high levels of pS757-ULK1 (A) or pS236-RPS6 (C) are seen at 78h. Embryos cultured in –G medium show a dramatic decrease in the levels of pS757-ULK1 (B) and pS236-RPS6 (D).

(E-H) CDX2 expression is lost upon mTOR inhibition with Torin2 (F) and INK128 (G) and inhibition of S1P signaling by JTE-013 (H).

(I-P) Inhibition of mTORC1 and S1P signaling does not perturb OCT4 and YAP1 expression.
mTOR inhibition with Torin2 (J, N) and INK128 (K, O) and S1P signaling by JTE-013 (L, P) does not affect OCT4 (I-L) and YAP1 (M-P).

(Q-T) Inhibition of purine synthesis decreases TFAP2C expression. The expression of TFAP2C is eliminated in the presence of purine synthesis inhibitors, lometrexol (LTX, Q), methotrexate (MTX, R), mizoribine (Miz, S) and AVN-944 (T).

(U-X) Inhibition of purine synthesis does not perturb YAP1 expression. Purine synthesis inhibition with LTX (U), MTX (V), Miz (W) and AVN-944 (X) does not affect YAP1.

(Y) Quantitation of TFAP2C expression in embryos in which the purine synthesis is inhibited.

(Z) Quantitation of phosphorylation of 4E-BP1 in embryos in which the mTOR and S1P pathways are inhibited (the control data are shared with Figure 3-6D.

Chapter 4 Concluding remarks

The formulation of in vitro preimplantation embryo culture medium enables us to study the metabolic roles during early embryogenesis. In this thesis, I investigated the relationship between the metabolic status and developmental progression of mouse preimplantation embryos.

In Chapter 2, the central finding is that multiple TCA cycle and associated enzymes are temporarily localized to the nucleus, while also maintaining a mitochondrial pool. Functional analysis indicates that such proteins (class I enzymes) are enzymatically active within the nucleus. These enzyme complexes are the ones that belong to the first half-cycle of the TCA cycle, and the data support a model in which they are important contributors of metabolites (class I metabolites) such as acetyl-CoA and α-KG essential for epigenetic control and activation of the zygotic genome during the 1- to 2-cell stage of preimplantation development (Figure 2-6A). The enzymes in the second half of the TCA cycle (class II enzymes) are not seen in the nucleus and their corresponding class II metabolites such as succinate and fumarate are not favorable for genome activation (Xiao et al., 2012). Strong support for the model is provided by the rescue of the developmental and transport defects due to pyruvate deprivation by exogenously provided α-KG.

Our results show that, at the 1- and 2-cell stages, PDH (that converts pyruvate to acetyl-CoA) is localized both to the mitochondrion and the nucleus. The enzyme PDK

(that inactivates PDH) is localized to the mitochondrion, while PDP (the activator of PDH) is largely confined to the nucleus. The simplest explanation is that the PDK in the mitochondrion renders PDH less active than at later stages of development, while the PDH that enters the nucleus is activated by PDP. The most significant finding of Chapter 2 is that multiple enzymes of the TCA cycle and additional proteins related to entry into the TCA cycle: pyruvate carboxylase, pyruvate dehydrogenase, pyruvate dehydrogenase phosphatase, citrate synthase, aconitase-2, and isocitrate dehydrogenase 3A (class I enzymes) are all transiently seen in the nucleus. The nuclear localization of TCA components is not an artifact of the ex vivo culture conditions since identical results are obtained from embryos isolated at different stages of in vivo development and never subject to the ex vivo culture conditions.

Enzyme activity assays adapted for very small number of isolated nuclei established that the enzyme complexes PDH and IDH3, the initiating and terminal class I enzymes are active inside the nucleus. Both dynamic measurements following brief pyruvate starvation and re-feeding as well as steady-state measurements in the presence and absence of pyruvate show a clear distinction in the dynamic property and pyruvate responses of class I and class II metabolites.

Nutrients such as pyruvate are essential for many independent functions within the cell. In this context, the rescue of ZGA and post-2-cell development by α-KG provides a unique perspective. The cells deprived of exogenously provided pyruvate continue to be under redox and energetic stress and yet are able to proceed through

ZGA when α-KG is supplied. It is pertinent that the rescue by α-KG requires the presence of lactate. This observation suggests that lactate can be utilized in the absence of pyruvate, but, due to the low NAD^+/NADH ratio, the rate of lactate to pyruvate conversion is not sufficiently high to maintain class I metabolite levels. Currently, it is unclear at which point the perturbed NAD^+/NADH ratio limits lactate utilization. It is likely that the conversion of lactate to pyruvate by LDH is affected, but it is also possible that subsequent steps of the pathway are also limited. The decrease in the levels of class I metabolites will compromise the important biosynthetic and signaling processes that drive developmental progression and are fueled by carbon from lactate and pyruvate. The provision of exogenous α-KG supplies a portion of the carbon requirement of these processes, rendering the redox state less critical, allowing the embryos to progress beyond the 2-cell stage even under energetic or redox stress. It is surprising that proline is able to rescue development, but glutamine is not. Our preliminary (data not shown) metabolite measurements suggest that exogenously provided α-KG or proline raises glutamate level in the embryo, but, for reasons still unclear, providing glutamine is much less effective in causing this change.

Most strikingly, we also detect active (unphosphorylated) PDH in the nucleus of human embryos at a stage that is different from that seen in mouse, but one that precisely matches the timing of genome activation in humans. Thus, this entire process linking nuclear localization of TCA enzymes to ZGA seems to be conserved. But this also raises some difficult questions. Our first-level model was that class I enzyme entry into the nucleus aids in ZGA. The human embryo results suggest instead that some

other signaling event marking ZGA timing instructs pyruvate-dependent nuclear transport. The simplest model for the trigger would be one that responds to nutrition levels, but this needs to be investigated further.

TCA enzyme complexes are large and require complex folding patterns. Several possible models, to be investigated in the future, can be proposed for the mechanism of their transport to the nucleus. The recently characterized “mitochondrial-derived vesicles” (MDVs) (Sugiura et al., 2014) could play a role in this process. These vesicles facilitate translocation of mitochondrial matrix proteins to several organelles including peroxisomes and lysosomes. While a possible involvement of MDVs in nuclear transport has not been explored, electron microscopy (EM) studies have shown that the early embryo displays a ring of mitochondria closely apposed to the nucleus and displaying a “blebbing” of vesicles into the nucleus (Szöllösi and Szöllösi, 1988). Only a fraction of TCA enzymes are involved in the transport process, but MDVs are reported to be selective for their cargo (Shutt and McBride, 2013). Another model involves pyruvate-dependent O-glycosylation of class I enzymes binding to Hsp90 or similar chaperones and then gliding through the nuclear pore (Hardivillé and Hart, 2014). This mechanism does not exclude a role of MDV-like vesicles in the transport process.

Published literature provides precedence for extra-mitochondrial localization of PDH (Chueh et al., 2011, Mitra et al., 2005, Sutendra et al., 2014). Similar to our results in the preimplantation embryo, all three subunits of PDH can be detected during the S phase of the cell cycle in the nucleus of lung cancer cell lines (Sutendra et al., 2014).

Also, this nuclear PDH enzyme complex is active and influences only a subset of histone acetylation patterns (Sutendra et al., 2014). Notable differences include the need for large amounts of growth factors for nuclear PDH to be detected in cancer cell lines and, more importantly, that no TCA cycle enzyme such as citrate synthase and IDH, that were included in the study, were detected in the nucleus. These differences between the embryo and the cancer cell lines will be important in resolving questions regarding metabolic control of normal development and cancer. It will also be very interesting to determine whether the process outlined here for normal development is found either in part or in full in the context of any other cancer or stem cell development. An additional avenue to explore will be to determine whether these observations have clinical relevance in infertility research, including the efficiency of the in vitro fertilization procedures. Infertility is often associated with metabolic disorders and cellular stress signals. Whether some of these dysfunctions result from perturbation of processes described here warrants future analysis.

A model that summarizes the analysis presented in Chapter 3 is presented in Figure 3-7J. Following formation of the 8-cell compacted morula, the next cell division generates apical and basal cells (Sasaki, 2017). This polarity arises independently of glucose and relies in part on mechanical forces (White et al., 2018). YAP1 is sequestered and activated in apical cells and its inactive form is degraded in basal cells (Rossant, 2018) by mechanisms that too are independent of any input from glucose. The basal cells, devoid of YAP1 function will eventually adopt an ICM fate.

In the apical cells, active YAP1 needs to be localized to the nucleus in order for it to be functional as a transcription factor, and this event of nuclear localization is glucose/HBP/O-linked glycosylation dependent. TFAP2C expression is translationally controlled by mTOR in all cells at the 8-cell stage. This process requires a dual input into the mTOR pathway by a signaling lipid, S1P, and by an unidentified PPP generated metabolite. The HBP plays no role in TFAP2C regulation. Although TFAP2C expression is ubiquitous at this stage, it forms a complex with YAP1/TEAD4 in only the apical cells that have all three proteins in the nucleus. The heterotrimer functions as a transcription factor, and activates TE-specific markers such as CDX2. Loss of Tead4 causes a similar loss of TE but not ICM markers (Cao et al., 2015; Yagi et al., 2007).

Amongst the metabolic curiosities of the system, we find that glucose and glycolysis do not function to generate energy since glucose does not fuel the TCA cycle and does not support anabolic pathways that are TCA cycle dependent. Pyruvate takes over these functions and the prominence of the lactate/pyruvate system over glucose for fulfilling bioenergetic needs is a metabolic signature of the preimplantation embryo. The importance of pyruvate has been emphasized in many classical studies (Biggers et al., 1965; Biggers et al., 1967; Brown and Whittingham, 1991; Whittingham and Biggers, 1967; Leese and Barton, 1984; Lane and Gardner, 2000; Barbehenn et al., 1974; O'Fallon and Wright, 1987). Combined with this current analysis, we conclude that the embryo, unlike cancer cells, utilizes only a small amount of glucose that is not used for bioenergetic functions. However, this small amount is necessary and sufficient for the signaling functions that drive an important developmental transition. Also in stark

contrast with cancer cells (Locasale et al., 2011; Snell, 1984), glucose does not generate fatty acids and cholesterol, amino acids including glycine and serine or purine nucleobases.

Bioenergetic needs could be met by a plethora of metabolites, for example, pyruvate in the embryo and glutamine in many cancer cells. But only glucose provides anabolic and protein modification functions that are essential for lineage specification, differentiation and morphogenesis during the morula to blastocyst transition. Keeping the flux through glycolysis at a minimum allows glucose derivatives to be used for the PPP and the HBP that are otherwise minor arms of the pathway. The relatively free exchange of carbon between the metabolites generated in PPP, HBP and glycolysis in spite of the divergent function of each arm is a surprising finding of this study. It is worth investigating, if this extent of cross-talk occurs in other systems and whether low activity through the PFK-step of glycolysis is especially conducive to exchange of metabolite carbons between the arms.

Several unique features of metabolic control make the preimplantation mammalian embryo a superb system in which to study “Developmental Metabolism” or the metabolic control of normal development. The relative solitude of the preimplantation embryo demands self-sufficiency and requires built-in metabolic mechanisms that compensate for the paucity of extracellularly triggered signal transduction events. The interplay between metabolic pathways and proliferation or differentiation has been studied extensively in the context of cancer cell expansion and

tumor growth (Pavlova and Thompson, 2016; Kang et al., 2018) or in model systems (Mandal et al., 2005; Owusu-Ansah and Banerjee, 2009). As in cancer, metabolic and signaling pathways are closely intertwined during development, with the role of intrinsic metabolic pathways difficult to dissect away from interactions between cells and their environment. Any imbalance between these two fundamentally important sets of pathways would lead to developmental disorders and malignancies suggesting that "Developmental Metabolism" would provide valuable insights for "Cancer Metabolism".

Reference

Barbehenn, E.K., Wales, R.G., and Lowry, O.H. (1974). The explanation for the blockade of glycolysis in early mouse embryos. Proc Natl Acad Sci U S A 71, 1056-1060.

Biggers, J.D., Moore, B.D., and Whittingham, D.G. (1965). Development of mouse embryos in vivo after cultivation from two-cell ova to blastocysts in vitro. Nature 206, 734-735.

Biggers, J.D., Whittingham, D.G., and Donahue, R.P. (1967). The pattern of energy metabolism in the mouse oocyte and zygote. Proc Natl Acad Sci U S A 58, 560-567.

Brown, J.J., and Whittingham, D.G. (1991). The roles of pyruvate, lactate and glucose during preimplantation development of embryos from F1 hybrid mice in vitro. Development 112, 99-105.

Cao, Z., Carey, T.S., Ganguly, A., Wilson, C.A., Paul, S., and Knott, J.G. (2015a). Transcription factor AP-2gamma induces early Cdx2 expression and represses HIPPO signaling to specify the trophectoderm lineage. Development 142, 1606-1615.

Chueh, F.Y., Leong, K.F., Cronk, R.J., Venkitachalam, S., Pabich, S., and Yu, C.L. (2011). Nuclear localization of pyruvate dehydrogenase complex-E2 (PDC-E2), a mitochondrial enzyme, and its role in signal transducer and activator of transcription 5 (STAT5)-dependent gene transcription. Cell Signal 23, 1170-1178.

Hardiville, S., and Hart, G.W. (2014). Nutrient regulation of signaling, transcription, and cell physiology by O-GlcNAcylation. Cell Metab 20, 208-213.

Kang, Y.P., Ward, N.P., and DeNicola, G.M. (2018). Recent advances in cancer metabolism: a technological perspective. Experimental & Molecular Medicine 50, 31.

Lane, M., and Gardner, D.K. (2000). Lactate regulates pyruvate uptake and metabolism in the preimplantation mouse embryo. Biol Reprod 62, 16-22.

Leese, H.J., and Barton, A.M. (1984). Pyruvate and glucose uptake by mouse ova and preimplantation embryos. Journal of reproduction and fertility 72, 9-13.

Locasale, J.W., Grassian, A.R., Melman, T., Lyssiotis, C.A., Mattaini, K.R., Bass, A.J., Heffron, G., Metallo, C.M., Muranen, T., Sharfi, H., et al. (2011). Phosphoglycerate dehydrogenase diverts glycolytic flux and contributes to oncogenesis. Nat Genet 43, 869-874.

Mandal, S., Guptan, P., Owusu-Ansah, E., and Banerjee, U. (2005). Mitochondrial regulation of cell cycle progression during development as revealed by the tenured mutation in Drosophila. Dev Cell 9, 843-854.

Mitra, K., Rangaraj, N., and Shivaji, S. (2005). Novelty of the pyruvate metabolic enzyme dihydrolipoamide dehydrogenase in spermatozoa: correlation of its localization, tyrosine phosphorylation, and activity during sperm capacitation. The Journal of biological chemistry 280, 25743-25753.

O'Fallon, J.V., and Wright, R.W., Jr. (1987). Calculation of the pentose phosphate and Embden-Myerhoff pathways from a single incubation with [U-14C]- and [5-3H]glucose. Anal Biochem 162, 33-38.

Owusu-Ansah, E., and Banerjee, U. (2009). Reactive oxygen species prime Drosophila haematopoietic progenitors for differentiation. Nature 461, 537-541.

Pavlova, N.N., and Thompson, C.B. (2016). The Emerging Hallmarks of Cancer Metabolism. Cell Metab 23, 27-47.

Rossant, J. (2018). Genetic Control of Early Cell Lineages in the Mammalian Embryo. Annu Rev Genet 52, 185-201.

Sasaki, H. (2017). Roles and regulations of Hippo signaling during preimplantation mouse development. Development, Growth & Differentiation 59, 12-20.

Shutt, T.E., and McBride, H.M. (2013). Staying cool in difficult times: mitochondrial dynamics, quality control and the stress response. Biochimica et biophysica acta 1833, 417-424.

Snell, K. (1984). Enzymes of serine metabolism in normal, developing and neoplastic rat tissues. Adv Enzyme Regul 22, 325-400.

Sugiura, A., McLelland, G.L., Fon, E.A., and McBride, H.M. (2014). A new pathway for mitochondrial quality control: mitochondrial-derived vesicles. EMBO J 33, 2142-2156.

Sutendra, G., Kinnaird, A., Dromparis, P., Paulin, R., Stenson, T.H., Haromy, A., Hashimoto, K., Zhang, N., Flaim, E., and Michelakis, E.D. (2014). A nuclear pyruvate dehydrogenase complex is important for the generation of acetyl-CoA and histone acetylation. Cell 158, 84-97.

Szollosi, M.S., and Szollosi, D. (1988). 'Blebbing' of the nuclear envelope of mouse zygotes, early embryos and hybrid cells. J Cell Sci 91 (Pt 2), 257-267.

White, M.D., Zenker, J., Bissiere, S., and Plachta, N. (2018). Instructions for Assembling the Early Mammalian Embryo. Dev Cell 45, 667-679.

Whittingham, D.G., and Biggers, J.D. (1967). Fallopian tube and early cleavage in the

mouse. Nature 213, 942-943.

Xiao, M., Yang, H., Xu, W., Ma, S., Lin, H., Zhu, H., Liu, L., Liu, Y., Yang, C., Xu, Y., et al. (2012). Inhibition of alpha-KG-dependent histone and DNA demethylases by fumarate and succinate that are accumulated in mutations of FH and SDH tumor suppressors. Genes Dev 26, 1326-1338.

Yagi, R., Kohn, M.J., Karavanova, I., Kaneko, K.J., Vullhorst, D., DePamphilis, M.L., and Buonanno, A. (2007). Transcription factor TEAD4 specifies the trophectoderm lineage at the beginning of mammalian development. Development 134, 3827-3836.